ENERGY STORAGE TECHNOLOGIES FOR OFF-GRID HOUSES

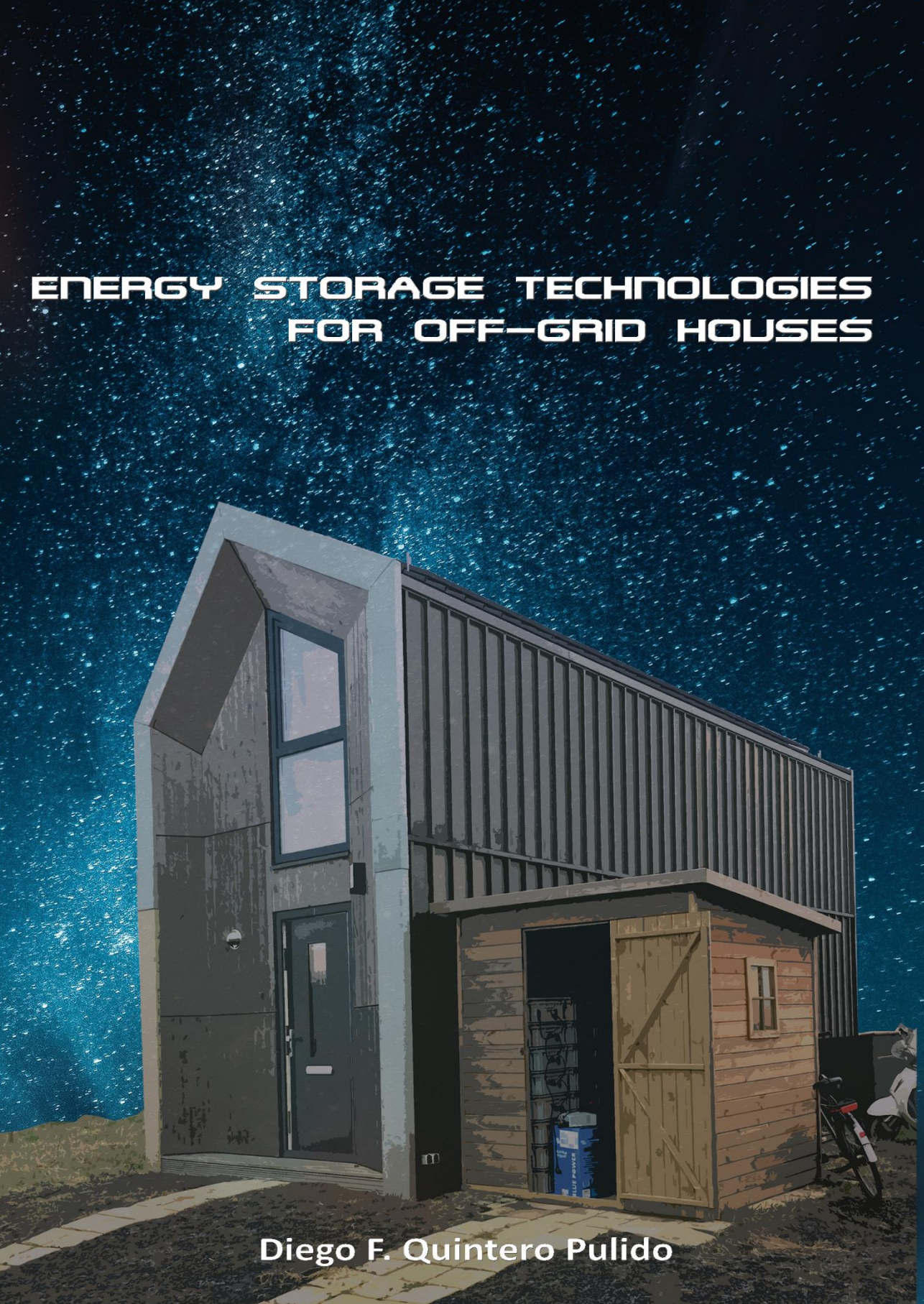

Diego F. Quintero Pulido

Energy Storage Technologies for Off-grid Houses

Diego F. Quintero Pulido

Promotiecommissie

Prof. dr.	J.N Kok	University of Twente (dean)
Prof. dr.ir.	G.J.M Smit	University of Twente (promotor)
Prof. dr.	J.L Hurink	University of Twente (promotor)
Prof. dr.ir.	M. Huyben	University of Twente
Dr.	M.J. Arentsen	University of Twente
Dr.ir.	M.V ten Kortenaar	Dr Ten B.V (referent)
Prof. ir.	R.R. Balda Ayala	Universidad de la Salle
Prof. dr.ir.	Z. Lukszo	Delft University of Technology

This research is funded by the Netherlands Organisation for Scientific Knowledge (NWO), which falls under the responsibility of the Ministry of Education, Culture and Science of the Netherlands. This research is part of the I-Care project number 11854.

This research is partly sponsored by Dr Ten BV, in the Netherlands as part of its ongoing development research and demonstration of storage systems for smart grid integration.

This research is partly funded by the Administrative Department of Science, Technology and Innovation of Colombia, COLCIENCIAS.

UNIVERSITY OF TWENTE. | DIGITAL SOCIETY INSTITUTE

Faculty of Electrical Engineering, Mathematics and Computer Science

Digital Society Institute
P>O Box 217, 7500 AE Enschede, the Netherlands

DSI PhD thesis series No 19-016
ISSN 2589-7721
ISBN 978-90-365-4826-7
DOI 10.3990/1.9789036548267

ENERGY STORAGE TECHNOLOGIES FOR OFF-GRID HOUSES

PROEFSCHRIFT

ter verkrijging van
de graad van doctor aan de Universiteit Twente,
op gezag van de rector magnificus,
prof. dr. T.T.M. Palstra,
volgens besluit van het College voor Promoties
in het openbaar te verdedigen
op vrijdag 4 oktober 2019 om 10:45 uur

door

Diego Fernando Quintero Pulido
geboren op 8 augustus 1985
Bogotá- Colombia

Dit proefschrift is goedgekeurd door:

Prof.dr.ir. G. J. M. Smit (promotor)
Prof. dr. J. L. Hurink (promotor)

Cover design: Diego F Quintero Pulido, Julian R. Daza “Tiny House Almkerk”

ISBN 978-90-365-4826-7
DOI 10.3990/1.9789036548267

Abstract

Off-grid houses have the potential to become an important asset for tomorrow's electricity grid. Access to electricity inside homes is an important ingredient for creating quality of life. On the one hand, off-grid houses may enable such an access in regions without a proper grid infrastructure such as Sub-Saharan regions in Africa. On the other hand, due to the predicted consequences of a world-wide climate change, the vast majority of countries are making plans towards a massive integration of renewable energy; especially solar photovoltaics (PV) and wind turbines. The introduction of this huge amount of renewable energy leads to a lot of challenges. Off-grid houses may become an important asset which can support the integration of renewable energy as they tend to keep the generated energy locally.

In this thesis we research off-grid houses, in particular (semi)off-grid or standalone houses that are capable of being electrically self-sustained for a certain period of time. These houses should depend electrically primarily on renewable sources (e.g. solar PV), used storage units (e.g. batteries) and backup power (e.g. fuel cells or the grid if it is present).

We consider a setup for an off-grid house based on research on new storage technologies done by University of Twente and the company Dr Ten in the Netherlands. The setup focusses on electrical devices in a house and in particular a wastewater treatment unit, which are powered mainly by Solar PV combined with a Sea-Salt battery and a Glycerol Fuel Cell as backup power.

In the first part of this thesis, the Sea-Salt battery and the Glycerol Fuel Cell are studied separately with regard to their electrochemical behaviour. In the second part, we study the sizing of Solar PV, the Sea-Salt battery and the Glycerol Fuel Cell for use in two cases: a standalone wastewater unit and for a house in the US and in NL.

We study the Sea-Salt battery in more detail in Chapter 2. In this part, we consider the kinetics and mechanisms that rule the bromide oxidation at graphite electrode in an aqueous solution in conditions as close as possible to real Sea-Salt batteries. The reason for this is that we want to get a better understanding of the electrochemical processes that occur in halide batteries, which are relevant for large scale implementation in microgrids. We show the electrochemical analysis of a possible cathode materials for the

Sea-Salt battery. We observe that oxidation kinetics with NaBr solutions are much higher than $ZnBr_2$ at 7M while no large differences are observed at 2M. This may be related to the effect that positive ions (Na^+ and Zn^+) may have an influence on the halide oxidation kinetics at large positive electrode potentials which indicates that local ionic potential effects affect the oxidation rate of the reaction.

In Chapter 3, we show the research for the development of a Glycerol Fuel Cell by investigating the glycerol oxidation mechanisms and kinetics using a gold electrode in alkaline media. The Glycerol Fuel Cell is used in this thesis as possible backup power in an off-grid house. The study shows that gold has the highest current density for glycerol oxidation in alkaline media when compared with another catalysts at a potential of -0.2V (Pt, Ag, GC and Cu). It is further observed that the gold surface can change in cyclic voltammetry. Moreover, the Zn-Au and the Cu-Au electrodes show voltammetry behaviour similar to the gold electrode in cyclic voltammetry at different scan rate. The discharge chronoamperometry test shows that the Zn-Au and Cu-Au electrode has higher current densities than the gold electrode at a potential of -0.25V vs Ag/AgCl (5 mA cm^{-2}, 4.5mA $cm^{-2,}$ and 3mA cm^{-2} respectively).

In Chapter 4, we present an example of the energy infrastructure for an off-grid decentralized wastewater treatment plant (DWWTP) using Sea-Salt batteries and solar PV. The goal is to investigate whether a combination of solar PV and Sea-Salt batteries is able to provide electrical power for a DWWTP for a whole year. The results indicate that, solar PV and a Sea-Salt battery can provide the energy requirements of the DWWTPs. However, in order to power the DWWTPs during the months of low sunlight the dimensions of the solar PV and the Sea-Salt battery need to be increased by a factor of three compared to the periods with high sunlight. Alternatively, a Glycerol Fuel Cell as backup power may be added. The simulations performed show that a solar PV of 15kWp and a 20kWh Sea-Salt battery provide 100% of the necessary electricity during the summer and up to 75% during the winter in NL for the Bever III DWWTP. In the case of the MBR DWWTP, a PV system of 30kWp and a Sea-salt battery of 50kWh are necessary to provide 100% electricity supply during the summer and up to 65% during the winter in the Netherlands.

In Chapter 5, we investigate whether the combination of a solar PV system and Sea-Salt batteries is able to provide electrical power to a house for a summer period. For this, we use measured data collected in the US and in the Netherlands for the electricity consumption of a house and for generation from solar PV. Using this data the necessary size of storage needed to create an off-grid house is determined. Based on the experimental

data collected in the summer of 2016 for the houses in Austin-USz and Nunspeet-NL, it is observed that during this period a PV installation combined with a battery may provide the necessary electricity for a 100% off-grid house without showing a blackout. The Austin house needs a solar PV system of 38 kWp and a storage of 226 kWh, and the Nunspeet house needs a solar PV system of 11.5 kWp with a storage of 45 kWh. Furthermore, a practical test is presented in which scaled solar PV and load data for one week was used to test whether a real Sea-Salt battery would be able to deal with the fluctuations of electricity for the considered off-grid scenario in Austin or not. The results of this test indicate that the Sea-Salt battery has the potential to be used for such off-grid applications, although more field tests are needed to support this conclusion.

Samenvatting

Off-grid huizen hebben het potentieel om een belangrijke troef te worden voor het elektriciteitsnet van de toekomst. Toegang tot elektriciteit in huizen is een belangrijk ingrediënt voor het creëren van levenskwaliteit. Aan de ene kant kunnen off-grid huizen een dergelijke toegang mogelijk maken in regio's zonder een goede netwerkinfrastructuur zoals de Sub-Sahara-regio's in Afrika. Anderzijds, vanwege de voorspelde gevolgen van een wereldwijde klimaatverandering, maakt de overgrote meerderheid van landen plannen voor een massale integratie van hernieuwbare energie; vooral fotovoltaïsche zonne-energie (PV) en windturbines. De introductie van deze enorme hoeveelheid hernieuwbare energie leidt tot veel uitdagingen. Off-grid huizen kunnen een belangrijke troef worden die de integratie van hernieuwbare energie ondersteunen kan omdat ze de gegenereerde energie lokaal houden. In dit proefschrift onderzoeken we off-grid huizen, in het bijzonder (semi) off-grid of vrijstaande huizen die in staat zijn om gedurende een bepaalde periode elektrisch zelfstandig te zijn. Deze huizen moeten in de eerste plaats elektrisch afhankelijk zijn van hernieuwbare bronnen (bijv. Zonne-PV), gebruikte opslageenheden (bijv. Batterijen) en back-upvermogen (bijv. Brandstofcellen of het net indien aanwezig).

We bekijken een opstelling voor een off-grid huis op basis van onderzoek naar nieuwe opslagtechnologieën uitgevoerd door de Universiteit Twente en het bedrijf Dr Ten in Nederland. De opstelling is gericht op elektrische apparaten in een huis en in het bijzonder een afvalwaterzuiveringseenheid, die hoofdzakelijk worden gevoed door zonne-PV in combinatie met een Sea-Salt-batterij en een Glycerol Fuel Cell als back-up stroom.

In het eerste deel van dit proefschrift wordt de Sea-Salt-batterij en de Glycerol Fuel Cell afzonderlijk bestudeerd met betrekking tot hun elektrochemisch gedrag. In het tweede deel bestuderen we de dimensionering van zonne-PV, de Sea-Salt batterij en de Glycerol Fuel Cell voor gebruik in twee situaties: Als een zelfstandige afvalwatereenheid en voor een huis in de VS en in Nederland.

We bestuderen de Sea-Salt-batterij in meer detail in hoofdstuk 2. In dit deel beschouwen we de kinetiek en mechanismen die de bromide-oxidatie aan grafietelektrode in een waterige oplossing bepalen in omstandigheden die zo dicht mogelijk bij echte Sea-Salt-batterijen liggen. De reden hiervoor is dat we een beter inzicht willen krijgen in de elektrochemische processen die zich voordoen in halide-batterijen, die relevant zijn voor grootschalige implementatie in microgrids. We tonen de elektrochemische analyse van

mogelijke kathodematerialen voor de Sea-Salt-batterij. We zien dat oxidatiekinetiek met NaBr-oplossingen veel hoger is dan $ZnBr_2$ bij 7M, terwijl er geen grote verschillen worden waargenomen bij 2M. Dit kan verband houden met het effect dat positieve ionen (Na^+ en Zn^+) een invloed kunnen hebben op de halide-oxidatie kinetiek bij grote positieve elektrodepotentialen, wat aangeeft dat lokale ionische potentiaaleffecten de oxidatiesnelheid van de reactie beïnvloeden.

In hoofdstuk 3 tonen we het onderzoek voor de ontwikkeling van een Glycerol Fuel Cell door onderzoek naar de glyceroloxidatiemechanismen en kinetiek met behulp van een gouden elektrode in alkalische media. De Glycerol Fuel Cell wordt in dit proefschrift gebruikt als mogelijke back-upstroom in een off-grid huis. De studie toont aan dat goud de hoogste stroomdichtheid voor glyceroloxidatie in alkalische media heeft in vergelijking met andere katalysatoren met een potentiaal van -0,2V (Pt, Ag, GC en Cu). Verder wordt opgemerkt dat het goudoppervlak kan veranderen in cyclische voltammetrie. Bovendien vertonen de Zn-Au en de Cu-Au elektroden voltammetriegedrag vergelijkbaar met de gouden elektrode in cyclische voltammetrie met verschillende scansnelheid. De ontlading chronoamperometrie test toont aan dat de Zn-Au en Cu-Au elektrode hogere stroomdichtheden hebben dan de gouden elektrode bij een potentiaal van -0,25V versus Ag/AgCl. (5 mA cm^{-2} en 4,5 mA cm^{-2} respectievelijk, versus 3 mA cm^{-2}).

In hoofdstuk 4 presenteren we een voorbeeld van de energie-infrastructuur voor een off-grid gedecentraliseerde afvalwaterzuiveringsinstallatie (DWWTP) met behulp van Sea-Salt-batterijen en een PV-systeem. Het doel is om te onderzoeken of een combinatie van zonne- en Sea-Salt-batterijen in staat is om een DWWTP gedurende een heel jaar van stroom te voorzien. De resultaten geven aan dat PV en een Sea-Salt-batterij voor de energiebehoeften van de DWWTP's kunnen zorgen. Om de DWWTP's tijdens de maanden van weinig zonlicht van stroom te voorzien, moeten de afmetingen van het PV-systeem en de Sea-Salt-batterijen echter met een factor drie worden verhoogd in vergelijking met de perioden met veel zonlicht. Als alternatief kan een Glycerol Fuel Cell als back-upstroom worden toegevoegd. De uitgevoerde simulaties laten zien dat een PV-systeem van 15kWp en een 20kWh Sea-Saltbatterij 100% van de benodigde elektriciteit leveren in de zomer en tot 75% in de winter in NL voor de Bever III DWWTP. In het geval van de MBR DWWTP zijn een PV-systeem van 30kWp en een Sea-Salt-batterijen van 50kWh nodig om 100% elektriciteitsvoorziening te bieden in de zomer en tot 65% in de winter in Nederland.

In hoofdstuk 5 onderzoeken we of de combinatie van een zonne-PV-systeem en Sea-Salt-batterijen in staat is om een huis voor een zomerperiode van stroom te voorzien. Hiervoor gebruiken we meetgegevens verzameld in de VS en in Nederland voor het elektriciteitsverbruik van een huis en voor de opwekking van PV-systemen. Met behulp van deze gegevens wordt de benodigde opslagruimte bepaald die nodig is om een off-grid-huis te creëren. Op basis van de experimentele gegevens die in de zomer van 2016 zijn verzameld voor de huizen in Austin-VS en Nunspeet-Nederland, wordt opgemerkt dat een PV-installatie in combinatie met een batterij in deze periode de benodigde elektriciteit kan leveren voor een 100% off-grid huis zonder een black-out te tonen. Het huis in Austin heeft een PV-systeem van 38 kWp en een opslag van 226 kWh nodig, en het huis in Nunspeet heeft een PV-systeem van 11,5 kWp met een opslag van 45 kWh nodig. Verder wordt een praktische test gepresenteerd waarin geschaalde PV-installaties en belastinggegevens voor een week werden gebruikt om te testen of een echte Sea-Salt-batterij in staat zou zijn om de fluctuaties van elektriciteit voor het beschouwde off-grid scenario in Austin wel of niet te behandelen. De resultaten van deze test geven aan dat de Sea-Salt-batterij potentieel kan worden gebruikt voor dergelijke off-grid toepassingen, hoewel meer veldtesten nodig zijn om deze conclusie te ondersteunen.

Acknowledgment

This thesis has been a collective effort to arrive to a book that shows a long process of work and sharing experiences in the scientific community. This thesis would not have been possible without the help and support of many people. I would like to thank my family for their support. To my mother Esther Pulido, who has always talked to me and give me courage to continue working on the massive piece of work that I tried to develop in this thesis. To my father Jairo Quintero who has been always the rational part of my live, he has showed me that problems can be really simple and it is possible to let many things go in order to have relax mind. I want to thank my wife who has been next to me for many years and she has to endure with me all the changes that we have during this time. She has given me all the space I needed to accomplish this work and without her this process would have been longer and less enjoyable, I will always be thankful to her. Thanks to my aunt Rosalba who has been there for me when I needed her and also thanks for let me collect data in her own house for future projects. I also would like to thank the rest of my closest family, my sister Paola and my brother Leonardo, they have always been an important part in any project I do. Also, thanks to my cousin Miguel for his time and talks in which we shared our ideas and dreams.

I would like to thank the company Dr Ten. Specially, Marnix ten Kortenaar who has been an inspiring tutor before and during this process. He has been working with me and helped me in many aspects of my life. I am very thankful to him and I am glad that he has shared his knowledge with me. I am trustful that all our efforts to create new technologies to help the world will be possible in the near future. I will keep working hard to achieve this, hopefully as part of Dr Ten. In addition, thanks to Gerrit Miedema who has been a very good friend and colleague, I consider him the best manager of Dr Ten and during these years he has helped me to find new ideas to address problems and to understand how to deal with politics as part of the daily job. I am also grateful for the rest of the team, especially Margriet, Rajat and Bart, thank you for being part of this process.

I would like to thank my supervisors and colleagues at University of Twente. To Prof. Gerard who since the beginning gave me his trust and patience in my chaotic creativity, thanks for helping me to understand the process of been a PhD and to spend time checking my wild ideas. Also, to Prof, Johann who gave me always meaningful and substantial feedbacks that made me realize the importance of having a good tutor that understands the technical

processes of the students. Thanks for giving me the courage to improve my writing skills. Thanks to the CAES group, Gerwin for the paper we wrote and collaborate. Thanks to Martijn, Gijs, Viktor, Richard, Thijs, Herman, Marco and Marloes, I appreciate the talks during brakes and the fun activities we had with the group during this period. Also, thanks to all the students that I supervised at University of Twente, TU Delft and HBO Delft. Additionally, thanks to Carlos Barreto from IHE Delft who helped me during the days working at Delft and for the time we spent writing a paper.

Thanks to Prof. Roberto Balda, from La Salle University in Colombia who has been a good role model for me, high appreciation for his knowledge during my bachelor degree and for all these years working together, thanks to him I was able to gain a valuable friend and someone that I respect and trust deeply. To the people at the University of Texas at Austin in the United States, especially the group of mechanical engineering at CEMS. To Prof. Hebner, thanks for hosting me during my PhD and to Liz for her support and the space she gave in her publications for UT.

Contents

1

Introduction

Abstract –In the first part of this chapter the research background for off-grid houses is presented and some of the problems of access of electricity in some areas are illustrated. Furthermore, an analysis of the current alternatives for off-grid electricity solutions are given and the main problem statement and research questions are formulated. Finally, the outline of the thesis is presented[1].

1.1 Motivation for an off-grid house.

In this thesis we refer to an electrical (semi)off-grid house as a house that is capable to be electrically self-sustained for a certain period of time. Such a house, should electrically primarily depend on renewable sources (e.g. solar photovoltaics (PV)), storage units (e.g. batteries) and a backup power unit (e.g. fuel cells). In general, two different motivations are given for considering an off-grid house. First, off-grid houses may provide an interesting option to increase access to electricity in developing countries like e.g. in the case of Sub-Saharan Africa where electricity from the main grid is scarce or not available. Secondly, such houses may help to increase

[1] *Large parts of this chapter have been published in [DFQP 1]*

the amount of renewable electricity which can be integrated in the distribution grid. This is especially the case in developed areas, like for instance Europe. One goal of this thesis is to define possible configurations for a (semi) off-grid house. Those configurations in general comprise the following: a generation system, a main storage unit, a backup power, and specific flexible devices. Within the thesis we mainly focus on the following specific setup for an (semi)off-grid house:

1. Generation: Solar PV.

2. Storage: The Sea-Salt battery.

3. Backup power: The Glycerol Fuel Cell.

4. Flexible devices: appliances in a house in the US, the Netherlands and Colombia and in particular a Wastewater unit.

5. Tool for energy management: DEMkit.

The Sea-Salt battery and the Glycerol Fuel Cell are further discussed in Chapter 2 and 3 respectively. The Solar PV is studied in combination with the Sea-Salt battery and the Glycerol Fuel Cell in Chapter 4 and 5 whereby DEMkit is used as a simulation environment to determine the best size of storage and backup power for a house and for a wastewater unit. Lastly, in Chapter 6 conclusions are presented together with recommendations for future work.

In the remainder of this introduction chapter, we review recent advances in access to electricity in the world and the literature that supports the implementation of off-grid houses in different scenarios. We present an overview of different efforts to create off-grid houses considering both a top down and a bottom up approach. Moreover, some potential research directions for technologies in off-grid houses are presented in more detail.

The remainder of this Chapter is organized as follows. In Section 1.2 and 1.3, we describe the importance of off-grid houses and the current situation of electricity access in the world. In Section 1.4, the current status of electricity grids in developed countries is discussed followed by an overview of different types of off-grid solutions in Section 1.5. In Section 1.6 the challenges of off-grid electrification are described and in Section 1.7, the general set up used in this thesis for an off-grid house is presented in more detail. Finally, in Section 1.8 we give the main problem statement and the outline of this thesis.

1.2 The importance of off-grid and semi-off grid houses

Houses not connected to the electricity grid or being able to operate (almost) without the electricity grid (we call them off-grid houses), may become an important element in the future electricity system. On the one hand, as worldwide the access to electricity inside homes is an important element for creating quality of life, off-grid houses may enable such an access in regions without a proper grid infrastructure. On the other hand, due to the consequences of a world-wide climate change, the vast majority of countries are making plans towards a massive introduction of renewable energy; especially solar photovoltaics and wind turbines. This massive introduction of renewable energy leads to a lot of challenges that need to be overcome. Off-grid houses may be an element which can support the integration of renewable energy as they tend to keep generated energy locally. The two mentioned topics lead to two trends of developing and implementing off-grid houses, the top down approach and the bottom up approach.

The top down approach is suitable for countries that currently already have a stable connection to the electricity grid and that want to introduce more renewable energy in the existing system. Such situation occurs in developed countries, but also in the main cities in the majority of the developing countries (stable connection refers to a connection in a grid with a connection coverage in cities and rural areas of 95%).

In the Netherlands energy-neutral houses are supported by the current net metering schemes. If a house owner purchases a large setup of solar PV the net metering implies that at the end of the year the total electricity cost is determined based on the difference between the total volume of electricity production and electricity consumption. If the difference is zero the house is called energy neutral. However, the system of net metering of solar PV is now under change due to their costs for the government but also due to the negative effect on stabilizing the electricity system [1,2]. It is expected that by 2022 or 2023 a feedback tariff for end users will be introduced which will be much lower than the tariff for consumed electricity.

The bottom up approach for implementing an off-grid house is observed in places where the electricity grid is non-existing or it is existing but it is not stable and reliable. E.g. in Sub-Saharan African countries currently solutions are implemented to connect more cities and rural areas to the main grid. However, in this part of Africa a large investment and a lot of infrastructure is needed to realize such a connection. Considering the current local economic trends in these areas it seems that there are not enough financial means to increase electricity access in this way. On the other hand,

environmental policies and data from the utility providers indicate that also in these regions there is a tendency towards the introduction of a considerable amount of renewable energies, such as solar photovoltaic (PV), wind turbine, among others. Especially, solar PV is a flexible and easy to use technology that provides electricity on the spot without the need of a complex electricity infrastructure. In this way, off-grid houses may e.g. be implemented using solar PV and lead acid batteries. These off-grid houses therefore may also be seen as an innovative way of fast integration of renewables. An example of such a development are systems combining solar PV, batteries and television systems in Tanzania and Kenia, which use mobile tariff applications to allow users to pay for their electricity [3]. Another example is in Bangladesh where by using a swarm electrification method, it has been possible to implement solar PV and batteries for low income villages [4]. The basic idea is to set up a local energy economy in a small village. Initially, electricity is provided by one of the businesses using only a small investment (e.g. for one solar panel, a battery and one LED light to work when it is dark). This business may start to share the electricity produced by the panels with its neighbours and get income from it. Adding these customers may help the first business to buy more solar PV and at the end expand the grid slowly until reaching a village with lights in all houses. Currently, this approach is still in the development stage and fare tariffs are a matter of discussion.

Both cases bottom up and top down, show that there is a tendency towards the implementation of solutions where houses or groups of houses produce (a large part of) their electricity for their own usage with a tendency to create 100% off-grid solutions, at least for a large fraction of the time.

1.3 Increasing access to electricity

Worldwide access to electricity is an important factor to reduce poverty, since without electricity the development of countries tends to be slow and complex. Currently, there is some progress in terms of extending the energy infrastructure. However, this growth is not fast enough and therefore the United Nations (UN) has created the Sustainable Development Goals (SDGs). The SDGs have identified 17 main topics which are part of the 2030 Agenda for Sustainable Development, adopted in September 2015. In this 2030 agenda countries agreed on creating a set of goals to end poverty, to protect the planet and to ensure prosperity for all as part of a new sustainable development.

One of the 17 SDGs is Energy (SDG 7), which does not only cover problems related to limited access to electricity but it involves also a more global sustainable framework. The SDG 7 calls for three main action points:

1. Access to universal and modern energy services.
2. Double the improvement in energy efficiency.
3. Double the share of renewable energy in global energy production.

These three action points were first mentioned in 2011 by the Sustainable Energy for All (SEforAll) initiative [5] and were adapted/included in the SDG 7 targets. In detail the SDG 7 is targeting the following goals (see [6]):

- By 2030, ensure universal access to affordable, reliable and modern energy services.
- By 2030, substantially increase the share of renewable energy in the global energy mix.
- By 2030, double the global rate of improvement in energy efficiency.
- By 2030, enhance international cooperation to facilitate access to clean energy and technology development, including renewable energy, energy efficiency and advanced and cleaner fossil-fuel technology, and promote investment in energy infrastructure and clean energy technology.
- By 2030, expand infrastructure and upgrade technology for supplying modern and sustainable energy services for all developing countries, in particular in the least developed countries, Small Island Developing States, and land-locked developing countries, in accordance with their respective programs of support.

These five targets indicate the areas where policies must be developed, (e.g. increasing the share for renewable energies in the global energy picture, and also improving the rate of implementation of energy efficient technologies). However, the SDG 7 Energy is also interconnected with all the other 16 SDGs, and it is linked to 125 out of 169 targets of the overall SDGs which accounts for almost 74% of the total targets. Nowadays, it is globally recognized that planning for universal access to modern electricity is a primary goal in the national plan for the development of countries and the SDGs.

The importance of a strong energy infrastructure is indicated in studies by the World Bank on power blackouts which indicate that loss of electricity

leads to a loss of economic value in communities [7]. For example in Tanzania the 2012 power blackouts cost businesses around 15% of their annual sales. On the other hand, when electricity is stable and available, this leads to more income, more work and better education for individuals in communities [8]. Additionally, when modern electricity is not available, this creates constrains on economic growth, but when it is stable and available, it increases growth and employment opportunities.

Figure 1.1 *Access to electricity (% of population) World Bank, Sustainable Energy for All (SE4ALL) database from the SE4ALL Global Tracking Framework led jointly by the World Bank* [9].

In the following, we consider the situation in developing countries in more detail. Calculations by the World Bank in 2014 showed that the deficit in access to electricity (people without access to electricity) is mostly concentrated in Africa. The main affected area is Sub-Saharan Africa for which it is estimated that 62.5 percent of the people do not have access to electricity. In total around one billion people are without access to electricity (see Figure 1.1), of which 20% are in South Asia, 60% in Sub-Sharan Africa and the rest of it is distributed over the Pacific, East Asia, Latin America, Middle East and North Africa.

The IEA (International Energy Agency) estimates that at country level alone India has more or less one third of the global deficit of electricity (270 million people), followed by Nigeria and Ethiopia [10]. Figure 1.2 shows the percentage of population with electricity access in the different regions of the world from 1990 to 2016 with a projection towards 2030. It may be noted that between 1990 and 2016 there has been a large improvement in access to electricity on a global view and the increase in coverage occurred both, in cities and rural areas.

In Europe and Central Asia the access to electricity is approaching 98% and this is already in line with the 2030 targets for development. East Asia & Pacific, Middle East & North Africa and Latin America & Caribbean show a constant improvement since 1990 and it is expected that by 2025 the energy access will be covered in cities and in rural areas assuming that political conditions and economic growth have the same trends as in the last decade. Also, in South Asia, the access of electricity shows a constant increase during the years 1990 to 2016.

The trend indicates that by 2030 most cities will be able to reach the stated goals. On the other hand rural areas in South Asia are falling short in the current trend, showing that in 2016 the coverage was 80% in cities and 70% in rural areas. Moreover, South Asia might be able to achieve the 2030 target at its current rate of development. Another situation occurs in Sub-Saharan Africa, which countries have the lowest access in electricity in both cities (30%) and rural areas (20%). At the current rate of economic development Sub-Saharan Africa will not be able to reach the target in 2030. In detail, Sub-Saharan Africa electricity access is growing at the moment at 5.4% annually against the needed 8.4% annually to reach the 2030 goal.

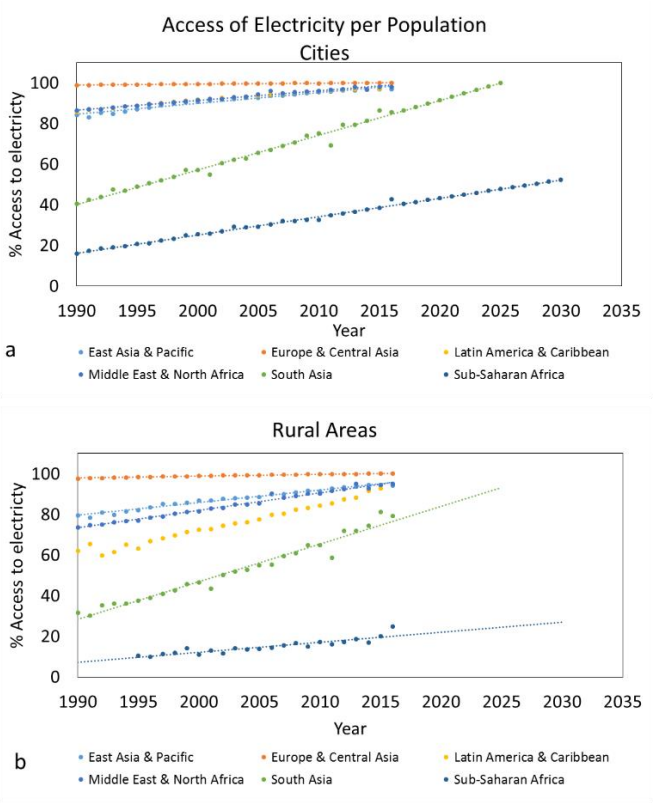

Figure 1.2 Percentage of population with electricity access during 1990 to 2016 with a projection to 2030 a) cities and b) rural areas. Data provided by the World Bank [9].

It can be observed that the improvements in electricity access in the world by 2014 was almost all in urban areas. Note that, the expected population growth of 1.5 billion by 2030 will create a growth mainly in urban cities, since a rural to urban migration is expected [11]. This implies that rural population will not increase considerably but will probably remain stable. Although, from a global perspective rural migration to cities may suggest an easier connection to electricity grids, the migration often leads to an increasing presence of slums which are in general not well connected to the basic infrastructures. This increasing demand in slums will require strong regulation, investments and infrastructure to warrant that enough electricity is available in future urban slums. Although, [12] shows that by 2040 one billion people in Sub-Saharan Africa may get access to electricity, due to population growth this still will leave 530 million people without access to electricity.

1.4 Increasing renewable energies infeed in the existing grid

In the previous section we considered the current situation of access to electricity in the world. We now focus energy savings and reduction of CO_2 emissions in developed countries in particular Europe, by observing the electricity flows within the grids.

The European Union has created guidelines and laws to ensure that the member states commit in reaching the stated targets for energy saving and increased renewable energy share by 2020. This is related to the 20-20-20 goals which were designed to have 20% increase in energy efficiency, 20% reduction of CO_2 emissions, and 20% of the energy from renewables by 2020 compared to the situation in 2014. For the period after 2020 there are also road maps that specify the goals to be achieved before 2050. Note that 2050 is the year in which it is expected to have a fully renewable energy system in the EU [13].

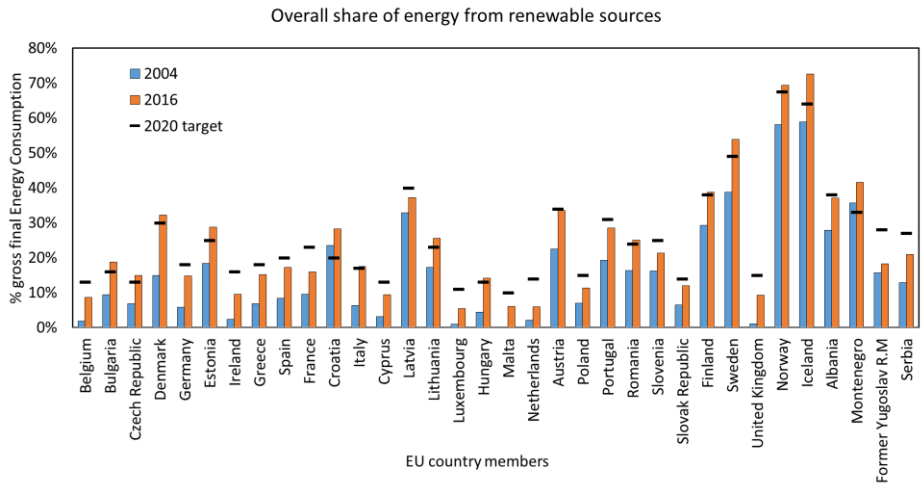

Figure 1.3 *Overall share of energy from renewable sources in European countries, with the percentage of share in 2004 and 2016 and the target for 2020. Based on data provided by Eurostat [14]*

Figure 1.3 shows the share of renewable energy in 2004, 2016 and the target for 2020 in the different countries of the European Union and Figure 1.4 gives the share for the whole European Union in these years [14]. The figures show that, 14 countries of the European Union have already reached their target level for 2020. The countries which are furthest away from the 2020 target are: Ireland (7 %), France (7%), Luxembourg (6%), the Netherlands (8%), United Kingdom (6%), Former Yugoslavia (10%) and Serbia (6%).

Although there was in 2016 still a total gap of 3% for the European Countries to reach the 2020 renewable energy target (see Figure 1.4), the European Environment Agency has issued a report in 2015 called "Trends and Projections in Europe" in which it states that the EU is on track to reach the 2020 targets and that there is a considerable improvement in reducing the Green House Gases (GHG) since 1990 [15]. The GHG emissions in Europe have been reduced since 1990 by approximately 19% in 2013-2014. This trend is linked with the implementation of renewable energies. Given the current trend, it is expected that the GHG reduction for the 2020 goals will be 24 %. Moreover, if additional measures are implemented, the reduction may increase to 26% of the values of 1990.

Next to the 2020 goals, the EU has already created a set of climate and energy targets for 2030 that are in line with SDG 7. Thereby, it is expected that the EU will reduce the use of fossil fuels and will increase the shares of renewable energy to at least 27% by 2030.

Although, many developed countries have already covered the energy reduction target of SDG 7, they still phase problems. These problems are in general not caused by non-existing infrastructures (like is the case of countries in Africa) but by the limitations of the grid capacity.

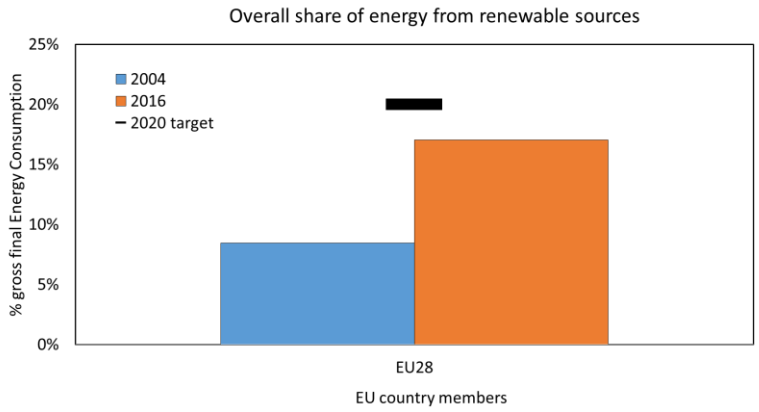

Figure 1.4 *Overall share of energy from renewable sources in the overall European Union, with the percentage of share in 2004 and 2016 and the target for 2020. Based on data provided by Eurostat [14]*

Although, in the case of the EU the electricity coverage in cities and rural areas is almost 100%, the stability of the grid tends to get affected, by the large increase in energy consumption of houses, buildings and industries due to the energy transition [16]. On the other hand, the need to reduce the use of fossil fuels has led to an increase in the installation of renewable

energy on a small scale (e.g. house level Solar PV) but also on a large scale (e.g. solar PV and wind farms). This large scale integration of renewables changes the flows in electricity grids and leads to extra uncertainty in the current electricity system. As the current electrical infrastructure was designed for a centralized power infrastructure in which only a small number of controllable energy sources on central locations were present, the increasing amount of decentralized renewable generation affects the stability of the grid and its reliability. Some of the major concerns are:

- Excess of Solar PV production in decentralized and centralized locations during sunny hours.
- Fluctuation of energy production coming from wind energy and solar farms.
- Increase in electricity demand e.g. due to replacement of gas-fired boilers for supplying the heating/cooling demand by heat pumps.
- Increase in electricity demand due to a large increase in the penetration of electric vehicles (EV).

1.5. Different types of off-grid renewable electricity systems.

In the previous sections we have identified two major concerns for the electricity sector. Firstly, there is a need to provide world wide access to electricity in line with the SDG 7. Hereby the most problematic situation is observed in Sub-Saharan Africa, where access to electricity is as low as 32% and current trends show that it is not enough to achieve the 2030 target. Secondly, in developed countries the SDGs in general are focusing on addressing climate change, protecting the environment and providing stable electricity supply. The SDG 7 in particular encourages countries to create a more stable and reliable electricity grid based on renewable energies and to reduce the use of fossil fuels.

In order to tackle the first concern and to secure access to electricity worldwide, there are two main paths that may be taken: The first is to set up a *grid base electrification*, in which current electricity grids are extended to urban and sub-urban areas; a second option is to enable off-grid electrification in rural areas on micro-level. This results in *mini grids, micro grids and islanded grids*.

These two different strategies operate on a different scale and they give different perspectives on electricity access and services. Furthermore, they both are different in investment and can serve different types of customers.

Grid based electrification

The conventional method to expand the electricity grid has been similar in most countries. Table 1.1 shows in more detail the characteristics of the different possibilities to extent the electricity grid. The electrification of an area usually comes with employment opportunities, improvement of communication, education, social services, and in general enriched quality of life. In the past decades at least 1.7 billion people have been connected to national grids (mostly in urban areas). However, there are still major problems in connecting rural areas to the electricity grid, especially when the location and geography complicates the construction of the grid. For instance in countries like Colombia, Chile, Mexico, China and Tanzania the grid expansion is an ongoing process and will lead to large extensions of the grid networks and power plants.

Off-grid electricity

An alternative way to extend energy access is by employing off-grid electrification. Hereby, off-grid electricity means that smaller grids are setup and that these grids are not connected to the main grid. In principal, there are three approaches for off-grid electrification: mini-grids, micro-grids and off-grid systems (for some characteristics of such grids see Table 1.1).

1. A mini-grid, operates usually with less than 10 MW of installed capacity and it covers an area of around 50km^2. These systems are usually used in communities and sometimes have a restricted connection to the national grid, which is not very reliable. However, in many cases they operate isolated in remote places and have to serve a larger demand mainly during the day.

2. A micro-grid distinguishes from a mini grid mainly by its size. It operates with less than 100kW of installed capacity and it works at a low voltage level covering areas of around 3km^2 to 8km^2.

3. Off-grid solutions (e.g. off grid buildings) are usually used in remote small communities. They may be implemented fast and they are used when a mini-grid or a micro-grid is still in the process to be implemented. Off-grid systems are used mainly for individual houses but they may possibly be extended to areas with approximately 1000 people. Nowadays, a new alternative for off-grid houses emerges,

when these houses are still connected to a weak main grid. In this case, houses (or buildings, industries) may be used in the grid as flexible assets, and they can even be temporarily disconnected. For example, a house may be disconnected in times when the electricity consumption in the grid is too high. In this way this approach may be used to reduce peaks in the main grid.

Table 1.1 *Methods for expanding electricity and utilities, based on* [17]

CHARACTERISTICS	GRID ELECTRICITY	OFF-GRID ELECTRICITY		
System type	Centralized	Mini-grids	Micro-grid	Stand-alone
Size	Large Cities, small cities, regional and multi countries	Communities		Individual houses
Example	Paris(Fr), Amsterdam(NL), Bogotá(COL), México city (MEX), Madrid(SPA), Nairobi(KEN) etc	American Samoa (US)[18], San Andres Island(COL) [19], Hawaii(USA), Among others	Heeten (NL) [20], Pecan Street TX (US)[21],	Partly implemented yet for all year round
Area that can cover	Lager than 50 km^2	8 to 49 km^2	3 to 8 km2	< 1 km^2
People benefit	100.000 to millions	10.000 to 100.000	1000 to 10.000	Usually 1 to 1000
Energy capacity	>10MW	<10MW	< 100kW	< 20 kW
Type of technology use	Power plants in large scale and centralized	Smaller power plants in Medium scale and small scale		Smallest scale
Approx. Required investment in Euro	Billions	Hundreds of Thousands to Billion		Thousands

Traditionally the mini- and micro-grid are mainly powered by fossil fuels. Hereby, diesel generators are the typical option, nevertheless some new technologies are already tested and implemented like fuel cells and renewable energies (e.g. solar PV, wind turbines etc.) combined with batteries. In the ideal case an environmentally friendly mini/micro-grid consist of generation based on renewable energy, storage and a backup system. When the mini/micro-grid are designed and configured properly,

they even may be more efficient and cost effective than a centralized grid. This is why in the past diesel power and small hydro power mini-grids have been implemented. An area where such solutions are used is Indonesia where about 6000 people on islands are using diesel generators and small hydro power plants to cover their electricity needs [22]. Nowadays solar PV systems are starting to take over the market of diesel generators thereby reducing the consumption of diesel fuel (which is generally expensive in these areas) [23]. Another example is observed in the Maldives where about 200 people are using diesel powered generators in a mini-grid structure to cover the needs of hotels and a few houses. Currently there is a transition in the Maldives towards 100% renewable energy and the first steps have been taken by replacing diesel power plants by hybrid solar PV systems [24].

Especially, when communities are far away from cities an off-grid energy solution can be of interest. In this case, an off-grid system can be implemented faster and with less complexity than a mini/or micro-grid, with a connection to the main grid. In developing countries small solar PV systems (called "pico" solar systems) are used, which produce from a few watts of solar PV up to 1kW and provide this electricity for lighting and charging mobile phones [25]. These systems are also used to power small water pumps and other systems with low power consumption. These stand-alone solutions are usually coupled with batteries, and they provide a simple electricity supply solution in situations where the grid is not present or not stable. Such solutions get more interesting since the cost of solar PV has been decreasing rapidly in recent years, which is due to the increase of the market volume, and their cost is expected to keep on decreasing. The report on off-grid solar market trends [26] shows that the value of solar PV products are expected to grow from around $ 700 million in 2018 to around $ 2.4 billion in 2024. This report also estimates that about one out of three off-grid houses will use off-grid solar PV by 2020. However, although the market for off-grid solutions is increasing considerably, there are still not enough incentives and strategies to speed-up the implementation of off-grid systems in order to attain the 2030 SDGs goals for electricity access. For this, off-grid electrification has to overcome some important challenges, which are discussed in the next section.

1.6. Challenges for off-grid electrification:

Off-grid electrification is facing major challenges regarding implementation and contribution to electricity access and the goals for 2030. These challenges involve political, financial, technical and regulatory issues. The

World Bank and Energy for All indicated that the following challenges are of most importance. They were also identified by other researchers [27]:

- high initial investment,
- regulatory uncertainties,
- tariffs,
- stranded assets,
- supply and demand mismatch.

Off-grid electrification usually has high initial investment costs. These initial costs are due to the fact that these off-grid power plants are often designed for a higher power demand than needed for the short term. The reason for this is that power plants are often expected to fulfil the requirements of a larger group of people in the future. However, if the location does not grow as expected the system is underutilized and the revenue for the power plant may never be reached, creating problems for financing the system in the future.

A second challenge concerns regulation. Usually investors need a regulatory system to reduce risks of their investments and to be able to provide services on a long term basis. When an off-grid system is in place it requires upfront legislation which specifies rules for tariffs, services, maintenance, and future plans for grid implementation. Furthermore, for example in India, there are efforts to create a more stable mini-grid system in which users are willing to pay for this stability and the government is willing to provide services for both the electrical grid and the off-grid power system [28]. Note that, tariffs for off-grid electrification are usually higher than for the regular connected often subsidized electricity grid, especially for those consuming small amounts of electricity. Furthermore, when there is no subsidy for the off-grid electrification system, the electricity tariff has to fully recover the investment costs of the power system.

Another problem for off-grid electrification is when technologies become obsolete or when they do not work properly during their life span. This is usually known as stranded assets. In perspective, when the main grid reaches areas where off-grid electrification is present, the off-grid assets may not be used anymore and if investments are not recovered up to that time, this will lead to financial losses. For this reason, it is necessary to create a protection for these assets with legislation to recover the investments even when a grid connection is established, in the future.

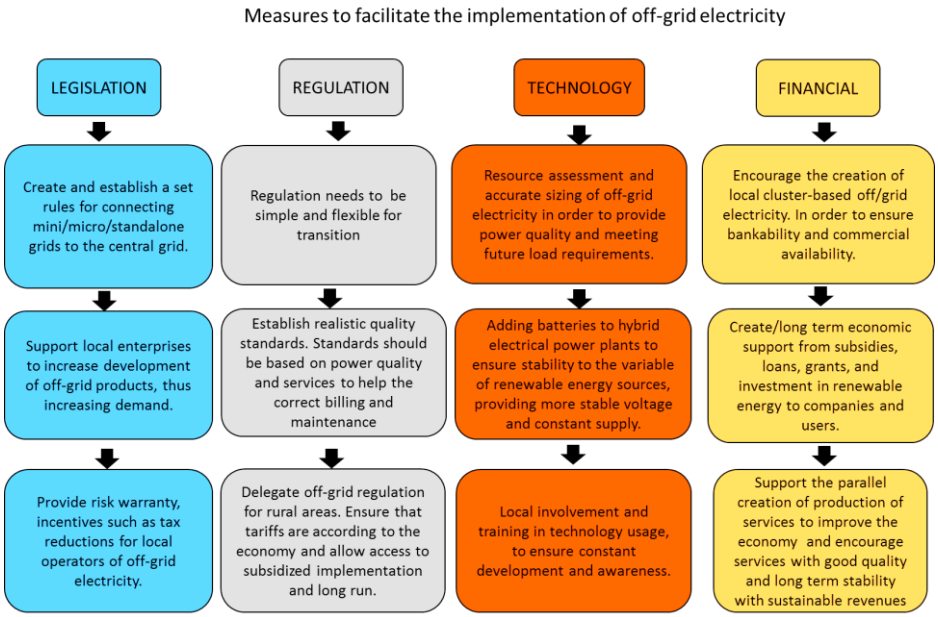

Figure 1.5 *Measures to facilitate the implementation of off-grid electricity, adapted from Energy Access Report and Clean Energy Ministerial 2013* [17][29]

A further challenge for off-grid electricity is the supply and demand mismatch, in particular due to the fluctuations of renewable energies like e.g. solar or wind. When powering a mini/micro or off-grid system with renewable energy in general it will have an underutilization of the resources for some parts of the year. The reason for this is that in order to provide sufficient electricity during months of low electricity production, the system needs to be oversized which leads to an increase in costs. To overcome this, diesel generators may be used to supply the remaining needed electricity when there is a too low production of renewable electricity. However, this creates also extra costs for the power system. Likewise, batteries may be used but they also have a high cost. Nevertheless, in some cases some demand can be steered, e.g. by using decentralized energy management to shift the use of appliances to times when electricity production is high thus reducing the need of backup power.

In order to achieve a better and cost-effective implementation of mini/micro- and off-grid system, schemes for off-grid electrification have to be evaluated in more detail. The transition to an electricity grid with massive generation from renewable energies may be achieved when all corresponding measures are taking into account. Furthermore, off-grid electricity may have a higher chance of success if actions are taken towards

legislation, regulation, technology, and financial issues. A few of such measures are shown in more detail in Figure 1.5.

Since the literature mentioned in the previous sections and our research at University of Twente have shown that an off-grid house may become an important asset for the electricity systems of the future, we focus now on creating an off-grid house to solve the challenges that this represents.

1.7. The Set up for a stand-alone off-grid house

An off-grid system may use different types of renewable electricity generation, and it is usually equipped with batteries and a backup power system to avoid power shortage. Furthermore, in rural off-grid situations the water supply, and wastewater treatment has to be done also locally and should be included in these considerations.

Figure 1.6 illustrates a common configuration of a rural islanded off-grid house. It takes into account the need of electricity for heating, electrical appliances, water and waste treatment (including wastewater). This off-grid house has the following main components:

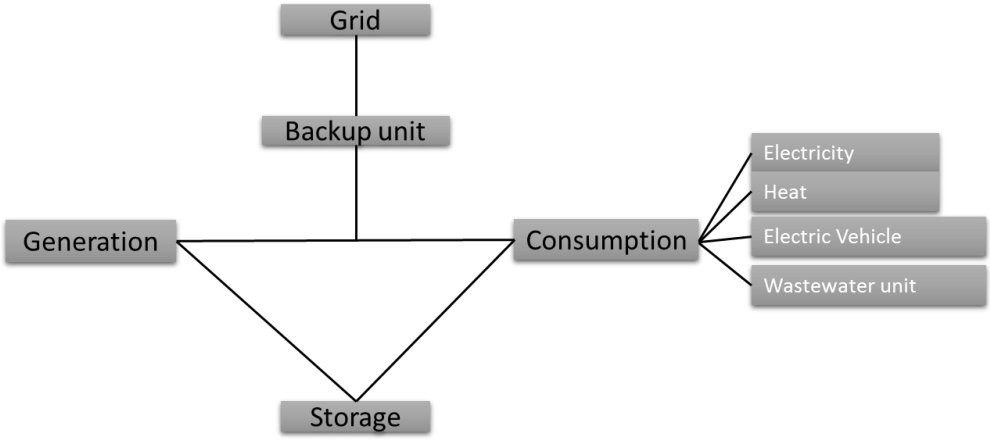

Figure 1.6 *Current setup for a stand-alone house off-grid system.*

1. Generation of electricity: often, Solar PV or Wind Turbines.
2. Energy Storage: usually Lead Acid, Li-ion or NiMH batteries
3. Back up units: a generator or a fuel cell, a micro CHP based on renewable sources (e.g. biogas or wood pellets) or small Biodiesel plants.

4. Devices in a house that consume electricity: e.g. lights, TV sets, water cleaning unit, waste and wastewater treatment system, and heating and cooling units.

5. A connection to an electric grid line when present, which is only included for taking up temporary electricity surplus or shortage.

This setup is the basic setup for off-grid houses as we considered in this thesis.

In principal the combination of the different technologies can provide all the energy that is needed for a house to function daily all around the year. However, in practice a cost-effective and efficient setup that may be embedded in different situations is to our knowledge still not available. There are only a few cases of off-grid houses in the world, whereby these approaches are related to small off-grid houses or compact livings, see e.g. in South Wales [30] and Italy [31]. These approaches show that current technologies are able to provide the energy required for an off-grid house, however, the all-year supply of electricity for all the energy needed in a house still is a major challenge.

Figure 1.7 shows the setup of an islanded off-grid house in the Netherlands which uses new sustainable technologies as described in this thesis. The setup uses various technologies to generate the electricity needed for a house and it is designed to also supply electricity for a decentralized wastewater treatment plant (DWWTP). In this setup, solar PV is combined with a Sea-Salt battery. During the day the solar PV provides electricity and during the night or during low solar irradiation the Sea-Salt battery is used as main electricity provider. Furthermore, a Glycerol Fuel Cell is used as a backup power unit. The fuel cell is only used when solar PV and the Sea-Salt battery are not capable of providing the electricity demand.

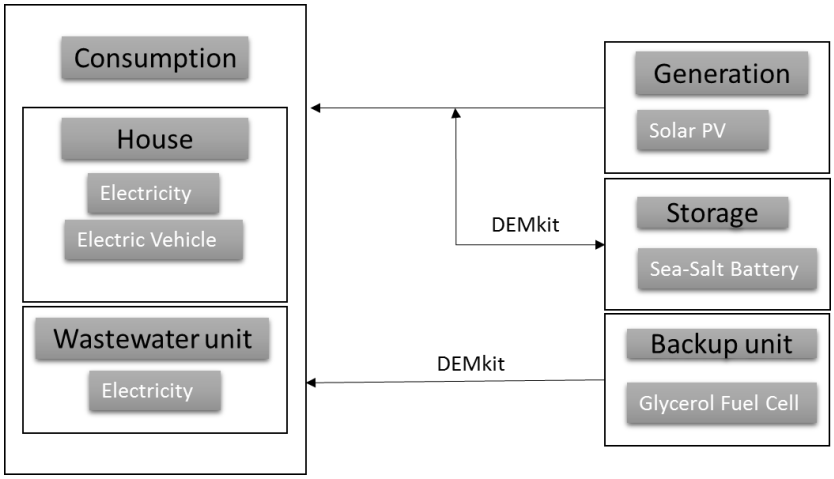

Figure 1.7. Prototype set up for an islanded off-grid house

In the following a short description of the technologies used in this thesis for the setup of a stand-alone house as given in Figure 1.7 is given:

- Solar PV: Various types of commercial solar photovoltaic panels may be used for off-grid houses. Data of solar PV electricity output can be found in different sources; see e.g. Pecan Street in USA [21], data from the electricity company Alliander in NL [32], or data collected from measurements of electricity production/consumption loggers [33].
- The Sea-Salt Battery: This battery is a new energy storage system based on carbon graphite using an electrolyte made of sea salts and additives. It has been developed in the Netherlands by the company Dr Ten BV [34]. The battery is currently under test in the Netherlands, USA, Belgium and Israel and it is expected that the battery will be on the market by 2022 [20][35]. This battery has also been used in research of our group at University of Twente for use in smart grids [35] [36].
- The Glycerol Fuel Cell: The glycerol fuel cell is an electrochemical system that is capable of transforming glycerol directly into electricity. This technology has been developed by the company Dr Ten and investigated by our research group at University of Twente [37] . Currently, the system is under development and it is expected to be on the market by 2025.

- DEMkit: The simulation package DEMkit is a tool for decentralized energy management developed at University of Twente [38,39]. DEMKit makes use of discrete time-series dynamic simulations using a bottom-up modelling approach. A library with device, grid and control components is available in the tool. Generic device components are available that describe the behaviour of a device and its operation constraints, such as e.g. the battery capacity. Attached control algorithms can be used to optimize the operation of devices taking into account the given constraints. The given devices can be connected to a physical grid model, such that it is possible to evaluate the effects of control actions on the delivered power and the power quality.

DEMkit can be used to evaluate the performance of an off-grid house equipped with solar PV, a Sea-Salt battery and a Glycerol Fuel Cell. Furthermore, DEMkit can be used to determine suitable parameters of the appliances (e.g. size of PV panels, storage capacity of the batteries and output power of the fuel cell), such that the house may be used off-grid all year around.

1.8 Main research topics

The overall problem statement of this thesis is as follows:

- *How to identify a setup for an off-grid house based on renewable energy generation, sustainable energy storage technologies and sustainable energy backup unit?*

As mentioned in the previous section the design of an off-grid house may consist of the following elements:

1. Generation of energy: e.g. Solar PV.
2. Energy storage: e.g. Sea-Salt battery.
3. Back up unit: e.g. Glycerol Fuel Cell.
4. Flexible appliances: e.g. Decentralized wastewater treatment unit.
5. Simulation and control software: e.g. DEMkit.

Each of these technologies addresses specific problems that need to be addressed in order to achieve an off-grid house. The central problem of this thesis is divided in the following concrete questions:

- *How can the Sea-Salt battery be characterized for storage in off-grid houses?*

- *How can a fuel cell based on glycerol be designed as backup power for an off-grid house?*
- *How can the near optimal sizing of energy storage units be determined for an off-grid house?*
- *How can the storage technologies and backup units be integrated in the energy management of a house?*

1.8.1 Outline:

This thesis is structured as follows:

1. In Chapter 2 we introduce the Sea-Salt battery technology and in particular we study the kinetics and the mechanisms that are observed in the oxidation of halides at a graphite electrode in an aqueous solution. This has to lead to a better understanding of the electrochemical processes that occur in the battery, which are relevant for large scale implementation in off-grid houses.
2. In Chapter 3 we demonstrate the feasibility of a fuel cell capable of using glycerol as fuel. The glycerol oxidation is studied on a gold electrode and its electrochemical behaviour is presented by means of voltammetry and electrochemical impedance spectroscopy. Furthermore, it is investigated how the glycerol fuel cell has to be scaled up in order to provide a possible back up in an off-grid house.
3. Using the energy management tool DEMkit we investigate in Chapter 4 which size the storage for an off-grid house is near optimal. For this we explain the use of DEMkit and the details of the chosen model for an off-grid house.
4. Chapter 5 presents an analysis of the energy storage needed for providing the required energy for an off-grid decentralized wastewater unit used in houses. This is used as an example for the methods to size of storage units necessary to provide energy for different units that are part of off-grid scenarios in smart grids.
5. In Chapter 6 conclusions and recommendations are given.

2

Electricity Storage
The Sea-Salt Battery

Abstract – This chapter presents a study of the chemical characteristics of a halide battery, which is related to the Sea-Salt battery and its use in off-grid houses. We study the electrochemical reactions that are involved during the process of charging a battery. In detail, the oxidation of halides, in particular bromide, is studied in aqueous solutions on graphite electrodes by voltammetry, electrochemical impedance spectroscopy (EIS) and UV-Vis spectroscopy for its application in halide/halogen batteries used for off-grid houses and for microgrids [2].

2.1 Introduction

Batteries are an appealing technology that can be used as storage technology for managing the mismatch between generation and consumption in buildings and houses [40–42]. Furthermore, recent advances in halide carbon based battery technologies have increased the potential for using this technology in off-grid houses [35]. The combination of renewable energy with these new batteries for usage within microgrids is studied at the University of Twente in the Netherlands [38,43,44]. However, before an actual large scale application of these batteries in a field test a detailed understanding of reliability, power behaviour, electrochemical and chemical properties is needed. In this paper, the last two aspects are addressed,

[2] *Large parts of this chapter have been published in [DFQP 2]*

whereby a focus is on a detailed description of the bromide (Br^-) oxidation at a graphite electrode.

A halide/halogen battery is a battery that has a halide element (Br^-, I^-, Cl^-, F^-) as cathode material and a metal ion (e.g. Zn, Fe, Ni, Li) as anode material. Current battery technologies in the market are still unable to obtain the maximal energy capacity of the halide/halogen redox couple. This is due to problems with the salt solubility and the complex halide reaction mechanisms [45]. However, halide compounds such as chloride, iodide, and bromide have attractive electrochemical properties, for instance, moderate theoretical standard reduction potential (Cl^- 1.358V, I^- 0.53V and Br^- 1.066V) and good theoretical specific energy and power [46,47]. Compared with electrochemical studies performed with halides such as chloride and iodine, not much can be found in the literature on the kinetics and mechanisms of bromide oxidation, e.g. at graphite (which is the most common electrode in halide batteries). Most of the work found about bromide electrochemistry has been done for the development of the zinc bromide flow battery [48–51], also as an alternative for the cathode material in the vanadium flow battery [52] and polysulphide flow battery [53]. In these technologies, the bromide oxidation operates in a complexed chemical bond with ammonium morpholine compounds. This to some extent, prevents halide/halogen recombination and reduces its volatility nature [54].

The mechanisms of the bromide oxidation without complexing agents are still a challenge for researchers. E.g. White [55] and Vogel [56] studied the kinetic behaviour of bromide oxidation at a Pt electrode. Diaz [57] researched the Br^-/Br_2 reaction and pH effect at an Au electrode, Conway [58] evaluated the exchange current density and Tafel behaviour at a Pt electrode, Heintz [59] studied the bromide oxidation concentration effect using cation membranes and Pell [60] investigated the bromide oxidation at low-temperature on carbon electrodes. Other work has been recently done by Walter [61] using carbon nanotubes and carbon cryogels electrodes. From these studies three main aspects can be concluded: First, in voltammetry it is possible to observe two electrochemical processes that govern the halide reaction, one when the halide is oxidising showing a linear increase in the current density and another when the halogen is reduced showing a clear wave in the cyclic voltammetry. These processes include the step formation of the trihalide/polihalide ions in an aqueous solution which leads to a semi-reversible redox reaction. The mentioned results were observed first by Faita [62] and supported recently by other authors for the halide water system [55,63]. Furthermore, the halide oxidation is a multistep process in which the increase in current may correspond to the oxidation of

polybromides (Br_x^-) in the form of Br^- - Br_x^- and of Br_x^- - Br_2^-. This was observed more clear using nitrobenzene as supported solution in $ZnBr_2$ electrolyte [64]. Finally, the studies of the halide oxidation have in common the use of a metal halide salt (e.g. $ZnBr_2$, NaBr and KBr) in an aqueous solution, which has implications in the aqueous form of the halide bond to the cation in which the halide-cation exist in balance in the form of e.g $Zn_{x+y}Br_{x+y}^-$ [65,66].

In this chapter, we study the kinetics and mechanisms that rule the bromide oxidation at a graphite electrode in an aqueous solution in conditions as close as possible to practical batteries. The reason for this is that we want to get a better understanding of the electrochemical processes that occur in halide batteries, which are relevant for large scale implementation in microgrids. This chapter is organized as follows: First, a cyclic voltammetry (CV) analysis is presented for different concentrations of halide salts and a detailed comparison of $ZnBr_2$ and NaBr aqueous solutions is given. Further, an electrochemical impedance spectroscopy (EIS) analysis is shown using a circuit fitting procedure and Kramers-Kronig (KK) transform validation method proposed by Boukamp [67,68]. Lastly, the chapter addresses UV-Vis spectra results to further analyse the studied aqueous solutions.

2.2 Experimental methods

In the following the basic elements used for the experiments are given.

The reagents: $ZnBr_2$ puriss anhydrous, ≥98%, Br_2 reagent grade, $ZnCl_2$ ACS reagent, ≥97% ,ZnI_2 purum p.a., ≥98.0% (AT), NaBr ReagentPlus®, ≥99% , HCl ACS reagent, 37% , and NaOH reagent grade, ≥98%, pellets all from Sigma Aldrich [69] were used with no further purification.

The equipment: The cyclic voltammetry-chronoamperometry experiments were performed with a PGSTAT 101 compact unit from the company Metrohm Autolab [70]. The pH and temperature were recorded with a Hanna HI 9811-5 [71]. The impedance spectroscopy measurements were performed with a Model 600E Series Electrochemical Analyser from the company CH instruments [72].

Voltammetry analysis: Figure 2.1 shows the electrochemical cell used for this work. Graphite was used as the working and counter electrode, the sizes of the electrodes were 3 mm and 20mm diameter respectively. The experiments were performed with Ag/AgCl as reference electrode. The working, counter and references electrode were immersed in 20ml of

electrolyte solution. The graphite was washed and polished with alumina paper caliber 15 after every single experiment. The experiments were performed in different aqueous solutions, with a scan rate of 100mV/s, in a potential window from -1.2V to 1.9V.

The EIS analysis: EIS analysis was done with the EIS fitting procedure in which the elements are analysed with the software-method EQUIVCRT developed by Boukamp [67,73,74]. This method provides more information on the kinetics of the reaction, and can be also validated by a linear KK transform test method developed by the same author [68].

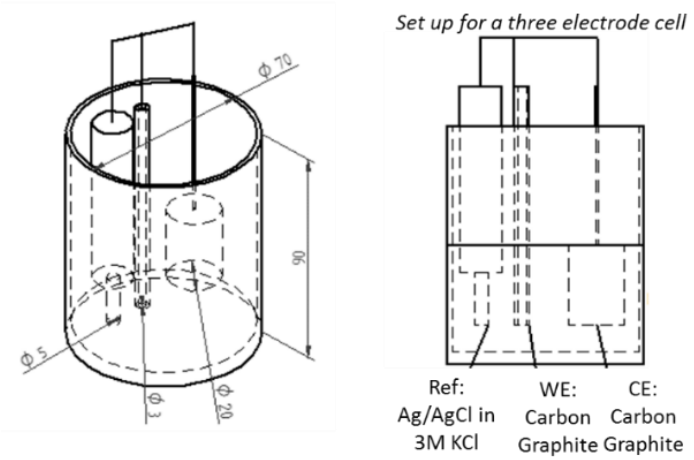

Figure 2.1. *The electrochemical cell*

2.3 Results and discussion

2.2.1. Halide oxidation reaction

Cyclic voltammetry experiments were conducted to gain an insight into the difference between various halides and their oxidation at graphite in an aqueous solution, the studied ions were Cl^-, I^- and Br^-. The analysis was performed using different halide compounds (2M $ZnBr_2$, 2M NaBr, 2M ZnI_2, and 2M $ZnCl_2$,). Figure 2a shows that the halide voltammograms have a similar shape between 0V to 1.9V. In detail, when a potential was applied to the electrochemical cell a current response was obtained, increasing the potential until a value of 1.9V showing linear behaviour, then the potential was reversed and the current reduces thus starting the reduction reaction. Here, all the studied halides defined a clear curve with peaks at different potentials. The peak potential depends on the studied halide thus varying the

current density. This effect may be related to the halide/halogen electrochemical reduction potential which varies between the different halide ions (E^o = Cl^- 1.358V, Br^- 1.066V and I^- 0.53V) and also may be affected by processes at the electrode that affect the current density response e.g. diffusion, side reactions and intercalation. This observations were also presented by the research performed by Arai [75] and Chen [76].

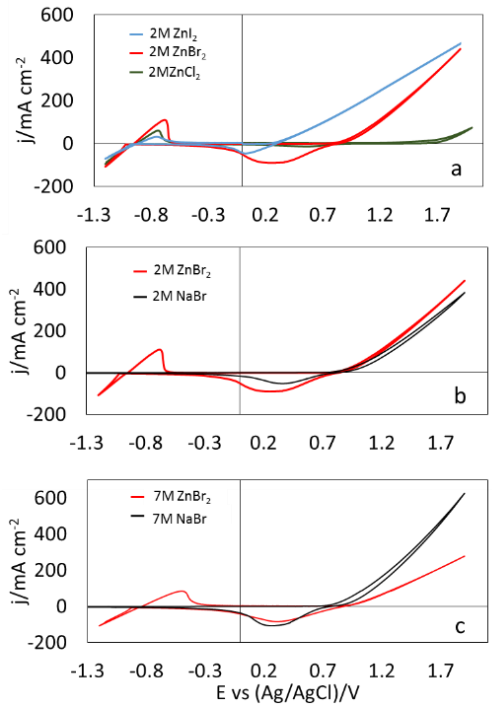

Figure 2.2. *Cyclic voltammetry of graphite in aqueous solutions at 100mV/s and Ag/AgCl reference electrode of a) 2M $ZnBr_2$, 2M ZnI_2 and 2M $ZnCl_2$ b) 2M NaBr and 2M $ZnBr_2$ and c) 7M $ZnBr_2$ and 7M NaBr*

Between 0V to -1.3V a change in the voltammogram shape was observed. This change is possibly related to the zinc deposition/reduction reaction at the graphite electrode, which occurs in a twostep process defining two peaks. The deeper study of the zinc reaction is beyond the scope of this study. However, the zinc reaction was included in the voltammetry in order to show the active presence of the ions in the studied halide compounds and to keep our research as close as possible to real battery processes that could affect the halide oxidation.

Table 2.1 *Current density from CV experiments at 1.5V of different metal halides*

Metal Halide	1.5V mA cm^{-2}
2M $ZnBr_2$	243
2M ZnI_2	359
2M NaBr	215
2M $ZnCl_2$	11.5
7M $ZnBr_2$	148
7M NaBr	346

A comparison between $ZnBr_2$ and NaBr at two different concentrations (2M and 7M) is shown in Figures 2.2b and 2.2c respectively. The voltammetry shows that although $ZnBr_2$ and NaBr have the same anion, the voltammetry potential and current density were different at 2M (Figure 2.2b) and the difference is greater at 7M (Figure 2.2c). Table 2.1 presents a comparison of the current density at 1.5V for the different halides oxidized at graphite in aqueous solutions. The 2M $ZnBr_2$ and 2M ZnI_2 have the highest current density in comparison with 2M $ZnCl_2$ and 2M NaBr. However, the current density in 7M $ZnBr_2$ (148mA cm^{-2}) is lower than at 2M $ZnBr_2$ (243mA cm^{-2}). On the contrary 7M NaBr has a higher current density than the 2M NaBr aqueous solution. This effect is observed in more detail in the voltammetry when the $ZnBr_2$ and NaBr are scanned at different concentrations (Figure 2.3).

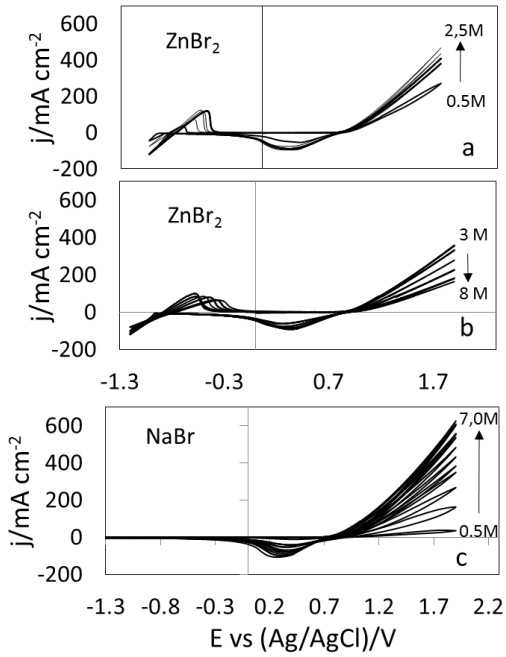

Figure 2.3. *Cyclic voltammetry of graphite at different concentrations of $ZnBr_2$ and NaBr in aqueous solutions at 100mV/s and Ag/AgCl reference electrode of: a) Concentration from 0.5M to 2.5M of $ZnBr_2$, b) Concentration from 3M to 8M of $ZnBr_2$ and c) Concentration from 0.5M to 8M of NaBr.*

When comparing in detail the effect of the Br- oxidation in the voltammetry at 1.5V between the $ZnBr_2$ and the NaBr (see Figure 2.4), it is observed that in the $ZnBr_2$ aqueous solutions the Br^- oxidation current density tends to increase gradually until a concentration of 2.5M, reaching a value of 259mA cm^{-2}. Then, it decreases progressively until 28 mA cm^{-2} at a concentration of 14.5M. In the case of NaBr, the Br^- oxidation current density in the voltammetry at 1.5V increases constantly until a value of 320mA cm^{-2} at a concentration of 7M (point in which no more NaBr was possible to be dissolved at room temperature). The current density increases proportional to the concentration of the solution, thereby behaving in correlation with the Randles-Sevcik equation (Eq 1) [46]. In this equation; i_p is the current density in amps, n is the number of electrons (usually 1), A is the electrode area (cm^2), F is the Faraday constant C mol^{-1}, D is the diffusion coefficient (cm^2 s^{-1}), C is the concentration (mol cm^{-3}) and ν is the scan rate (V/s).

$$I_p = (2.6 * 10^5) n^{3/2} A C D^{1/2} \nu^{1/2} \qquad (Eq1)$$

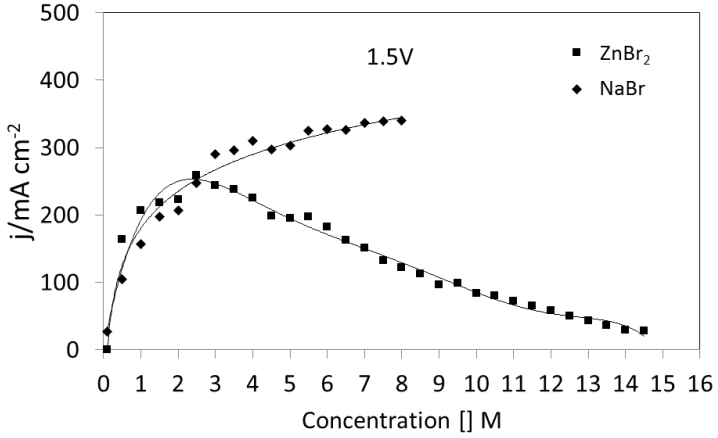

Figure 2.4. *Current density at 1.5V of graphite at different concentrations of $ZnBr_2$ and NaBr in aqueous solutions at 100mV/s and Ag/AgCl reference electrode*

Another difference observed between $ZnBr_2$ and NaBr aqueous solutions is in the pH. Figure 2.5 shows the pH vs concentration effect of $ZnBr_2$ and NaBr in an aqueous solution. In the case of the $ZnBr_2$ the pH decreases when the concentration increases and at the maximum concentration (14.5M) the pH value is 0.2. In the case of NaBr, the pH vs concentration showed a slightly increase from 7.0 (at 0.1M) to 8.5 (at 7M). The changes observed during the voltammetry and pH experiments showed that there is an interesting difference between bromide oxidation and the rest of the halide oxidation reactions and that depending on the studied halide the reaction kinetics differs. In the following section, we show a comparative analysis of the bromide oxidation reaction by studying the mechanism of the reaction at graphite electrode using $ZnBr_2$ and NaBr.

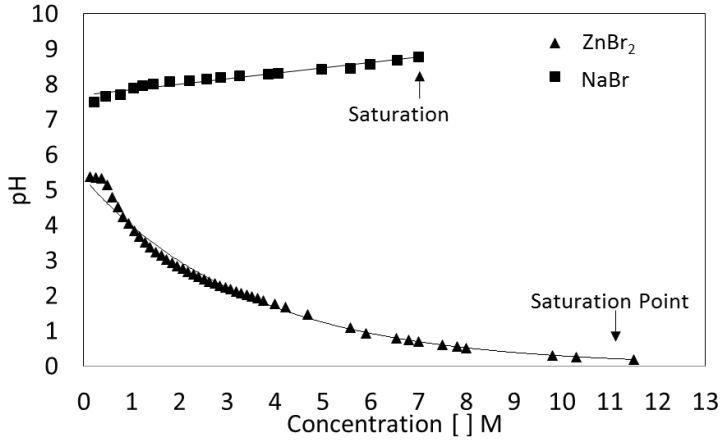

Figure 2.5. *Effect of pH on concentration on $ZnBr_2$ and NaBr aqueous solution*

2.2.2. Halide oxidation at graphite in $ZnBr_2$ and NaBr aqueous solutions

In this section the possible processes that are involved in the bromide oxidation voltammetry presented in Section 2.2.1 are discussed. Here, three different physical and chemical processes that affect the kinetics of the halide oxidation are explained: The aqueous crystal structure of $ZnBr_2$ and NaBr in aqueous solutions, the formation of the tribromide/polibromide species and the intercalated bromine on the graphite electrode.

2.2.2.1 The aqueous crystal structure of $ZnBr_2$ and NaBr in aqueous solutions

One possible explanation for the oxidation behaviour of Br- in an aqueous solution is its crystal structure which is different for $ZnBr_2$ and NaBr. In the case of $ZnBr_2$, Duvlet [65] proposed that there are two different kinds of Zn atoms in the crystal structure of $ZnBr_2$ solutions. The first Zn atom is a tetrahedral coordinated by four Br atoms, this forms dimeric $Zn_2Br_6^{2-}$ groups with mmm crystallographic symmetry. The bridging function of Br distorts both the bond distances and the angles around Zn from an ideal tetrahedron.

The second Zn atom forms a $Zn(H_2O)_6^{2+}$ octahedral also with crystallographic mmm symmetry. Which are linked to the $Zn_2Br_6^{2-}$ groups through of $O\text{-}H^+...Br^-$ hydrogen bonds to form infinite chains of $[Zn(H_2O)_6]^{2+}$-$[Zn_2Br_6]^{2-}$ extended along and through $O\text{-}H^+...Br^-$ hydrogen bonds into layers. Later research carried out by Simonet [77] suggest that both Zn and Br ions are largely hydrated under normal conditions in aqueous solutions and that Zn–Br pairs are formed in hydrothermal conditions. This is related to the

octahedral-to-tetrahedral evolution of the local Zn environment, where the majority of Zn atoms are surrounded by water octahedral in normal conditions and by distorted tetrahedral involving Br and O atoms in hydrothermal conditions. The two explanations for $ZnBr_2$ crystal structure showed that, the halide oxidation may be influenced by the bonds of Zn and Br atoms which at high molar concentration (7M), are influenced by Zn O^- H^+ in their crystal forms in aqueous solutions which may slow down the kinetics of the Br species towards the graphite electrode thus possibly reducing its current output.

In the case of NaBr, Omta [78] and later studies by Lin [79] showed that the average of hydrogen and oxygen molecules surrounded the Na^+ and Br^- in aqueous solutions have the same number compared with pure water in low concentrations. Also, that increasing the NaBr concentration only affects slightly the bond of Na^+ Br^- thus not creating infinite chains in the solution (like in the case of $ZnBr_2$). This behaviour suggest that Br- ions can move faster in NaBr aqueous solutions and the halide oxidation may occur at a faster rate than $ZnBr_2$ in aqueous solutions thus possibly explaining the effect in current density at higher concentrations (e.g. 7M), observed in Figure 2.3 and 2.4.

2.2.2.2 The formation of the tribromide and polibromide species in aqueous solution

Another important aspect that may influence the Br^- oxidation reaction is the formation of tribromide and polibromide. In literature information is found of the Br^- oxidized form. E.g. Adanuvor and White [80] researched the formation of the tribromide complex base on the step reaction proposed first by the Volmer-Heyrovsky (V-H) discharge desorption mechanism equation for Br^- oxidation (Eq 2 and Eq 3 respectively). The Br^- ions are present in the solution and are adsorbed during the oxidation process (Eq 2) creating bromide adsorbed (Br^-_{ads}). A second reaction step occurs when the Br^-_{ads} oxidases at the electrode surface in the presence of Br^- forming Br_2 (Eq 3). A third chemical reaction step occurs after the charge transfer, when Br_2 is in contact with the remaining Br^- ions forming the tribromide complexation (Br_3) (Eq 4), which has been studied in detail by different authors [58,81]. The chemical oxidation reaction is a series of continues processes between the new formed element (Br_2, Br_3) with Br^- ions forming different types of polybromides complexes (Br_x) (Eq 5). This effect is observed in more detail when using complexing agents. This type of mechanism of the Br- oxidation reaction has been studied in detail recently by Park [82]. Park, concluded that the Br- electrochemical oxidation is a reaction that occurs with the Br- transfer-water step. This is possibly occurring before (re)combining with

other elements in the aqueous environment, and this difference is relative to the current density and the concentration of Br^- ions in the electrolyte.

$$Br^- \rightarrow Br_{ads} + e^- \quad (V) \qquad (Eq\ 2)$$

$$Br^-_{ads} + Br^- \rightarrow Br_2 + e^- \quad (H) \qquad (Eq\ 3)$$

$$Br_2 + Br^- \rightarrow Br_3 \qquad (Eq\ 4)$$

$$Br_3 + Br^- \rightarrow Br_x \qquad (Eq\ 5)$$

2.2.2.3 Intercalated bromine

During the performed experiments on halogen oxidation, graphite was used as working electrode. In this case, it is possible that Br_2 intercalation[3] may contribute in the varying current density of the Br- oxidation in an aqueous solution. In literature, e.g. Izumi [83] researched the electrochemical intercalation of Br_2 on graphite in aqueous solutions. In the study it was observed that the Br- oxidation reaction at different concentrations had an effect in the current density during voltammetry studies. Izumi, concludes that the effect is related to the formation of intercalated Br_2 on the graphite electrode. This effect is supported by changes in electrode weight and the decrease in relative electrical resistivity. Later studies by Gaier [84], who studied the aqueous electrochemical intercalation of Br_2 on graphite fibers, showed that the effect observed on the graphite electrode was similar for carbon fibers. The mechanism to create intercalated Br_2 are related to the concentration of the halogen during the oxidation reaction near the graphite electrode. This effect was observed in temperatures from 5°C to 40°C. The observations by Izumi and Gaier are in accordance with the voltammetry recorded in this research for Br- oxidation at graphite (Figure 2.3 and 2.4), showing that graphite may have a contribution to the kinetics of the Br- oxidation.

2.4 EIS analysis of bromide oxidation at graphite

The three effects that are described in the previous section as a possible cause of kinetic changes during voltammetry for the Br- oxidation in aqueous solutions at a graphite electrode, were studied using electrochemical impedance spectroscopy (EIS). EIS is used in order to observe whether the Br^- oxidation at a carbon graphite electrode may be represented with an electrical circuit. If this is the case, it is possible to give an indication of the contributions of each step in the oxidation reaction, this

[3] Intercalation is a process in which a guest molecule or ion is inserted into a host lattice. The structure of the guest–host or intercalated compound is only slightly perturbed from the host structure and the reaction used to form the compound is reversible [174].

is possible by assuming that each step in the oxidation reaction can be represented of electrical elements (e.g. resistors and capacitors). The presence of the elements in the EIS study are not studied by other spectrometry methods. Based on the differences observed in the cyclic voltammetry in Figure 2.3 and 2.4 the EIS analysis is performed using $ZnBr_2$ and NaBr for comparison purposes.

The EIS analysis was performed in different steps: First, a plausible reaction pathway is taken from literature and a possible reaction model is created. Second, an expected circuit is suggested based on the assumption of the model for the reaction. Third, the circuit is compared against the lab results using the EQUIVCRT software and fourth the circuits are analysed with the KK transform test [67,68].

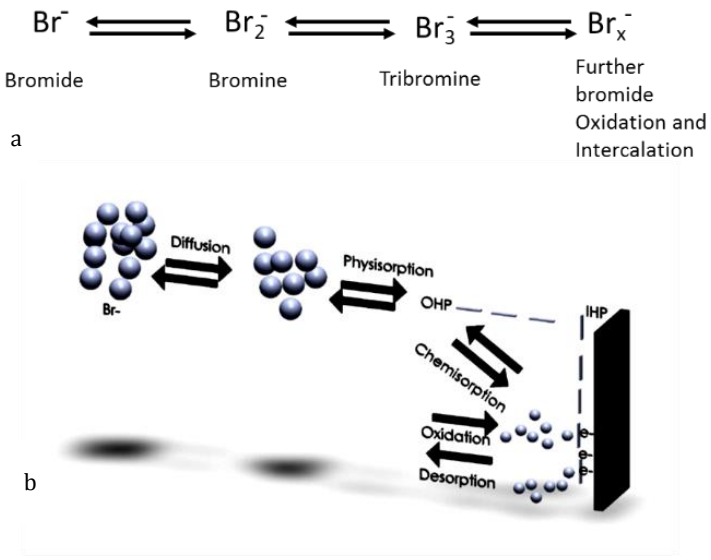

Figure 2.6 *Reaction representation of bromide oxidation pathway at graphite.*

2.3.1 Expected circuit

The Br^- oxidation reaction pathway at graphite considered for the analysis in EIS is shown in Figure 2.6a and 2.6b. Based on this pathway and the Br^- oxidation reaction equation an expected equivalent circuit was derived (see Figure 2.7a). The circuit is derived taking into account that each reaction step has a sub-analogue electrical circuit. First, we considered the chemical reaction that is shown in Figure 2.6b in which diffusion of Br^- ions is followed by physisorption in the outer Helmholtz plane (IHP). Also, it is observed that chemisorption processes presented in line to the double layer capacitance in

the inner Helmholtz plane (IHP) and various Br^- ions may be captured close to the electrode (oxidation-desorption) forming Br_2 and later the Br_3. The oxidation process will continue forming Br_x and possibly intercalated graphite with Br_2, Br_3, and Br_x close to the electrode. Based on the previous analysis of the Br^- oxidation reaction (see Section 2.2) the different sets of capacitors and resistors were designed (see Figure 2.7b). It is assumed that each pair of capacitor-resistance represents one of the steps in the reaction. Furthermore, after the expected circuit was designed it was tested with EQUIVCRT in order to observe whether the circuit fits the recorded impedance data or not.

2.3.2 Fitted circuit

The fitting of the circuit is a process based on the assumption that one particular circuit exists which fits (or mimics) all data that is found in the impedance measurements. For this, the impedance data was collected at four different potentials (0V, 0.5V, 1V and 1.5V) that were measured in the voltammetry of Br- oxidation at graphite presented previously in Figure 2.3 and 2.4.

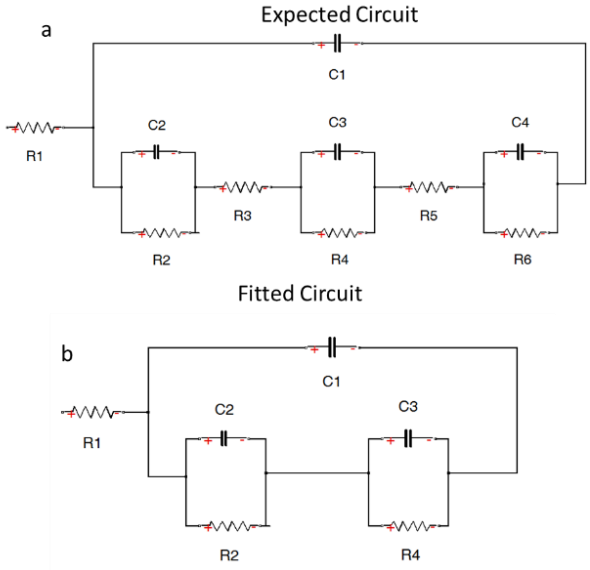

Figure 2.7 *Equivalent circuits for the bromide oxidation at graphite electrode with EIS software EQUIVCRT a) Expected circuit and b) Fitted circuit*

We first tested the expected circuit (Figure 2.7a) and we noticed that it did not completely fit the given EIS data. The software EQUIVCRT tested the data with the given circuit and started to iterate until finding the best match for the recorded data. In order to improve the fitting of the circuit with the EIS results we tested over 25 circuits, with a trial and error approach. In this process we tried to keep as close as possible to the literature and knowledge of the oxidation reaction. One circuit seemed to fit well the entire data at the studied potentials. In principal, some of the resistance and the diffusion elements are merged from the expected circuit, this might be due to the low influence in the studied frequency or due to extreme low noise in the system. The resulting circuit is shown in Figure 2.7b. The resulting fitting had an X^2 value of 10^{-3} or 10^{-4} (see Table 2.2). (The X^2 value represents the residuals of the correlation of data with the electrical proposed system. The X^2 results are explained in more detail in Section 2.3.3). The X^2 values are expected to be as close to zero as possible (10^{-6}). Although, the resulting X^2 values are not zero (10^{-6}), the circuit mimics reasonably the recorded impedance data and it is in line with our comprehension of the Br- oxidation reaction. Therefore, the fitted results were further analysed using the different concentrations of NaBr and $ZnBr_2$.

Table 2.2 *Circuit fitted values for the Impedance spectra of 7M, 2M $ZnBr_2$ and 7M, 2M N*

7M NaBr	V (V)	R1 (Ω)	C 1(F)	R2(Ω)	C2 (F)	R3(Ω)	C3(F)	X^2
	0	4.47E+00	4.70E-08	1.09E+02	2.53E-05	3.89E+01	2.04E-04	6.56E-04
	0.5	4.31E+00	7.14E-08	5.47E+01	2.22E-05	6.42E+01	1.22E-04	1.03E-03
	1	3.54E+00	2.09E-07	9.68E+01	1.91E-06	4.03E+01	1.71E-04	7.50E-04
	1.5	3.51E+00	2.83E-07	9.35E+11	6.72E-13	2.04E+01	1.71E-04	6.12E-04
7M $ZnBr_2$	V (V)	R1 (Ω)	C 1(F)	R2(Ω)	C2 (F)	R3(Ω)	C3 (F)	X^2
	0	8.55E+00	4.82E-08	9.55E+01	4.80E-05	-2.57E+14	2.60E-14	9.33E-04
	0.5	8.23E+00	5.56E-08	9.26E+01	5.11E-05	2.05E+13	1.42E-14	5.69E-04
	1	9.32E+00	2.47E-08	1.19E+03	4.01E-07	5.82E+02	1.49E-06	3.46E-04
	1.5	9.47E+00	2.73E-08	8.51E+02	9.32E-07	7.16E+11	-2.06E-12	2.46E-04
2M NaBr	V (V)	R1 (Ω)	C 1(F)	R2(Ω)	C2 (F)	R3(Ω)	C3(F)	X^2
	0	4.45E+00	8.51E-08	2.23E+02	2.77E-05	5.12E+01	1.47E-05	5.28E-04
	0.5	5.33E+00	5.18E-08	2.53E+02	1.86E-05	5.02E+01	1.34E-05	1.11E-03
	1	4.99E+00	6.88E-08	1.55E+03	-8.58E-04	4.06E+01	2.50E-05	1.29E-03
	1.5	2.77E+01	2.68E+00	-4.55E+01	1.62E-02	3.17E+11	3.63E-14	2.52E-04
2M $ZnBr_2$	V (V)	R1 (Ω)	C 1(F)	R2(Ω)	C2 (F)	R3(Ω)	C3 (F)	X^2
	0	5.14E+00	7.97E-08	3.94E+02	1.61E-05	5.93E+01	2.34E-05	5.77E-04
	0.5	5.49E+00	5.55E-08	1.30E+03	8.61E-07	3.87E+01	3.21E-05	9.50E-04
	1	5.34E+00	5.63E-08	2.54E+02	1.53E-01	3.52E+01	6.91E-05	6.26E-04
	1.5	4.18E+00	2.59E-07	3.13E+01	7.92E+00	4.03E+03	1.49E-13	2.16E-04

2.3.3 Spectra analysis

As shown in the voltammetry of Br- oxidation at graphite in aqueous solutions of NaBr and $ZnBr_2$ (Figure 2.3 and 2.4), there is a difference in the voltammetry when the concentration of the electrolyte is changed. The difference is more pronounced at a concentration of 7M than at 2M. Due to this observation, the analysis of this effect in both salts NaBr and $ZnBr_2$ was studied in more detail using EIS. Figure 2.8a shows the impedance spectra of 7M $ZnBr_2$ and 7M NaBr at the graphite electrode, with the real and fitted data at different positive potentials (0V, 0.5V, 1V and 1.5V) together with the steady state current in the region of -0.2V to 1.8V, the region in which, Br- oxidation is possibly occurring. The figure shows that, at the concentration of 7M in both $ZnBr_2$ and NaBr there was no substantial change in the impedance spectra at the potential of 0V and 0.5V.

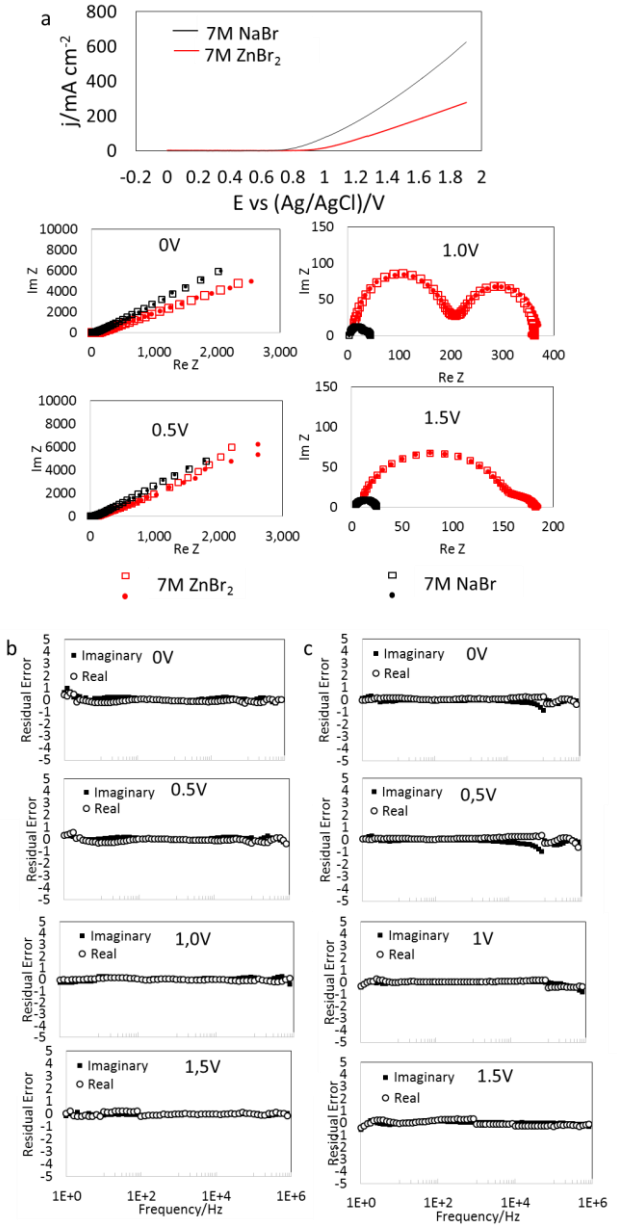

Figure 2.8 *a) Impedance spectra real (*) and fitted data(□) at different positive potentials together with the steady state current from graphite CV experiments on 7M $ZnBr_2$ and 7M NaBr, 100mV/s and Ag/AgCl reference electrode. b) Imaginary (*) and real (○) equivalent circuit frequency error 7M $ZnBr_2$ c) Imaginary (*) and real (○) equivalent circuit frequency error 7M NaBr*

However, when the impedance test was performed at 1V and 1.5V the spectra had a different shape, showing at 1V two clear loops and at 1.5V one large loop with a new loop at higher frequencies. The changes in the impedance spectra are possibly related to the standard redox potential of the Br- reaction which in literature [62] and in our study is observed at potentials about 0.9V. Moreover, the impedance in the 7M $ZnBr_2$ was overall larger than in the 7M NaBr aqueous solutions at the potential of 1.0V and 1.5V. This impedance behaviour may be related to the changes observed in the voltammetry where the current density recorded is lower in 7M $ZnBr_2$ than in 7M NaBr and also to the different pH of the solution as shown before in Figure 2.5. Previous tests performed by Jeffrey [85] support our results, showing that Br- oxidation in NaBr aqueous solutions at different concentrations have an effect on the kinetics of the reaction and on the pH of the solution.

On the other hand, the impedance spectra in 2M $ZnBr_2$ and 2M NaBr has a different behaviour than at 7M. Figure 2.9 shows the impedance spectra analysis at different positive potentials (0V, 0.5V, 1.0V and 1.5V) in 2M $ZnBr_2$ and 2M NaBr aqueous solutions at the graphite electrode. In this case, during both experiments the impedance spectra shape shows a similar behaviour. Here, in Figure 2.9a the changes in the spectra at potentials of 0V and 0.5V are not observed. However, the spectra change when the potential is increased to 1V showing two semicircles and one semicircle at 1.5V (this observation is also similar to 7M $ZnBr_2$ and 7M NaBr). At 1V the impedance spectrum shape maybe a representation of the Br- oxidation reaction as observed previously in Figure 2.8. In this case, it is observed that the impedance is larger in the 2M $ZnBr_2$ than in the 2M NaBr aqueous solution. Furthermore, at the potential of 1.5V the impedance is larger in the 2M NaBr than in the 2M $ZnBr_2$. Also, the values of the impedance are lower when they are tested at 1.5V than at 1V. These effects in the impedance spectra may be an effect of the Br- oxidation reaction which like in the 7M solutions occur at potentials higher than 1V. In order to verify the reliability of the impedance data, the relative residuals are plotted in Figure 2.8b and 2.9b. The data was calculated using equation 6 (Eq.6).

$$\Delta_{re,i} = X_{re,i} - X_{re}(w_i) / |X(w_i)| \quad and$$
$$\Delta_{re,i} = X_{im,i} - X_{im}(w_i) / |X(w_i)| \qquad (Eq6)$$

Here, as explained by Boukamp [73] $X_{re,i}$ and $X_{im,i}$ are the real and imaginary parts of the impedance at a data point (i), $X_{re}(w_i)$, $X_{im}(w_i)$ are the real and

imaginary parts of the modelling function for w_i. Furthermore, the $|X(w_i)|$ is the vector length expressed in absolute value of the modelling function (X also represents the statistical behaviour of the correlation for fitted data in the circuit). The residuals are in general between 0 - 1%, showing that the fitted data has a low error percentage in all the applied potentials.

As explained in Section 2.3.2 only one single circuit fitted all the impedance spectra shown in Figure 2.8 and 2.9. The resulting values of resistors and capacitors at different potentials are shown in Table 2.2. In general, when the potential is increased the fitted elements change proportional. The first resistance (R1) represents the distance of the particles that need to travel to the graphite electrode double layer. The first capacitor (C1) is representing the double layer capacitance, which has approximately the same value at all the potentials. The double layer capacitance is connected together with two sets of resistances-capacitors that are in series (R2C1 and R3C2). This set of resistors and capacitors may represent the steps that occur in the Br- oxidation reaction.

However, note that it is not possible by means of impedance spectroscopy to determine the precise reaction that is occurring. Nevertheless, our impedance measurements and fitted circuit show that there are two main reactions occurring in the Br- oxidation at graphite possibly related to the effect of Na^+ and Zn^+ in the solution, the presence of Br_2, Br_3, Br_x. and the effect of intercalation as explained in Section 2.2. Furthermore, it is observed that the capacitors and resistors have different values in the tested electrolytes at different concentrations and these differences are more pronounced at the potential of 1.5V (see Table 2.2). Figure 2.10 has been constructed in order to elucidate this effect in more detail. Here, a comparison is shown of the fitted values for capacitors and resistors at 1.5V in high (7M) and low (2M) concentrations of $ZnBr_2$ and NaBr.

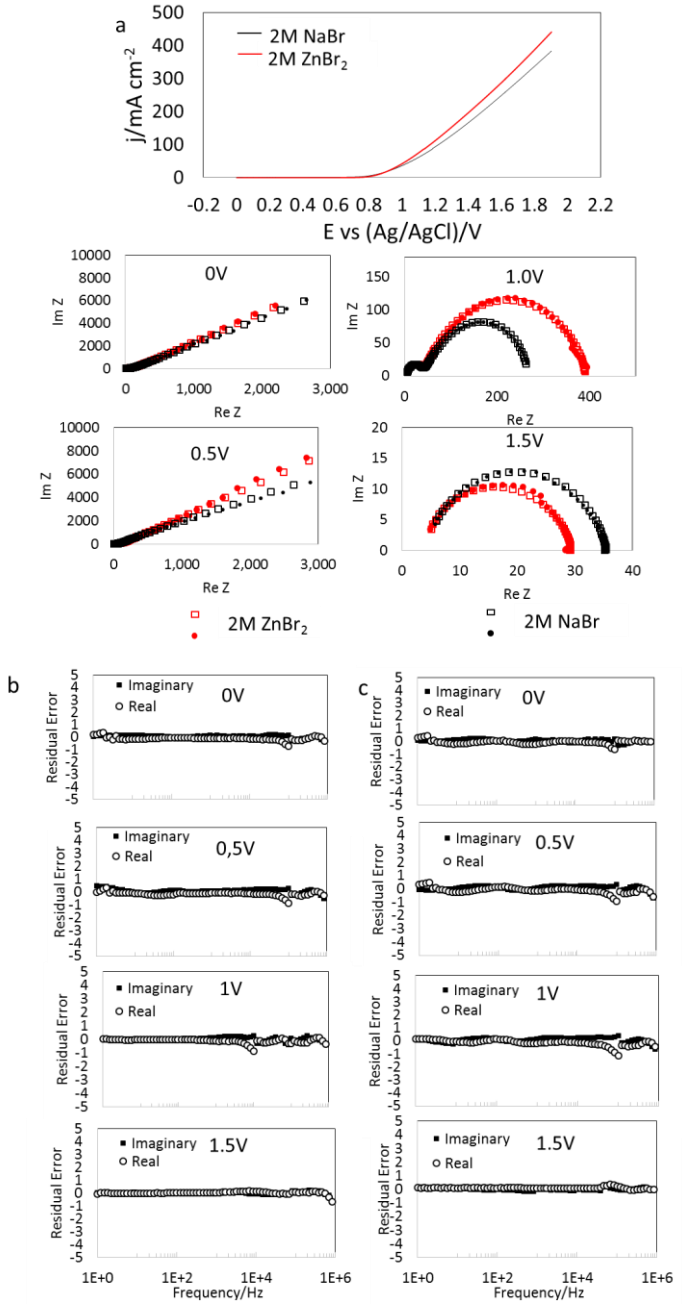

Figure 2.9 *a) Impedance spectra real (*) and fitted data(□) at different positive potentials together with the steady state current from graphite CV experiments on 2M $ZnBr_2$ and 2M NaBr, 100mV/s and Ag/AgCl reference electrode. b)) Imaginary (*) and real (○) equivalent circuit frequency error 2M $ZnBr_2$ c) Imaginary (*) and real (○) equivalent circuit frequency error 2M NaBr*

Figure 2.10a shows the capacitors in the fitted circuit for 7M $ZnBr_2$ and 7M NaBr. In principal, the values of C1 and C2 in both cases are similar with values close to zero. However, the capacitor C3 has a value of 1.71E-04 F for the 7M NaBr which is larger than in the 7M $ZnBr_2$ with a value close to zero. Furthermore, the resistor R2 shows a higher value for 7 NaBr than in the 7M $ZnBr_2$ (see Figure 2.10b) and the resistor R3 shows a larger value in the 7M $ZnBr_2$ (7.16E+11) than in the 7M NaBr (1.71E-04). The difference in the capacitors and the resistors in both electrolytes at 7M, may be related to the presence of the ions Zn^+ and Na^+ in the oxidation reaction, and this effect is possible related to the different in kinetics depicted previously in the voltammetry in Figure 2.3 and 2.4.

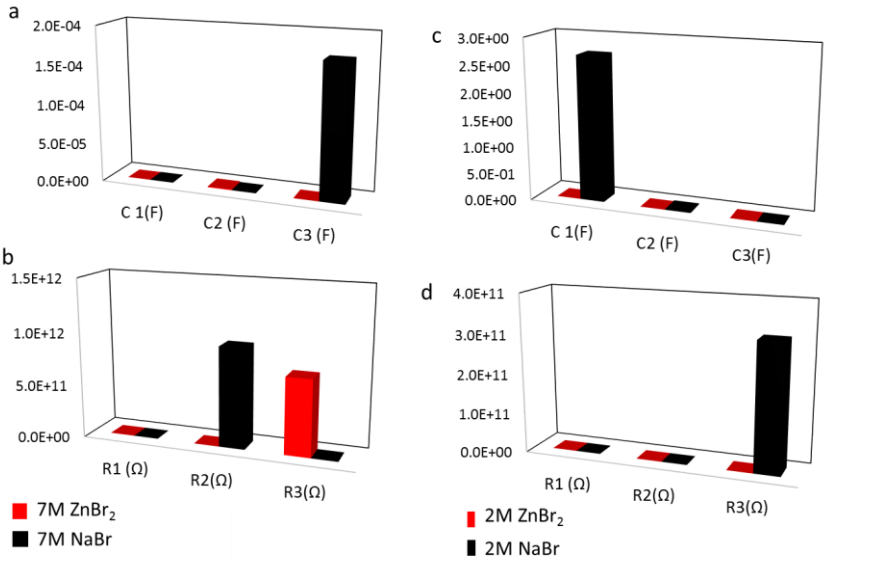

Figure 2.10 *Fitted circuit values at 1.5V of a) capacitors in 7M ZnBr2 and 7M NaBr b) Resistors in 7M ZnBr2 and 7M NaBr, c) Capacitor in 2M ZnBr2 and 2M NaBr and d) Resistors in 2M ZnBr2 and 2M NaBr*

On the other hand, the capacitors and resistors at a concentration of 2M in $ZnBr_2$ and NaBr (Figure 2.10c and 2.10d) show a different behaviour than at 7M. In Figure 2.10c, the capacitor C1 has a value of 2.68E+00 F in the 2M NaBr which is higher than in 2M $ZnBr_2$ and the capacitors C2 and C3 which have a similar values close to zero for both electrolytes. The resistors indicate that the highest resistance is in the resistor R3 in the 2M NaBr (3.17E+11), which is larger than in 2M $ZnBr_2$ (4.03E+03). The difference in capacitors and resistors is possible related to effect in the previous recorded cyclic voltammetry of 2M $ZnBr_2$ and 2M NaBr (See Figure 2.3 and 2.4) which

shows a difference in the Br- oxidation current density. Our results suggest that the capacitors and resistors changes at different potentials may have a correlation in the outcome of the current density in the Br^- oxidation reaction at the graphite electrode. However, note that the presented approach is only used to determine the presence of capacitors and resistors in the fitted circuit. In order to determinate the precise reaction that is ruling the Br^- oxidation it is necessary to use other in-situ spectrometric methods. Nevertheless, in order to test that our data has a mathematical validity, the fitted circuit was tested using the KK transform test [68].

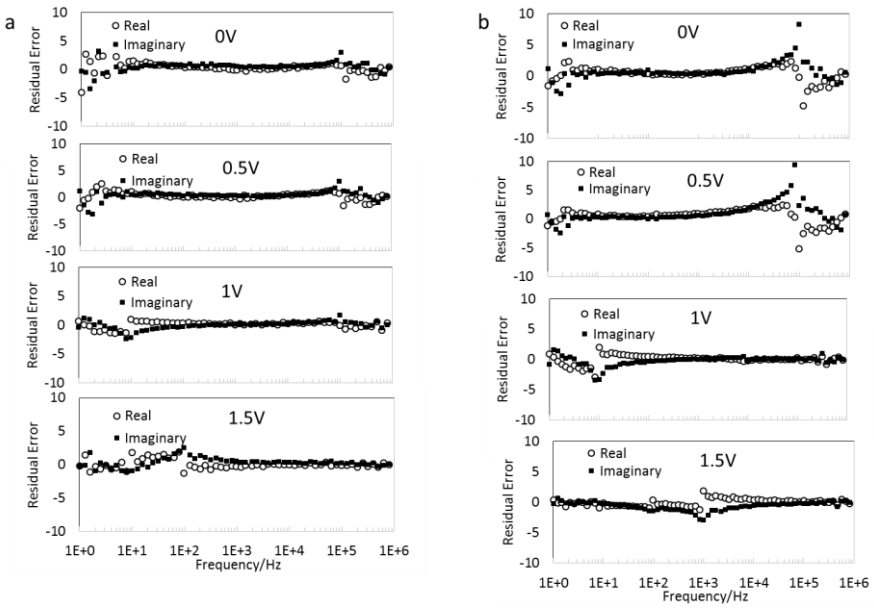

Figure 2.11 *KK transform analysis for experimental data of impedance measurements of Graphite electrode in a) 7M ZnBr and b) 7M NaBr*

2.3.4 Data reliability

In order to validate the modelled circuit a KK transform test was used with the method described by Boukamp [68]. The method gives a mathematical connection between the real part and imaginary part of a valid impedance spectrum. Figure 2.11 presents the results of the KK transform test for the impedance of a graphite electrode in 7M NaBr and 7M $ZnBr_2$. The test shows that the data can be transformed according to the KK theory thus confirming that the data has a certain degree of reliability. As described before, the capacitors and the resistors presented in this study are based on fitting and their actual presence in the reaction are not ascertained. However, based on the low frequency spectra it is possible to observe the presence of capacitors.

This could imply that the processes are slow. Also, the analysis of the residual error shows that the values stay in the range between 0 to 5%, thus supporting the presence of the capacitive structures in the reaction.

2.3.5 UV Vis analysis of charge experiments for Bromide oxidation

After observing the difference between the Br- oxidation reaction at a graphite electrode in different concentrations of $ZnBr_2$ and NaBr, an experiment was set up to test these differences in more detail. For this, the electrolytes were later analysed using UV Vis spectrophotometry. The spectrometry test is performed to observe the change in the electrolyte once the Br- oxidation reaction has occurred.

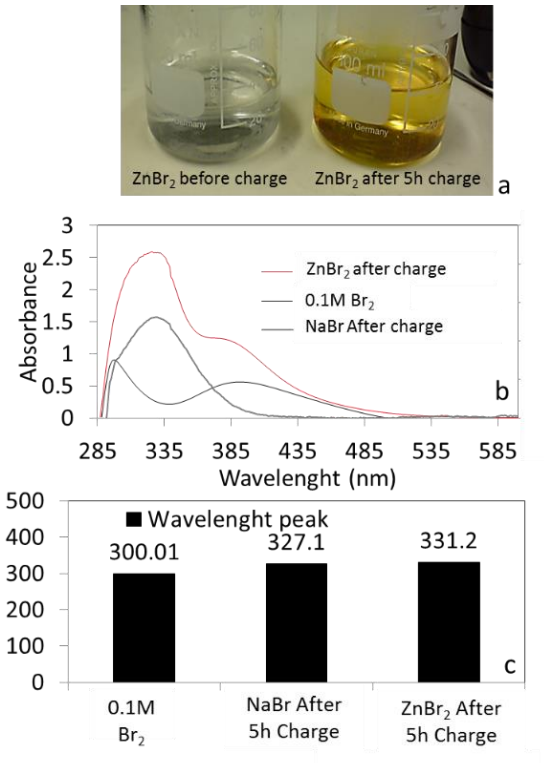

***Figure 2.12**.a) Picture 1M $ZnBr_2$ aqueous solution before charge and after 5h charge at 5 mA cm^{-2} b) UV Vis spectrophotometry of 1M $ZnBr_2$, 1M NaBr aqueous solution charge at 5 mA cm^{-2} for 5 hours and 0.1M Br_2. c)Peak wavelength of Br_2, Charged $ZnBr_2$, and Charged NaBr.*

The experiment was set up as follows: two different cells were built using two electrodes of graphite of 20cm^2. The graphite electrodes were immersed in a electrochemical cell with a solution of 20ml of 1M $ZnBr_2$ for the first

experiment and a new cell was built with 20ml 1M NaBr. Then, the graphite electrodes were connected as negative and positive electrode to a constant current power supply. A 100mA constant current source was used until a constant potential of 1.9V was observed. The electrolytes were in the cell with the described conditions for 5 hours. An example of the resulting electrolytes is shown in Figure 2.12a. Here the electrolyte changes to a light yellow colour after the experiment, which is characteristic for the Br^- oxidation reaction.

Moreover, UV Vis spectrophotometry was used to study the resulting electrolytes after the experiment finished. The $ZnBr_2$ and the NaBr were compared against pure Br_2 to observe the peak absorbance. Figure 2.12b shows the UV Vis spectra results. The experiment was recorded from 190nm to 1100nm wavelength. The Br_2 shows two wavelength peaks one at 287nm and one at 386nm. These peaks have been reported before by a few authors (see e.g Bell [85]). In his study, Bell reported the wavelengths at 285nm and 390nm. These values are close to the one measured in this study.

In the case of $ZnBr_2$ also two wavelengths peaks are observed one at 310nm and one at 386, however the second peak is less pronounced than the first wavelength peak. On the other hand the NaBr electrolyte shows one wavelength peak at 310nm. These results suggest that there is a difference in the UV Vis spectra between the Br_2, the $ZnBr_2$ and the NaBr electrolytes. Furthermore, the first wavelength peak at which Br_2 is observed (300 nm) was lower than the one produced electrochemically ($ZnBr_2$ 331nm-NaBr 327nm). Furthermore, the second wavelength peak has a different shape in the Br_2 than in the $ZnBr_2$ electrolyte. Although, both wavelengths peaks are present at close wavelength peaks and in the case of the NaBr the second wavelength peak was not present. In conclusion the UV Vis spectra showed that the Br^- oxidation in aqueous solution differs considerably between pure halogen (Br_2), NaBr and $ZnBr_2$.

2.5 Conclusions

The results with cyclic voltammetry indicated fairly large differences in current density between different halide salts, concentrations, cation type and pH. When comparing the absolute values of the tested aqueous solutions, it was observed current densities higher than 300mA cm^{-2} were observed at relative low electrode potentials (1.5V or 1.7 were no hydrogen evolution is observed). These high current densities suggest a large capacity to accept electrons. Moreover, oxidation kinetics with NaBr solutions were much higher than with $ZnBr_2$ at 7M while no large differences were observed at 2M. This may be related to the effect that positive ions (Na^+ and Zn^+) may

have an influence in halide oxidation kinetics at the large positive electrode potentials. This indicates that local ionic potential effects affect the oxidation rate of the reaction. Moreover, EIS spectra go in line with this view, as there was a large resistance difference between $ZnBr_2$ and NaBr in the electrolyte phase transfer element. This difference is possibly related to different polybromide formation rates (for the reaction $Br^- \rightarrow Br_x^- + x\ e^-$). Additionally, our results and literature shows that all data may be fitted by one equivalent circuit using the procedure proposed by Baukamp [67] with the fitted circuit and Nyquist plots showing the complexity of the reaction with the presence of different resistors and capacitors. Furthermore, the UV Vis spectra showed that the Br^- oxidation in aqueous solution differs considerably between pure halogen (Br_2), NaBr and $ZnBr_2$. In the case of the Sea-Salt battery, our results indicates that if the halide oxidation reaction is occurring in the battery, this may be a complex reaction that is related to the oxidation of the halide producing a multistep process at the graphite electrode, that needs to be studied more in detail. Nevertheless, the study of the cathode material indicates that the processes are constant and have a large current density which is an indication that the halide battery can be used for a large energy storage which is needed in off-grid houses.

3

Backup Power Glycerol Fuel Cell

Abstract: This chapter presents research on an electrochemical carbon molecule oxidation (i.e. glycerol) that started in the past years as new electrochemical solution for new fuel cells systems. This, in order to use the fuel cell as backup energy supply and long term (seasonal) storage systems in off-grid and on-grid microgrids. In particular, we show the electrochemical feasibility of a suitable cathode material for glycerol oxidation. Thereby the focus is on the use of Au, Zn-Au and Cu-Au electrodes[4].

3.1. Introduction

There is a need of a backup energy supply for periods when there is low production of electricity from renewable sources (e.g. in the night or during winter). In the case of off-grid houses a backup unit is required when the generation and storage are not capable of covering the demand of electricity. Currently the main alternative as backup power in this situation are diesel generators and combined heat and power systems. Both of these technologies work with fossil fuels. Due to the current environmental problems in the world, there is a need for developing new technologies that are better for the environment and close the cradle to cradle loop. In this chapter we consider a new fuel cell based on glycerol. Glycerol is nontoxic

[4] *Large parts of this chapter have been published in [DFQP 3]*

liquid, safe to store at ambient temperatures, low cost and a green energy source. The Glycerol Fuel Cell is a technology that uses glycerol as fuel and its oxidation produces CO_2 and H_2O. The CO_2 present in this type of fuel cells is low due to the high efficiency of conversion (80%-95%).

The growing amount of biodiesel produced worldwide leads to more than two million tons of glycerol entering the market yearly [86]. Glycerol is used in the pharmaceuticals, cosmetics and food industries. However, the current production rate already surpasses the capacities needed by these industries. The countries with high production of biodiesel (e.g USA, Germany and Colombia) are facing serious challenges with the glycerol overproduction reducing the value of glycerol dramatically [87]. This specific situation has led to low glycerol prices, making glycerol a bio-waste product and therefore new alternatives are needed to valorise glycerol. One alternative to valorise glycerol might come from electrochemical oxidation which may produce oxygenated materials with higher market value (tartronic acid, dihydroxyacetone, and glycolic acid, among others) [88]. The electrochemical oxidation of glycerol may be performed using a fuel cell. Fuel cells can directly convert a fuel into electricity [89]. One common fuel used in fuel cells is H_2 and its production is well known in chemical production plants. However, storage of hydrogen is still a challenge due to high volatility and safety concerns [90]. An alternative to the problem is to use a fuel that is liquid under ambient conditions. There are different types of fuels that were tested in the past as possible alternative fuels such as, hydrazine, organic compounds, and formic acid [91–93]. Nevertheless, there are technical and commercial requirements that a fuel must comply with in order to be used in a fuel cell e.g. availability, transport, safety and cost. Taking this into account, the range of possible fuels is reduced to a few types.

Electrochemical oxidation of glycerol has already been considered in the past, and special attention was given towards the selection of catalysts in alkaline and acid media. The following materials have been reported: Pt [94], Pt-Ru [95], Au, Pd [96,97], and Ag [98]. In the case of gold there are several advantages over other catalysts used for glycerol oxidation, e.g. it has a fast electrocatalytic response, it is stable in alkaline media, it is more abundant and it has a lower price than palladium or platinum [99]. Although gold has been studied as a catalyst for glycerol oxidation, the mechanism of the reaction is still far from being understood. E.g. in the study of Ureta [100], the mechanism of alcohol oxidation in alkaline media on a gold electrode was investigated and it is suggested that the optimal oxidation for alcohols is at pH 11. Also, Shi [101] studied the kinetics of low concentration of glycerol in alkaline media using voltammetry on a gold foil. Recently, Qi [102] studied

the generation of tartronade during glycerol oxidation in alkaline media, using an AuC coated electrode. From these studies it was concluded that glycerol oxidation reaction on a gold electrode begins with two primary -OH groups and the chemical reaction possibly decreases the over-oxidation of the secondary -OH and C-C bond cleavage. Also, Chornaja [103] proved that the glycerol oxidation pathways depends probably on the studied catalyst, leading to the formation of intermediate compounds such as tartronic, lactic, glycolic and oxalic ions. Marshall [104], studied the influence of gold nanoparticles loading on an Au/C electrode towards glycerol oxidation showing that the oxidation process is dependent on particle load and size distribution. Kwon [105,106] studied the mechanism of glycerol oxidation on polycrystalline gold and platinum electrodes. Kwon found that the glycerol oxidation is strongly influenced by pH and that no catalytic activity was observed in acid media. Padayachee [107] used electrochemical impedance spectroscopy (EIS) with an Au/MnO_2/Carbon alloy electrode to compare resistances at different potentials. In this study it was determined that the lowest cell resistance is at values of 0V to 0.2V vs Ag/AgCl implying an optimal potential for glycerol oxidation. However, no clear conclusion was drawn for the circuit fitted for the reaction.

In order to build a viable glycerol oxidation technology for a fuel cell, the mechanisms of the chemical reaction have to be studied in more detail to understand the reaction pathways and the kinetics. Also, to make this approach feasible, more studies need to be done towards development and research of stable electrodes with low catalyst load.

This chapter aims to develop an approach for the design of a glycerol fuel cell by observing the glycerol oxidation mechanisms and kinetics using a gold electrode in alkaline media. Next to that, it aims to compare the electrochemical behaviour of gold coated metals prepared in situ (Zn-Au and Cu-Au) in order to reduce the gold load used for glycerol oxidation and for practical implementation. The practical application is related to the use of the glycerol fuel cell in microgrids. However, the large-scale application of fuel cells requires a good understanding of the chemical, electrochemical and physical characteristics of the different technologies [108].

This chapter is organized as follows: Section 3.2 shows the experimental methods and the EIS fitting circuit is explained. In Section 3.3 the general approach used in this paper for data interpretation is presented. Section 3.4 shows the experimental results of testing the gold electrode, which is divided in three parts. First, voltammetry is used for comparison of catalysts for glycerol oxidation (Pt, Ag, Au, Cu and glassy carbon). Second, the cyclic voltammetry analysis of cycles and scan rate effect of glycerol oxidation in

alkaline aqueous solution on a gold electrode is shown. And third, the EIS results for the study of the mechanisms of the glycerol oxidation reaction when using the gold electrode. Section 3.5 and 3.6, shows a practical test with the gold coated Zn and Cu electrodes analyzed with cyclic voltammetry and chronoamperometry (cycles and scan rate effect) to observe the glycerol oxidation in alkaline media in comparison with the gold electrode. Lastly, in Section 3.7 conclusions are presented.

3.2 Experimental methods

The reagents: Glycerol ($C_3H_8O_3$)≥98%, H_2SO_4 ACS reagent, 37%, $AuBr_2$ reagent ≥ 99% and NaOH reagent grade ≥98%, pellets were purchased from Sigma-Aldrich [69] were used with no further purification.

The equipment: Cyclic voltammetry-chronoamperometry experiments were performed with a PGSTAT 101 compact unit from the company Metrohm Autolab [70]. The pH and temperature were recorded with a Hanna HI 9811-5 pH meter [71]. Impedance spectroscopy was performed with a Model 600E Series Electrochemical Analyzer from the company CH instruments [72].

The EIS analysis: EIS analysis was done with the EIS fitting procedure in which the elements are analyzed with the software method EQUIVCRT developed by Boukamp [67,73,74]. This method provides information on the kinetics of the reaction and are validated by a linear Kronig-Kramers transform test method developed by the same author [68]. In this paper, a circuit fitting test in Simulink-Matlab for a view of AC signal output is used, to validate the fitted circuit.

The Electrochemical set up: A three electrode ensemble was used for this study. Various working electrodes were used: Glassy carbon (GC), Au, Ag and Pt (Autolab electrodes) and metals such as Zn, Cu and carbon graphite (CG) 98% grade materials from Sigma-Aldrich. The counter electrode was carbon graphite and the reference electrode Ag/AgCl. The electrode ensemble was immersed in a 50ml aqueous electrolyte.

Electrochemical coating: Glassy carbon, Zn, and Cu (area 0.072cm^2) were immersed first in a solution of 1M H_2SO_4 for a few seconds to remove impurities, then rinsed with demi-water and dried for an hour. Each of the electrodes was immersed separately in an electrochemical cell with 0.01M $AuBr_2$ as the electrolyte. $AuBr_2$ was selected for electroplating as the sub-products of the electrodeposition are more environmentally friendly than common gold cyanate electrodeposition [109]. The cathode material used was carbon graphite and no reference electrode was used. Then, a potential of 2.0V was fixed (letting the current free) in the cell for 30 sec in order to

develop a layer of gold as witnessed by a change in colour on the electrode. During the experiment, any smell of bromine was not detected. After the electrode plating method, the electrodes were rinsed with demi-water and dried during the night.

3.3 General Approach

An ideal fuel cell system may be interpreted by means of cyclic voltammetry, taking anode and cathode reactions separated. If the two reactions are combined in one plot they may be depicted as shown in Figure 3.1. In a good glycerol fuel cell, glycerol is oxidized at the anode, and the current density, therefore, should start to rise at a potential as negative as possible (e.g -0.6V).

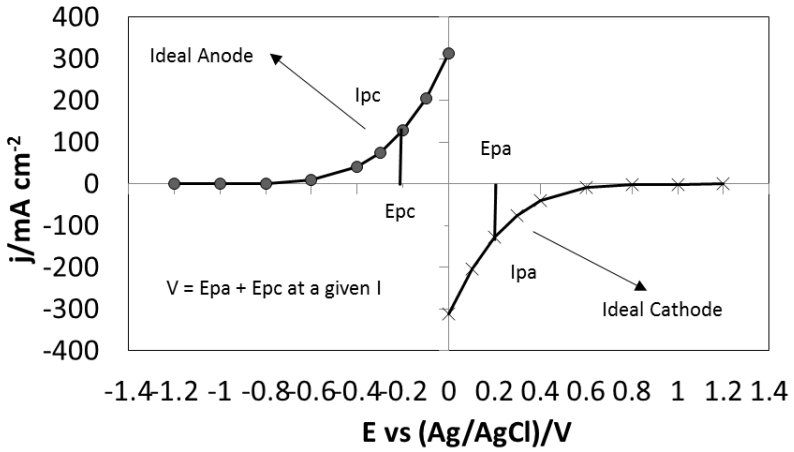

Figure 3.1 *Illustration of an ideal cyclic voltammetry of a fuel cell system with reactions occurring at the cathode and anode electrode*

The value of this potential is generally determined by the catalyst, side reactions, and cell resistance. Meanwhile, at the cathode oxygen is reduced and the current density should start to increase at a potential as positive as possible (e.g. -0.2 V). The max potential of the system is provided by the difference in the glycerol oxidation and oxygen reduction potentials (Epa + Epc) and the current by the steady state rates of this reactions at the anode and at the cathode respectively. This is possible by taking into account the lowest possible ohmic resistance, which is determined by cell geometry, impurities and reaction kinetics. Ideally the glycerol fuel cell has the following chemical reactions on the cathode and anode electrodes:

Anode reaction $C_3H_8O_3 + O_2 \rightarrow CO_2 + H_2O$
Cathode reaction $O_2 + 2H_2O + 4e^- \rightarrow 4OH^-$

Here, in the anode side glycerol is oxidase in presence of oxygen given carbon dioxide and water as products. On the other hand the cathode reaction is the oxygen reduction reaction (ORR) which has been study in detail before for used in other types of fuel cells [110,111]. This research focuses on analysing gold as an anode electrode for glycerol oxidation and its possible use in a fuel cell and the ORR system is not studied. As literature showed that gold is a relative good electrode, low corrosion and stable at different pH [112]. Consequently, we looked for the lowest ohmic resistances and low cost substrates for gold coating.

3.4 Results and discussion

Analysis of catalyst for glycerol oxidation

In order to gain insight into the glycerol oxidation, cyclic voltammetry is used on the different catalysts as shown in Figure 3.2. The goal was to get a comparison of the electrochemistry of different catalysts in the same electrolyte. The measurements were done at 100mV/s in 1M glycerol in 1M NaOH.

The voltammogram for the catalytic effect of Pt for glycerol oxidation in alkaline media in the potential window of -0.6V to 1V vs Ag/AgCl is shown in Figure 3.2a. The first peak (-0.3V and 10mA cm^{-2}) corresponds to Pt reduction and the second peak corresponds to glycerol oxidation (around 0.1V and 5mA cm^{-2}) in accordance with research reported by Akinbayowa [95]. The Figures 3.2b and 3.2c show the voltammetry of a silver and glassy carbon electrode for glycerol oxidation in alkaline media respectively. Clearly, silver and a glassy carbon have less catalytic effect for glycerol oxidation which is in-line with research performed by Song [113]. The voltammetry for the copper show three current density peaks at different potentials at -0.3V,-0.1V and 0.1V vs Ag/AgCl (Figure 3.2d). The first two current density peaks (from left to right) might correspond to copper oxidation in different states (Cu^{3+} to Cu and Cu^{2+} to Cu) as studied by Rozali [114]. The third peak may be interpreted as a glycerol oxidation. However, it may also be related to corrosion as explained in literature [115].

The glycerol oxidation in alkaline aqueous solution on gold is shown in Figure 3.2e, where two current density peaks at -0.2V and -0.1V potential are observed. The first peak corresponds to a typical sudden increase in

oxidation upon reducing gold from its oxidized state in alkaline media. The second peak corresponds to the glycerol oxidation which is presented in the literature by different authors [96–104].

In general, the catalytic activity for glycerol oxidation is observed with Pt, Cu, and Au electrodes. However, for the Ag and GC electrodes, no clear evidence of glycerol oxidation is observed, when comparing the current densities of the different metals at a potential of -0.2V. The results show that the gold electrode has the highest value (11mA cm^{-2}) followed by copper (8mA cm^{-2}) and the platinum electrode has the lowest current density (4mA cm^{-2}). Based on these observations. We focused on the catalytic activity of gold and gold coated Zn and Cu electrodes for glycerol oxidation, as further reported below.

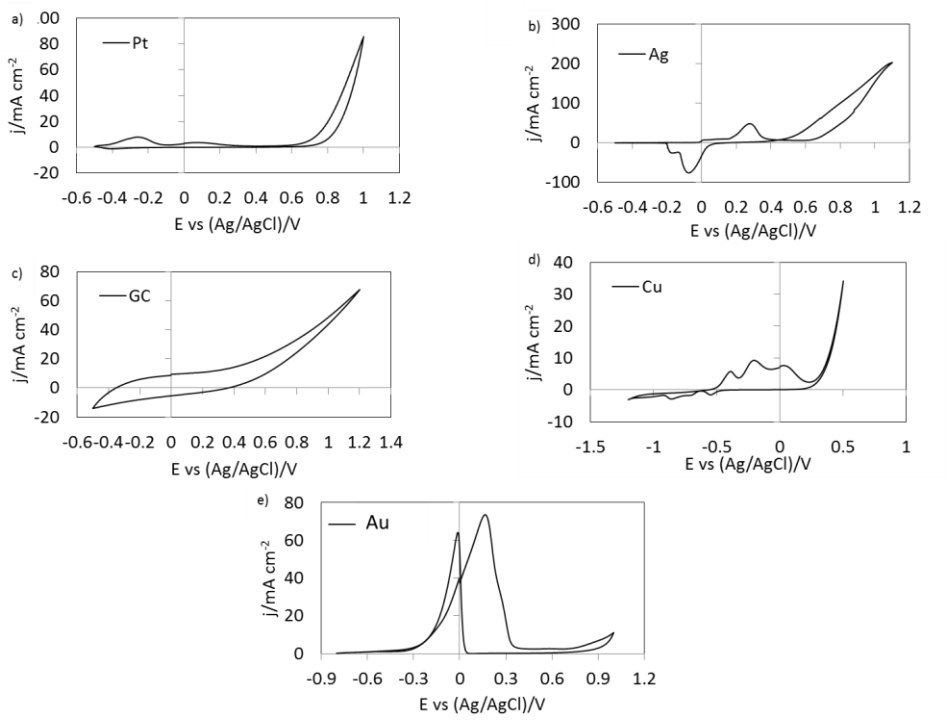

Figure 3.2 *Cyclic voltammetry of a) Pt, b) Ag, c) GC, d) Cu and e) Au electrode on 1M $C_3H_8O_3$+1M NaOH electrolyte, 100mV/s and Ag/AgCl reference electrode.*

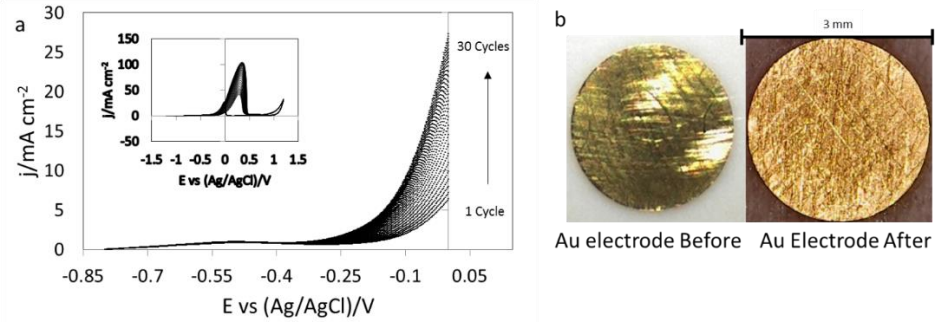

Figure 3.3 *Cyclic voltammetry at an Au electrode on 1M $C_3H_8O_3$+1M NaOH electrolyte, 100mV/s and Ag/AgCl reference electrode, a) Glycerol oxidation region between -0.85V and 0V showing 30 cycles and b) Au electrode before and after the experiment.*

Au electrode kinetics

Figure 3.3a shows repeated voltammetry cycling (30 cycles) in the potential window between -0.85V to 0V vs Ag/AgCl at Au electrode in 1M glycerol + 1M NaOH. After each cycle, an increase in current density is observed. This increase in current density may be related to changes in the surface of the electrode. The change in the surface was observed before and after the cycling experiment in Figure 3.3b. Each cycle may have an effect on the electrode surface, which could affect the catalytic area for the oxidation reaction, thus increasing the current density during the experiment. The changes in the current density are related also to losses in the faradic activity (a short-duration interrupted current). Glycerol oxidation is affected by the increase in the surface area, as the glycerol ions approaching the electrode interact with the surface. Furthermore, the prolonged oxidation process will create larger spaces on the electrode. The current started to increase at around -0.25V and the steady increase continues until all glycerol near the surface of the electrode has been oxidized.

To understand more about the kinetics of the glycerol oxidation in alkaline media at the gold electrode, the influence of the scan rate is studied in Figure 3.4. The current density gradually increased with the scan rates. The correlation between the scan rate and the current density at -0.15V vs Ag/AgCl was linear at a scan rate coefficient of 1/5 (I vs $v^{1/5}$) and not at 1/2 a coefficient (Figure 3.4b). Other scan rate coefficients were tested but no linearity was observed. This possibly suggests that the glycerol oxidation on

gold electrode is not totally controlled by diffusion and does not follow Levich behaviour. Also, with the increase of the scan rate the potential was negatively shifted. The varied potential may represent an alteration in the gold surface due to the interaction with glycerol and OH ions [116]. However, no clear evidence was observed in the voltammogram for the formation of oxidase compounds. EIS studies could elucidate details about the mechanism of the glycerol oxidation at the gold electrode and find close related oxidized compounds.

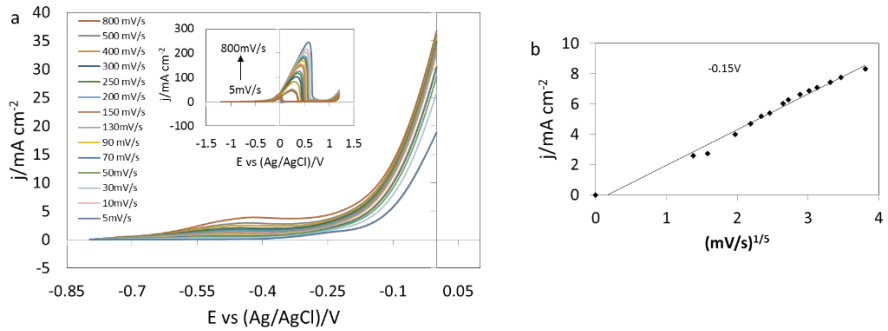

Figure 3.4 *a) Cyclic voltammetry, scan rate effect of an Au electrode spectra between -0.8 and 0V b) Current density at -0.15V in relation with the scan rate (I vs $v^{1/5}$) All experiments used 1M $C_3H_8O_3$+1M NaOH electrolyte and Ag/AgCl reference electrode.*

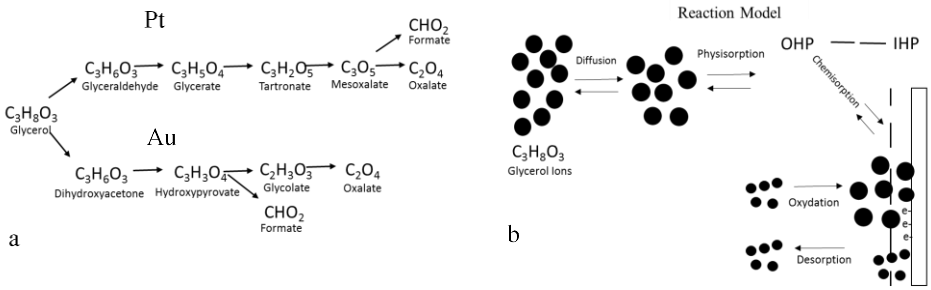

Figure 3.5 *Reaction representation of glycerol oxidation in alkaline media a) Pt and Au catalyst chemical oxidation pathways*[94] *b) Reaction model for glycerol oxidation in alkaline media on Au electrode, based on data taking from literature.*

Au electrode mechanism for glycerol oxidation in alkaline media and EIS analysis

EIS analysis was performed in different steps: first, a plausible reaction pathway was taken from literature and a possible reaction model was created. Second, an expected circuit was drawn based on the assumption of the model for the reaction. Third, the circuit was compared with the lab results using the EQUIVCRT software and fourth the fitted circuits were analysed with the Kramers-Kroning transform and AC Simulink-Matlab circuit signal output to validate the data obtained.

Reaction pathways: Wang [94], explained that glycerol oxidation in an alkaline aqueous solution has two pathways depending on the catalyst. The first reaction path was derived for Pt in which, glyceric acid is the main glycerol oxidation product with tartronic, lactic, glycolic and oxalic acids as by-products (Figure 3.5a). Glycolic and oxalic acids are formed during the oxidation of tartronic acid. In the same study, it was shown that the reaction products of tartronic acid oxidation with dioxygen in the presence of the 5.7 % Pt–2.4 % Bi/C catalyst are mesoxalic and oxalic acids. However, the formation of glycolic acid was not detected. For the glycerol oxidation on a 1 % Au/C catalyst, the authors found that there is another pathway for the reaction in which glycolate and oxalate ions may be created only by the presence of hydroxypyrovate (with the intermediate dihydroxyacetone).

One plausible explanation for the two glycerol oxidation paths is the behaviour of the glycerol molecule in an aqueous solution as shown in literature [117]. It is assumed that glycerol oxidation will take place where the electron goes towards the electrode. In an aqueous solution, this happens at the electrode-electrolyte interface. This can be considered as a characteristic of a surface phase, in which there is an electric field, which is caused by the separation of charges that are in the bulk phases in contact, depending on the catalyst the rate of the reaction may be different and this can contribute to the different paths observed with the different catalysts.

Expected circuit: By using the glycerol oxidation reaction pathway for gold (Figure 3.5a), an equivalent circuit was derived. Under the assumption that each reaction step maybe represented by a sub electrical element. First, we considered the chemical reaction that is shown in Figure 3.5b in which diffusion is followed by physisorption in the outer Helmholtz plane (OHP). Chemisorption processes are presented in parallel to the double layer capacitance in the inner Helmholtz plane (IHP) and various species are captured close to the electrode (oxidation-desorption steps).

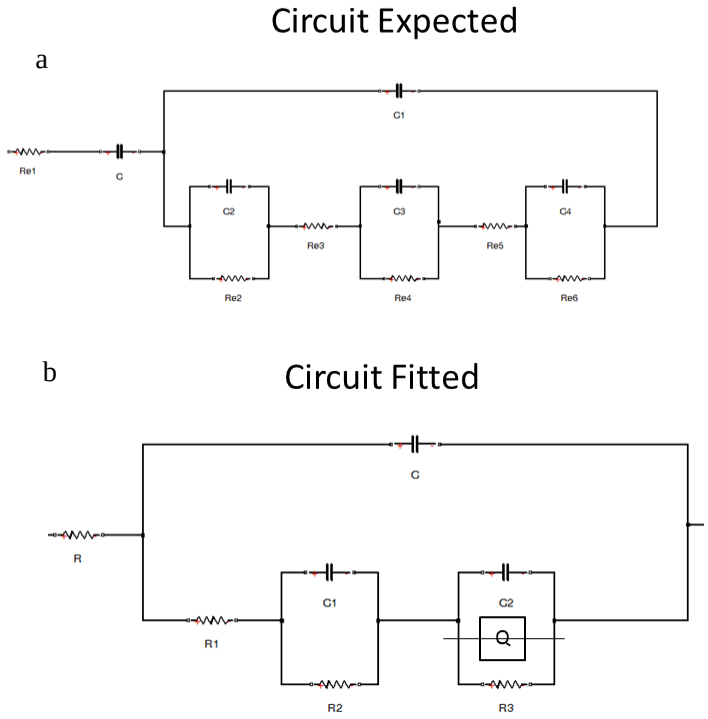

Figure 3.6 *Equivalent circuits for the glycerol oxidation in alkaline media at an Au electrode a) Circuit expected for EIS fitting from data in literature and b) Circuit fitted with EIS software EQUIVCRT*

The concept of a diffusion effect at the beginning of the reaction is related to faradic currents that could occur. This assumption is based on the formation of a thinner Nernst diffusion layer, or with a smaller similar contribution of the absorbed species that are in the overall electrode impedance. The parallel connections in the circuit are associated with the resistances provided by the reactions that occur during physisorption and chemisorption which are related to the oxidation and desorption of ions.

Fitted circuit: The fitting of the circuit was based on the assumption that one particular circuit may fit (or mimic) all data that was found in the impedance measurements. The impedance data was collected at three different potentials -0.25V,-0.15V and -0.05V vs Ag/AgCl that are in relation with the voltammetry of gold for glycerol oxidation.

After testing over 20 circuits in the software EQUIVCRT developed by Boukamp [67], one circuit seemed to fit well the potentials studied for the glycerol oxidation in alkaline media at the gold electrode (Figure 3.6b). All

spectra had an X^2 value below 10^{-4}, but although these X^2 values are large, the circuit mimics reasonably the presented data and is in line with our comprehension of the reaction. Therefore the fitted results were further analysed. In principal, some of the resistance and the diffusion element are merged. This might be due to the low influence on the frequency studied or due to extreme low noise in the system. A diffusion element (Warburg) is observed in the circuit in parallel with the double layer capacitance, and it is treated as a CPE (constant phase element (Q)) with a value of n = 0.5 with a capacitor and a resistor in parallel.

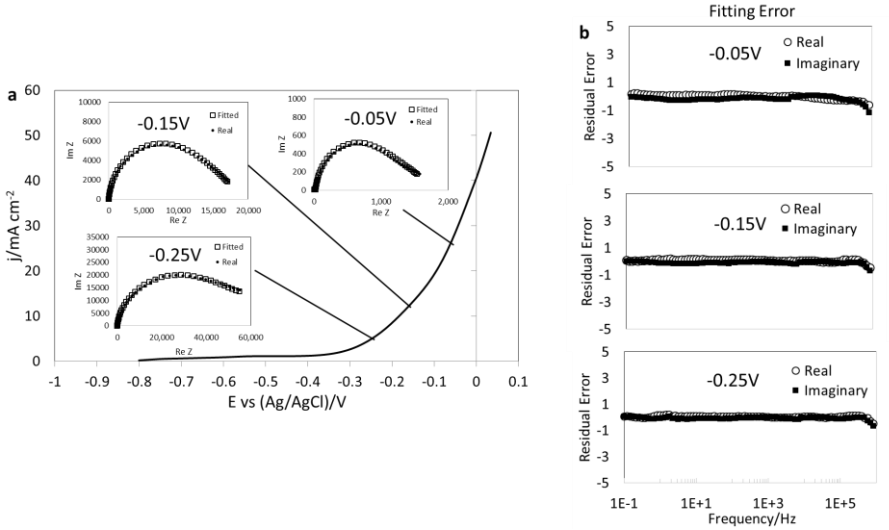

Figure 3.7 *a) Impedance spectra real (*) and fitted data(□) at different negative potentials together with the steady-state current from Au CV experiments on 1M $C_3H_8O_3$+1M NaOH electrolyte 100mV/s and an Ag/AgCl reference electrode.b) fitted (*) and real (□) equivalent circuit frequency error.*

Table 3. 1 *Values obtained for the circuit fitted for the Impedance spectra of 1M $C_3H_8O_3$+1M NaOH*

V (V)	R (Ω)	C (F)	R1(Ω)	R2(Ω)	C1	R3(Ω)	Q (F)	n	C3 (F)	X^2
-0.05	3.81E+00	6.51E-08	1.66E+01	4.08E+02	3.23E-04	1.36E+03	5.65E-05	4.34E-01	2.09E-06	4.83E-04
-0.15	3.68E+00	7.36E-08	1.69E+01	1.20E+02	2.22E-04	1.95E+04	1.08E-05	4.02E-01	1.40E-06	1.45E-04
-0.25	3.54E+00	7.97E-08	1.61E+01	2.14E+04	1.62E-04	6.05E+04	4.74E-06	4.78E-01	1.31E-06	1.17E-04

Spectra analysis

The impedance plot at different potentials (-0.05V, -0.15V and -0.25V vs Ag/AgCl) plotted with the real and fitted values, in the voltammetry region for the oxidation of glycerol in alkaline media with the gold electrode are

shown in Figure 3.7a. The lowest resistance is observed in the EIS experiment for the potential of -0.05V vs Ag/AgCl which was also related to the largest current in the reaction voltammogram (30mA cm^{-2}) when compared with the other analysed potentials.

In order to verify the reliability of the data, the relative residuals are plotted in Figure 3.7b. The data were obtained by Equation (3.1):

$$\Delta_{re,i} = (X_{re,i} - X_{re}(w_i)) / |X(w_i)| \text{ and}$$

$$\Delta_{re,i} = (X_{im,i} - X_{im}(w_i)) / |X(w_i)| \quad (3.1)$$

Here, $X_{re,i}$ and $X_{im,i}$ are the real and imaginary parts of the impedance at a data point (i) and $X_{re}(w_i)$, $X_{im}(w_i)$ are the real and imaginary parts of the modelling function for w_i. The $|X(w_i)|$ is the vector length expressed in the absolute value of the modelling function. The residuals show a trend that is close to values between 0 - 1% for the error in the data fitting, showing that data in the fitting correlation has a low error percentage in all the applied potentials.

Table 3.1 shows the values of the elements collected from the fitted circuit (resistors, capacitors, and Q element). With the change of potential the fitted elements change proportionally. The first resistance (R) reduces as the potential is reduced from -0.25V to -0.05V. The first capacitor (C) represents the double layer capacitance, which is approximately the same at all the potentials. Together with the resistance in parallel (R1) that is connected to the second set of resistances-capacitor that are in series (R2C1 and R3C2). In all the cases Q has an n value of closely to 0.5 indicating the possible presence of the Warburg element.

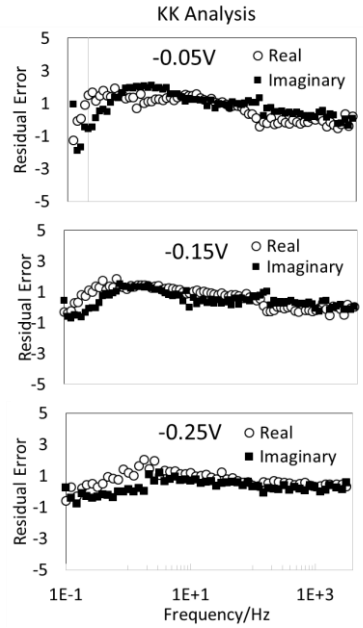

Figure 3.8 *K-K transform analysis for experimental data of impedance measurements of Au electrode in 1M $C_3H_8O_3$+1M NaOH and Ag/AgCl reference electrode.*

Data reliability

In order to validate the modelled circuit the K-K transform can be used. The method has been described by Boukamp [68]. Figure 3.8 shows the data that was transformed according to K-K theory. It confirms that the calculated magnitudes match the experimental magnitudes, thus we can have some confidence in the data. The capacitors and the resistors presented in this studied are based on fitting and their actual presence in the reaction are not ascertained. However, based on the low-frequency spectra it is possible to observe the presence of capacitors. This could imply that the processes are slow. Also, the analysis of the residual error supports the theory of the presence of capacitive structures in the reaction. Furthermore, in order to validate the data further Simulink-Matlab was used, and the resulting Simulink circuit fitting is shown in Figure 3.9. The fitted circuit is connected in series with regular AC circuit elements available in the Simulink package and the output of the system is given by the scope unit. The signal from the circuit indicates that the circuit has a logical frequency output, and it may be used as an electronic system.

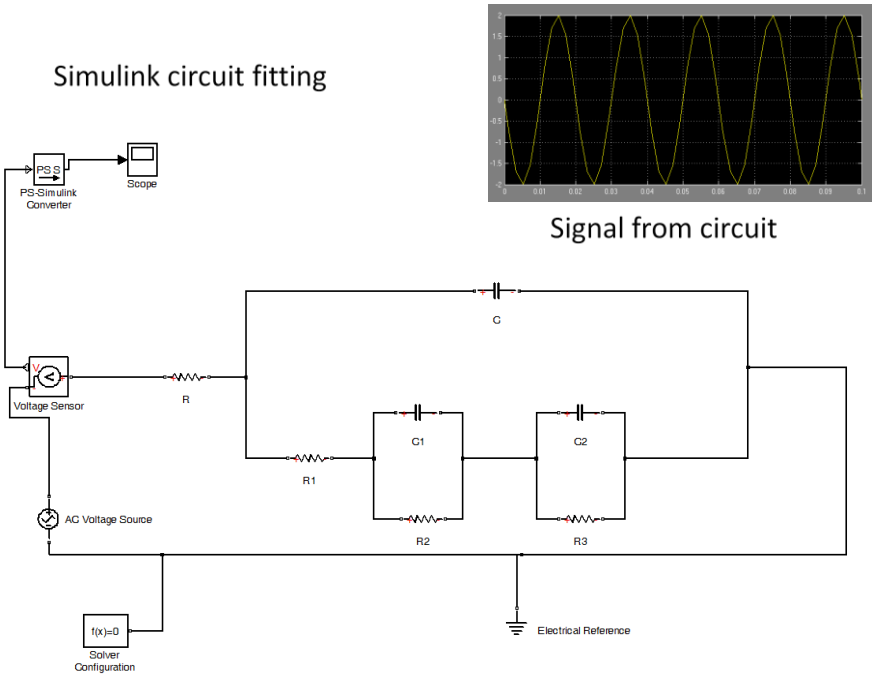

Figure 3.9 *Simulink-Matlab test with AC signal output for the circuit fitted for glycerol oxidation in alkaline media on a gold electrode.*

3.5 Gold coated metals proof of concept

Although the analysis with the gold electrode showed good results for glycerol oxidation in alkaline media, current densities and potentials are still low for a realistic scenario in a fuel cell construction. In order to offer an alternative for the gold electrode, this section presents first, a gold coating method for glassy carbon and the voltammetry test which is compared with gold in alkaline and in acid media to observe the changes in current density and potential in a 1M glycerol aqueous solution. Second, two gold coated metals are tested (Zn-Au and a Cu-Au) in order to compare their electrochemical behaviour against pure gold.

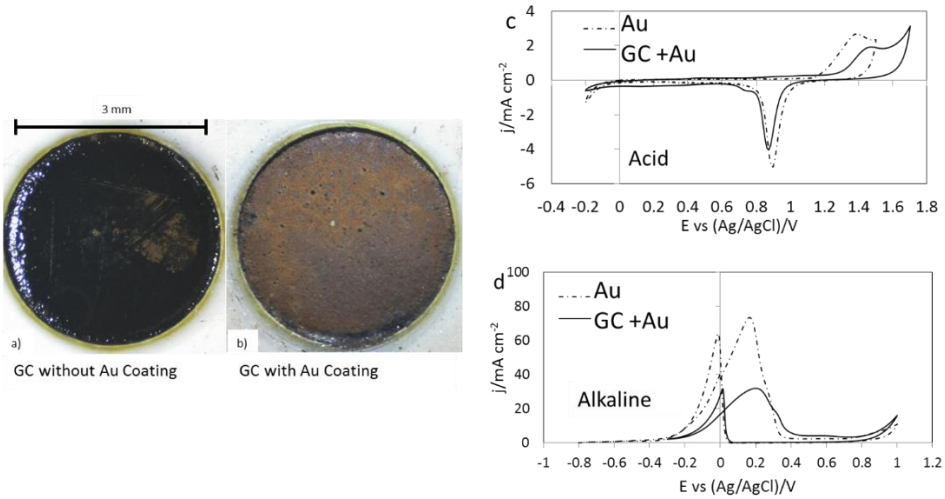

Figure 3.10 *a) GC electrode without Au coating, b) GC electrode with Au coating and cyclic voltammetry of gold electrode and GC-Au electrode on c) Acid media (1M $C_3H_8O_3$ +1M H_2SO_4), d) Alkaline media (1M $C_3H_8O_3$ +1M NaOH). Both at 100mV/s and Ag/AgCl reference electrode.*

Gold Coating effect

Glassy carbon (GC) was used as material to deposit gold with the method described in Section 3.2. The used GC electrode without gold is shown in Figure 3.10a. A clear layer of gold was deposited (Figure 3.10b). The gold deposition corresponds to the classical electrochemical-nucleation phenomenon in which the gold ions are traveling through the electrolyte in a diffusion control behaviour [118]. After the electrode was prepared, two cyclic voltammograms were measured one with glycerol in acidic media (Figure 3.10c) and one with glycerol in alkaline media (Figure 3.10d). Both voltammograms were compared with the gold electrode.

The CV of GC-Au electrode and of the gold electrode in acid media is shown in Figure 3.10c. When the potential increases in the positive direction of the scan first a current density peak was observed, possibly, corresponding to gold oxidation. Then the potential changed and the gold reduction current density peak was observed. This behaviour is typical for a gold electrode in acid media [99]. In both the GC-Au and the gold electrode, cathodic and anodic current density peaks were observed. This is an indication that gold was present on the GC electrode showing similar behaviour as the gold electrode. However, no clear evidence of glycerol oxidation during the experiment was observed. Also, the GC-Au showed lower current densities than the gold electrode. The reasons for this may be related to the size of the

gold layer, the GC-Au stability and possibly intrinsic resistances between the materials [119].

Figure 3.10d shows the CV of gold and GC-Au electrodes in 1M glycerol in 1M NaOH. It was observed that the GC-Au electrode has a similar behaviour than the gold electrode showing two current density peaks, (one for the gold reduction at approximately 0V and one for glycerol oxidation at approximately 0.2V vs Ag/AgCl). The comparison showed that similar voltammograms may be achieved by using the gold coating method. However, lower current densities were observed when using GC electrode as a substrate for gold deposition in comparison with the gold electrode.

In both acid and alkaline media, the CV behaviour of the gold electrode was observed when using GC-Au electrode. Furthermore, it may be concluded that using GC as a substrate material for gold plating has an effect on the current density, potential, and the capacitive plateau during voltammetry. This effect may be due to the electrochemical nature of GC, which may affect the normal behaviour of the gold electrode for glycerol oxidation [100]. Similar observations were done by Othman[120], in which an Au-PVC electrode was used for glycerol oxidation and it was observed that the gold coated material can mimic the electrochemical behaviour of gold.

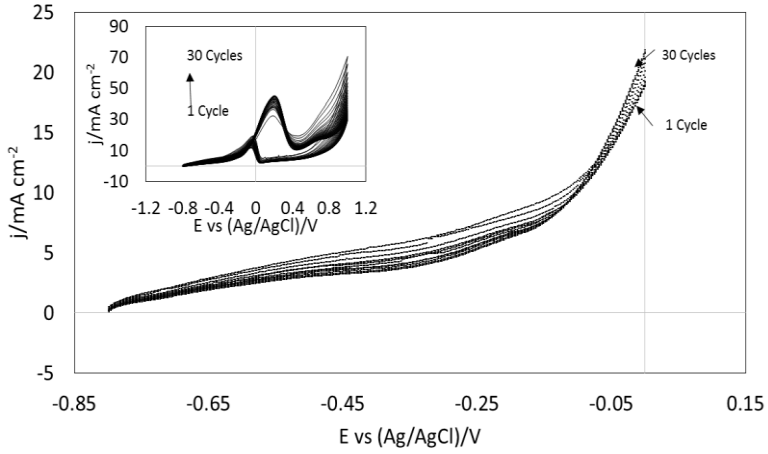

Figure 3.11 *Cyclic voltammetry cycles effect at Zn-Au electrode on 1M $C_3H_8O_3$+1M NaOH electrolyte, 100mV/s and Ag/AgCl reference electrode.*

The Zn-Au electrode

Based on the observations done with the GC electrode, it is plausible that changing the substrate material for gold electrodeposition may affect the

current density and potential in the voltammetry of glycerol in alkaline media. A Zn-Au electrode was prepared using the same procedure as for the GC-Au electrode. The electrode was checked visually before and after been in the aqueous solution of $AuBr_2$ and a change in colour on the surface of the zinc electrode was observed. the change may be related to zinc oxidation [121] and also to a displacement of zinc ions for gold ions [122]. In order to observe if gold is presented on the surface of the zinc electrode voltammetry was used. The effect of cyclic voltammetry cycling is presented in Figure 3.11 where thirty cycles are shown at a scan rate of 100mV/s. The shape of the voltammetry is similar to the gold electrode implying, that a gold layer was created on the surface of the zinc electrode and that possibly glycerol oxidation may be achieved similarly than with gold. After each cycle in the voltammetry, the current density increased, having a similar effect than for the GC-Au electrode. This observation also suggests that the Zn-Au electrode has a layer of gold tick enough to continue the glycerol oxidation during each cycle.

To understand more about the kinetics of the glycerol oxidation in alkaline media at a Zn-Au electrode, the influence of the scan rate is studied in Figure 3.12. Similarly to the GC-Au electrode, the current density gradually increased with the scan rates. The correlation between the scan rate and the current density at -0.15V is linear at a scan rate coefficient of 1/5 (I vs $v^{1/5}$) and not linear at 1/2 (Figure 3.12b). Other exponential coefficients were tested but no linearity was observed. This observation may suggest that the glycerol oxidation using the Zn-Au electrode is not totally controlled by diffusion, as in the case with the GC-Au electrode. Also, with the increase of scan rate the potential is negatively shifted. The varied potential may represent both an alteration in the Zn-Au surface due to the interaction with glycerol and OH^- ions [116], and the interaction between gold and zinc that shifted the potential to negative values. This is possibly related to the negative electrochemical potential of zinc and possible side reaction of zinc in alkaline media forming zinc oxide and zinc hydroxide both with larger negative potential than zinc as shown in Equation (3.2). However, the actual presence of these reactions was not characterized in detail in this study.

Reaction	E°/V	
$Au^{2+} + e - \rightleftharpoons Au$	+ 1.8	
$Zn^{2+} + 2\ e \rightleftharpoons Zn$	–0.7618	
$Zn(OH)_4^{2-} + 2\ e \rightleftharpoons Zn + 4\ OH^-$	–1.199	
$Zn(OH)_2 + 2\ e \rightleftharpoons Zn + 2\ OH^-$	–1.249	
$ZnO + H_2O + 2\ e \rightleftharpoons Zn + 2\ OH^-$	–1.260	(3.2)

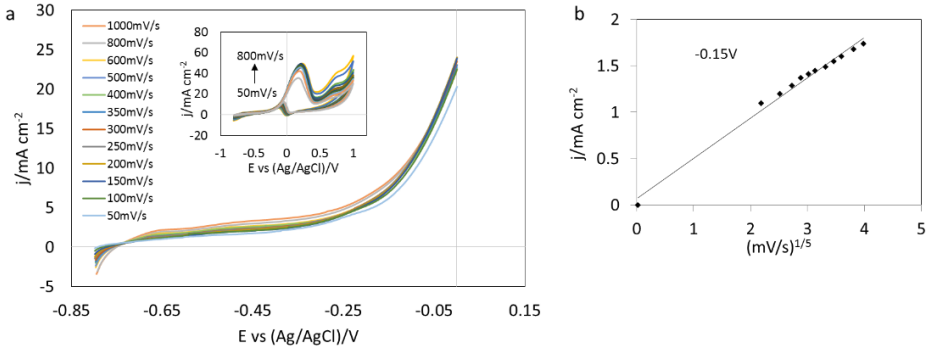

Figure 3.12 *a) Scan rate effect on Cyclic Voltammetry of Zn-Au electrode b) Current density at -0.15V relation with scan rate (I vs $v^{1/5}$), on 1M $C_3H_8O_3$+1M NaOH electrolyte and Ag/AgCl reference electrode.*

The Cu-Au electrode

The Cu-Au electrode was studied using the same conditions as for the GC-Au electrode and the Zn-Au electrode. The electrode was checked visually before and after being in the aqueous solution of $AuBr_2$ we observed that the colour on the surface of the copper electrode changed. The change may be possibly related to copper oxidation [123]. Also, it may result from displacement of copper ions for the more noble gold ions [122]. The effect of cyclic voltammetry cycling is presented in Figure 3.13. The shape of the voltammetry is similar to the gold electrode the GC-Au and Zn-Au electrode, showing that a gold layer was created on the surface of the copper and that similar shape can be observed in the voltammetry of glycerol oxidation as compared with the Au electrode. After each cycle in the voltammetry, the current density increased similarly to the GC-Au and the Zn-Au electrodes. This observation also suggests that the Cu-Au electrode had enough gold to continue the constant cycling.

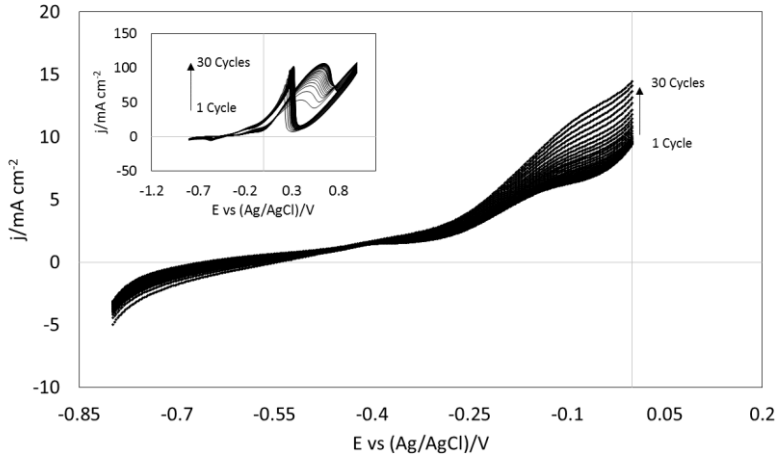

Figure 3.13 *Cyclic voltammetry cycles effect at Cu-Au electrode on 1M $C_3H_8O_3$+1M NaOH electrolyte, 100mV/s and Ag/AgCl reference electrode*

The influence of the scan rate is shown in Figure 3.14. It can be seen that the current density gradually increased with the scan rates. The correlation between the scan rate and the current density was measured at a potential of -0.15V vs Ag/AgCl and it was found to be linear at a scan rate coefficient of 1/5 (I vs $v^{1/5}$) and not at 1/2 (Figure 3.14c). These observations suggest that the glycerol oxidation at a Cu-Au electrode is not totally controlled by diffusion. Also, with the increase of scan rate the potential is negatively shifted similarly to the Zn-Au electrode. The varied potential possibly represents both an alteration in the copper-gold surface due to the interaction with glycerol and OH^- ions produced during the voltammetry [116]. The voltammetry of the Cu-Au electrode shows a change in the voltammetry shape towards more negative potential. This may be explained by the electrochemical potential of copper and other copper ions in alkaline solution (copper oxide and copper hydroxide) which are more negative than for gold in an alkaline solution. (Equation 3.3).

Reaction	E°/V	
$Au^{2+} + e - \rightleftharpoons Au$	+ 1.8	
$Cu_2O + H_2O + 2\ e \rightleftharpoons 2\ Cu + 2\ OH^-$	–0.360	
$Cu(OH)_2 + 2\ e \rightleftharpoons Cu + 2\ OH^-$	–0.222	(3.3)

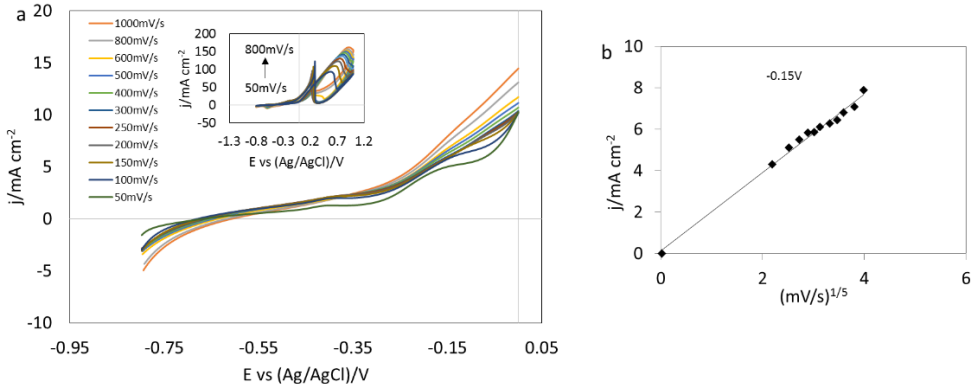

Figure 3.14. *a) Scan rate effect on Cyclic Voltammetry of Cu-Au electrode b) Current density at -0.15V in relation with scan rate (I vs $v^{1/5}$), on 1M $C_3H_8O_3$+1M NaOH electrolyte and Ag-AgCl reference electrode.*

3.6 Comparison of Au, Zn-Au and Cu-Au electrode

The behaviour of Au, Zn-Au, and Cu-Au electrodes is compared in Figure 3.15a. The comparison has been done using the ideal plot for an anode material in a glycerol fuel cell (Figure 3.1), using the region between -0.8V and 0 in the cyclic voltammetry for glycerol oxidation in alkaline aqueous solution. Both Zn-Au and Cu-Au have similar behaviour than the Au electrode in a solution of 1M glycerol and 1M NaOH at 100mV/s. When analysing the current densities at a potential of -0.15V (Figure 3.15b), the largest current density observed is from the Zn-Au electrode with a value of 7mA cm^{-2}.The lowest current density observed is from the Au electrode with 0.7mA cm^{-2} at a potential of -0.45V. For all the electrodes studied the current density decreases while the potential goes to negative values. This behaviour is lower in the Zn-Au electrode and the Cu-Au electrode when compared with the Au electrode. The experiment showed that changing the metal for gold deposition may have an effect on current density and potential and that Zn-Au and Cu-Au electrodes are possible materials to be used for glycerol oxidation in alkaline media.

Table 3.2 *Comparison of different catalyst for glycerol oxidation from literature with the present study*

		Experimental conditions			
Catalyst	Supported material	Temperature C°	pH	Main electrolyte	Observations
Pt	MCN (mesoporous carbon nitrides) [94]	60	Neutral	0.3M Glycerol	There is a decrease of catalytic activity after reusing of the catalyst also the experiments were performed in a base free environment.
Pt-Ru	MWCNT (multi-walled carbon nanotubes) [95]	20-90	Alkaline	0.7M Glycerol+ 2M KOH	Superior catalytic activity than Pd -MWCNT
Pd	MWCNT (multi-walled carbon nanotubes)[95]	20-90	Alkaline	0.7M Glycerol+ 2M KOH	It is observed higher current densities at temperatures of 80 Co
	CCE (Carbon ceramic electrode)[96]	25	Alkaline	0.5m Glycerol+ 0.3m NaOH	The concentration of NaOH influences the current density of glycerol oxidation
Au	Carbon [102,124]	50-60	Alkaline	0.1M Glycerol + 0.1 NaOH + 0.1M Tartronic Acid	The added tartronate improved the glycerol oxidation due to selectivity of Au for tartronate ions at high temperature
	MnO_2-Carbon [107]	60	Alkaline	0.5M Glycerol + 1M KOH	MnO_2 gave support for gold nanoparticles and better electrode stability
This research					
Au	Au	23	Alkaline	1M Glycerol + 1M NaOH	High catalytic activity
	GC				Similar catalytic activity than gold
	Zn				Higher current densities are observed and potentially shifted to negative values
	Cu				Higher current densities are observed and potentially shifted to negative values

Table 3.2 shows a list of different catalyst for glycerol oxidation compared with the catalyst used in our research. The experimental conditions show that different electrolyte compositions are used for the study of the glycerol oxidation. Furthermore, the comparison of the performance of the catalyst has not been studied in detail to our knowledge. E.g. the Pt, and Pd catalyst have different alkaline media (NaOH or KOH), temperature and pH. Nevertheless, the analysis of different authors suggest that the glycerol oxidation is a complex reaction that is influenced by physical, chemical and electrochemical conditions and finding the right set of characteristics is still a challenge to research.

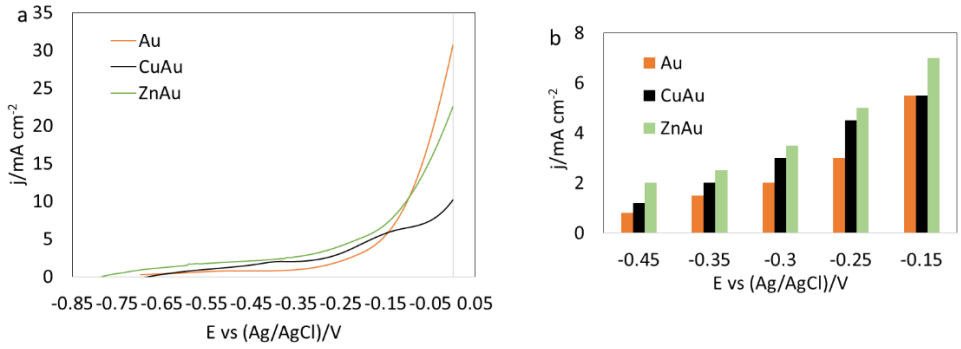

Figure 3.15 *Cyclic voltammetry of Au, Zn-Au, and Cu-Au in 1M $C_3H_8O_3$+1M NaOH electrolyte, 100mV/s and Ag-AgCl reference electrode. a) Zoom in voltammetry area between -0.8V to 0V and b) Comparison of negative potentials with current density.*

3.7 Proof of concept: Chronoamperometry discharge analysis

A prototype system was built to observe the discharge performance of the anode electrodes studied in this paper. Copper and zinc foils of 20cm^2 with electrodeposit gold were used as anodes for glycerol oxidation using the process described in Section 3.2. The cathode was carbon graphite for the oxygen reduction reaction. The graphical representation of the cell is shown in Figure 3.16a. The two materials were immersed in a solution of 1M glycerol and 1M NaOH. Two different potentials were tested for 900 seconds in each cell (-0.05V and -0.15V), the values were selected based on the results of EIS and CV analysis, taking into account the lowest resistance observed. The results are shown in Figure 3.16. Overall, it is observed that when the load potential is increased the current density decreases. In the case of the gold cell (Figure 3.16b), at -0.05V the current density average discharge is equal to 0.07mA cm^{-2} and at -0.15V is equal to 0.01mA cm^{-2}. In the case of the Zn-Au electrode (Figure 3.16c), the current density changes from 1.5mA cm^{-2} (at -0.05V) to 1mA cm^{-2} (at -0.15V) and for the Cu-Au electrode (Figure 3.16d) the average current density is 3mA cm^{-2} (at -0.05V) and 1.5mA cm^{-2} (at -0.15V).

The difference between the current densities of the cells is possibly related to resistance that can be created between the electrodes. In the three cells tested gold was observed to have the lowest current output at the given potentials, followed by Zn-Au and the highest current density was observed in the Cu-Au electrode. However, in the case of Cu-Au at the end of the last discharge, a double line is observed, indicating conductivity problems with the cell, this could be due to surface changes in the electrode after the discharge and possible surface oxidation (Cu_2O and/or $Cu(OH)_2$). Further

experimentation needs to be done in order to determine the exact maximum capacity of the electrode and the gold bonding. Figure 3.16e shows the analysis of a three electrode fuel cell connected in series, the test was performed using different current densities in order to observe the discharge potential response and the stability of the cathode electrode for a period of 300s. While the current density increases the potential of the cell reduces constantly. At 0 mA cm^{-2}, the voltage of the cell is stable at 0.7V. However, the potential changes during the time when no load is applied. This behaviour suggests that the stability of the carbon electrode is changing during the 300s experiment.

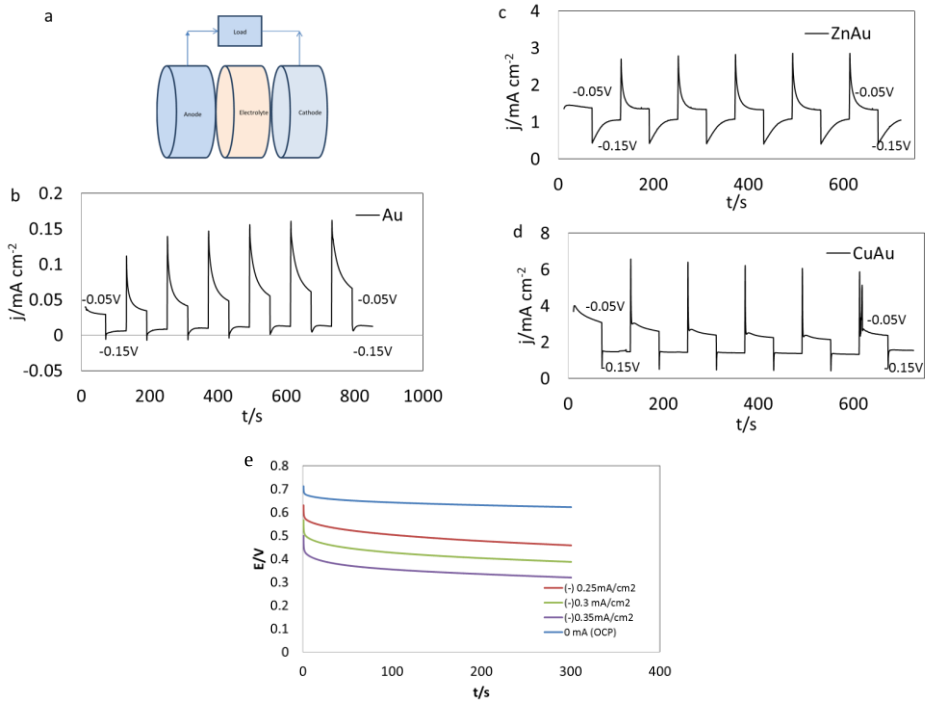

Figure 3.16 *Discharge chronoamperometry at -0.05V and -0.15V using Carbon graphite as a cathode electrode, $C_3H_8O_3$+1M NaOH electrolyte and a) representation of the fuel cell b) Au electrode c) Zn-Au electrode, d) Cu-Au electrode and e) Discharge potential curve of a three series connected cells with carbon graphite as cathode electrode*

3.8 Conclusions

Our analysis shows that gold has the highest current density for glycerol oxidation in alkaline media when compared with another catalysts at a

potential of -0.2V (Pt, Ag, GC and Cu). It is further observed that the gold surface can change in cyclic voltammetry. The current density shows linear behaviour with the scan rate at an exponential value of 1/5. One equivalent circuit fitted the data well at potentials of -0.05V,-0.15V and -0.25V vs Ag/AgCl, with resistors and a Warburg element in parallel with the double layer capacitance. The resistors and the capacitors are related to the possible presence of hydroxypyrovate and oxalate ions. Our results were consistent with the low-frequency error fitting analysis (10^{-4}). The AC Simulink-Matlab fitting responds and the Kronig-Kramers transform test. The Zn-Au and the Cu-Au electrodes showed voltammetry behaviour similar to the gold electrode in cyclic voltammetry at the different scan rates. The discharge chronoamperometry test showed that the Zn-Au and Cu-Au electrode had higher current densities than the gold electrode at a potential of -0.25V vs Ag/AgCl (5 mA cm^{-2}, 4.5mA $cm^{-2,}$ and 3mA cm^{-2} respectively). Au, Zn-Au, and Cu-Au are possible candidates for glycerol oxidation technologies and the gold coated metals are possibly suitable electrodes for building a fuel cell. In this study, the air electrodes used in the fuel cell test had limited instability. In future work, we may address stable air electrodes for our glycerol fuel cell approach. Upon success in prototyping, we aim to use fuel cells as backup systems in microgrids or as an alternative to replace diesel generators in some situations, although more R&D is needed to confirm this insight. Furthermore, simulations are needed to investigate how these fuel cells ma behave in such scenarios. This is a topic of ongoing research ion our group.

4

Sizing of Electricity Storage for an Off-Grid Wastewater System

Abstract: In this chapter we investigate how to supply a specific off-grid device with energy. More specific, we consider a decentralized wastewater treatment plant (DWWTP). For this device a constant energy supply is crucial in order to guarantee its functionality and to prevent contamination of rivers and thereby human illnesses due to pollution. However, power blackouts are a common problem in rural areas can affect the reliability of wastewater treatment plants. This chapter presents a study of how to size solar photovoltaics, Sea-Salt batteries and Glycerol Fuel Cells for powering a DWWTP working in 100% off-grid mode. The analysis is performed for two different DWWTPs, a prototype MBR and a Bever III compact wastewater aerobic system[5].

4.1. Introduction

Decentralized wastewater treatment plants (DWWTP) are intended to treat wastewater before it is discharged back into natural watercourses when a centralized solution is not suitable. Such plants are specifically suitable for rural areas. The DWWTPs are usually a recommendable alternative for sanitation in settlements which can range between one to a hundred houses. However, in rural areas electricity blackouts are more common than in cities, especially in developing countries. This situation is often due to the unreliability of the existing power grid. In literature a few cases are reported

[5]*Large parts of this chapter have been published in [DFQP 4]*

and explained in detail for countries such as India [125], Zambia [126], Tanzania [127], and Colombia [128] among others. These studies all report that electricity supply is unreliable in rural areas and causes problems for the development, implementation, and control of technologies that protect people and the environment. For instance, in the case of Colombia, the country has been increasing the sanitation coverage of wastewater treatment plants in the last years. Nevertheless, the selected solutions are mostly centralized systems for large communities. Even after the wastewater treatment systems are implemented, the rapid growth and poor planning make these technologies insufficient for treating the large wastewater flows and the organic loads that are generated in the cities. This can be observed by heavily polluted rivers near highly populated areas around cities like Bogota, Medellin, and Cali [129].

To stay at the example of Colombia, rural areas here have lower coverage of wastewater treatment plants compared to large cities. The National Statistics Department of Colombia (DANE in Spanish) reported that only 17.3% of the rural population in 2016 are treating the waste water before it is discharged in the rivers [130]. Economic and technical aspects are large boundary conditions when implementing a DWWTP. Therefore, often alternative solutions like the installation of conventional septic tanks are implemented. However, this technology is not capable of achieving the removal of solids and organic matter required to protect the rivers and aquifers from pollution [131]. A low cost, low foot print, and simple to implement DWWTP may be a good and possible alternative for houses in rural areas with untreated or partly treated wastewater. However, a DWWTP requires electricity to power mechanical pumps, blowers, and electrical parts for its normal operation. A possible solution to warrant the constant supply of electricity for a DWWTP could come from creating a 100% off-grid solution based on renewable energies.

In literature attempts have been reported to create off-grid, self-sufficient DWWTPs that are powered by renewable energy using technologies such as hydropower [132], wind turbines [133] , biomass [134], microbial fuel cells [135] and solar PV [136]. However, the implementation of these technologies as the only source of electricity for a DWWTP is still a challenge for large scale implementation. E.g Gu [137] researched the feasibility of implementing self-sufficient wastewater systems and Schäfer [138] investigated the available flexibility of the electricity supply of wastewater treatment plants. These studies concluded that the implementation of self-sufficient wastewater treatment systems is in principal possible but more

analysis on technologies, simulations and methods to warrant their reliable behaviour need to be done in order to prevent environmental concerns.

In this chapter, we investigate whether a combination of solar PV and Sea-Salt batteries is able to provide electrical power to a DWWTP for a whole year. We use a distributed energy management methodology (DEM) developed by our research group in the Netherlands for smart grids to model energy flows [44,139]. Specifically, we analysed the energy consumption of two innovative DWWTPs implemented in two cities in the Netherlands (a compact wastewater treatment system (commercial name Bever III) and a prototype membrane bioreactor (MBR) that can be operated at high biomass concentrations). The electricity consumption and the behaviour of these systems are measured and monitored to observe their electrical behaviour. Based on these results, the size of solar PV and Sea-Salt battery necessary to operate the DWWTPs in a 100% off-grid mode can be determined. This chapter is organized as follows. In the next section, the background information on the two DWWTPs, the considered solar PV system, the Sea-Salt batteries and the DEMKit tool are described. In the following section, the experimental results are presented in two parts: The analysis of the static sizing of solar PV and Sea-Salt batteries followed by the dynamic sizing/characterization of solar PV, the Sea-Salt battery and the Glycerol Fuel Cell to power the DWWTPs. The last section presents the conclusions.

4.2 Background information

The decentralized wastewater treatment plants

The two considered DWWTPs were tested under real conditions for the treatment of domestic wastewater. The goal of this chapter is to model them in a scenario where they can operate entirely on electricity from photovoltaics and batteries. The wastewater treatment units have two main characteristics: first, low foot print for installation and second, high wastewater treatment efficiency. The electricity consumption of both systems was monitored during an operating period of 30 days under real conditions to observe the energy consumption during the day and night. Then, based on the power load for 30 days an estimate of the power consumption profile for a year was extrapolated. Before we come to these outcomes, first the two DWWTPs are described.

a)

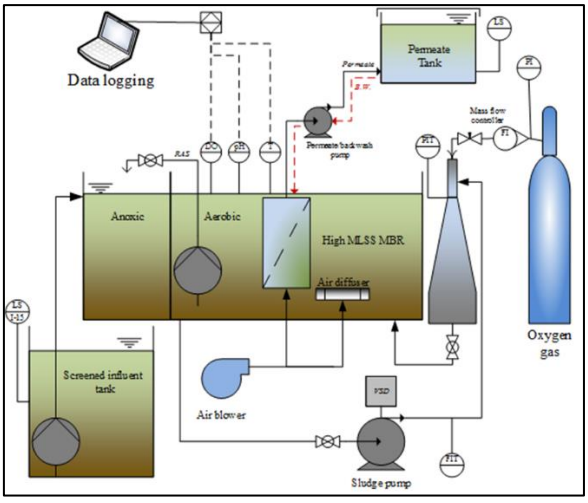

b)

Figure 4.1 *a)Schematic process flow diagram and pictures of installed prototype MBR setup in Delft-the Netherlands b) Decentralized wastewater treatment system Bever III from the company Afmitech in Friesland the Netherlands.*

Prototype MBR:

The innovative MBR system described by Barreto [140] is capable of increasing the treatment capacity of a conventional MBR with high efficiencies. Figure 4.1a shows the setup and some pictures of the prototype MBR. The system was designed to cover the demand of 25 houses. The MBR uses a supersaturated aeration system to provide oxygen at high biomass concentrations, allowing a higher treatment capacity. The system was installed in the Netherlands in the Harnaschpolder wastewater treatment plant in Delft and has been constantly researched during recent years.

Decentralized wastewater treatment system (Bever III)*:* The Bever III is a decentralized wastewater treatment system developed by the company Afmitech Friesland [141]. Figure 4.1b shows the setup of the DWWTP Bever III and some pictures of the installed system. The Bever III was designed for the treatment of wastewater equivalent to 10 houses in the city of Joure in the Netherlands. The Bever III is a compact biological wastewater treatment unit. The system combines the aerobic treatment tank with a settler in one single unit. This system has BOD (biological oxygen demand) and COD (chemical oxygen demand) removal of up to 95%.

Solar PV and the Sea-Salt Battery:

Solar PV panels of 300W (LG Neon 2 black Cello Design) were used as a main electrical source for the design characterization. The modules have an energy efficiency of up to 18%. The used solar irradiation data was collected from a real case study in Lochem-the Netherlands during the year 2016 [139] and is given with a minute time resolution.

In order to be able to store the electricity from solar PV for usage at periods with low PV generation, a Sea-Salt battery and a Glycerol Fuel Cell was used. More information of the Sea-Salt battery is presented in Chapter 1 and 2 and of the Glycerol Fuel Cell in Chapter 3. In this paper, we used the Sea-Salt battery as an ideal device which can be charged to 90% and discharge until 20% of its full capacity. During the simulation deterioration of the battery is not taken into account.

The DEMKit software:

The DEMKit is a software tool developed at the University of Twente [44]. The goal of the software is to provide a simple way for simulating and evaluating distributed energy management (DEM) technologies. The tool is used in smart grids applications for controlling devices. Note, that many DEM methodologies are used in academia for simulations that are developed

in complex software environments that require various specific tools. The complexity of this system usually hampers the transition from such models to a proof of concept. In contrast to this, the DEMKit is capable of simulate, co-simulate and generate simple demonstrations with real hardware in the loop simulations. The software is developed in Python, this allows users to use this platform with different operating systems. Furthermore, the provided data is stored in an Influx Data Base (InfluxDB) and it can be visualized in Grafana or any other graphic environment.

The system configuration in the DEMKit with the solar PV, Sea-Salt battery, and the DWWTPs is shown in Figure 4.2. All the components in the system provide constant feedback to validate the data and the fleet controller is connected to the controllers for the DWWTP, the battery and solar PV. The data used to study the devices gets collected by the host system and is stored in the data base.

4.3 Results

Table 4.1 shows a standard static calculation for sizing solar PV and batteries for an off-grid scenario of the two DWWTPs. The calculation is performed to power a Bever III and a MBR for wastewater treatment for one year. In order to calculate the total solar PV power production in one day, 3 h/day of sunlight is estimated (this value is based on an average sun light per day in a year in the Netherlands). Based on the numbers presented in Table 4.1, the MBR needs a solar PV of 30.2 kWp and a Sea-Salt battery of 48V and 4.6 kAh. On the other hand, the Bever III needs a Solar PV of 14.4kWp and a Sea-Salt battery of 48V and 2.2 kAh. The calculation is performed only on the basis of the average power that can be harvest using solar PV in a day. No seasonal effects are incorporated in these calculations. In the following, we use these numbers for the PV and battery size as a base to start the simulation.

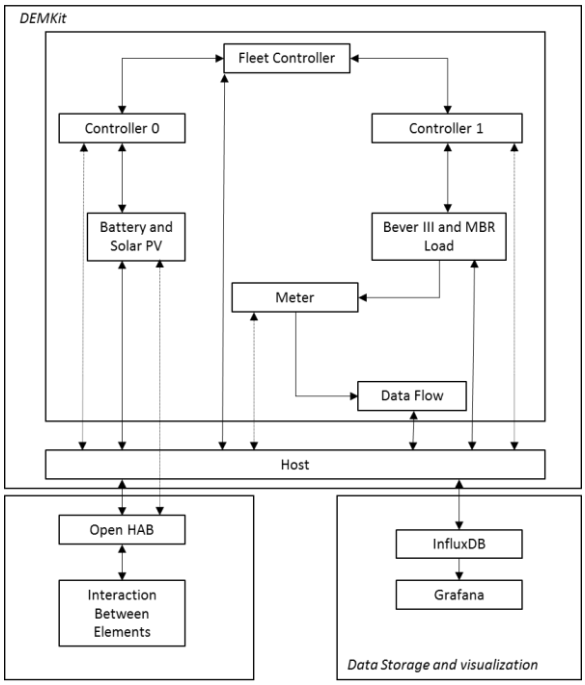

Figure 4.2 *Diagram of the DEMKit platform with a model and external software*

4.4 Performance simulation of Solar PV and the Sea-Salt battery

For the dynamic simulation, the effect of seasons was incorporated. As base the data collected from solar energy during the year 2016 is used with one-minute resolution. As mentioned, the MBR and the Bever III power load was measured for a period of 30 days. This data was extended for one year assuming a constant electricity consumption behaviour of the DWWTPs over the different months.

***Table 4.1**. Solar PV and Sea-Salt battery sizing calculation based on the power consumption of MBR and Bever III.*

SOLAR PV CHARACTERISTICS	Bever III	MBR	Unit
DWWTP Avg. Energy Consumption	1080	2300	kWh/ month
AC/0.85 = DC Correction Factor	1271	2706	kWh/ month
DC Consumption per month	42	90	kWh/ day
DC Consumption per day	42353	90196	Wh/ day
PV Modules			
Power	300		Wp
Solar PV Voltage	32.5		V
Solar PV Current	9		A
Daily avg. Solar Radiation in NL	3		h/ day
Total power produce daily by each PV module	900		Wh/ day
Number of modules needed	48	101	
Possible System Configuration			
Current	18	18	A
Power produce/day	43200	90900	Wh/ day
Modules in Series	24	50	
Modules in Parallel	2	2	

SEA-SALT BATTERY CHARACTERISTICS	Bever III	MBR	
Capacity	2000	2000	Ah
Voltage battery system	48	48	V
Total daily Ah requirements	882	1879	Ah/ day
Recommended reserve time	2	2	days
Percent of usable battery capacity	0.8	0.8	%
Minimum battery capacity	2206	4698	Ah
Batteries in Parallel	2	3	
Batteries in Series	32	32	
Total number of batteries	64	96	
STANDARD BATTERY DIMENSIONS CELL			
Voltage	1.5		V
Capacity	2000		Ah
Length	51.3		cm
With	27.3		cm
High	24.2		cm
Weight	85		kg
Area needed for batteries	89631	134447	cm^2
	9	13	m^2
Total Weight	5440	8160	kg
	5.44	8.16	Tons

Both, the data from the solar PV and the DWWTPs power load are loaded in the DEMKit simulation environment in order to power the DWWTPs when electricity is available from solar PV. The surplus of electricity from the solar PV is stored in an ideal Sea-Salt battery. The battery is charged with the solar energy and discharged during the periods when sunlight is not available or not sufficient to power the DWWTPs. Note that, the used design of the batteries and PV are part of the corresponding static calculations. Figure 4.3 shows the simulation results of the Solar PV and the Sea-Salt battery used to power a DWWTP during the months of June 2016 and November 2016. In the case of the MBR (Figure 4.3a and 4.3b), the results of June 2016 show that the battery state of charge (SOC) is above 20kW during the entire month and the solar PV produced a peak power of 30kWp on the sunniest day (4th of June).

On the other hand, during November 2016 the solar PV generated a peak power of 12kWp on the sunniest day of the month (10th of November) and the Sea-Salt battery is discharged fully during the periods of low sun irradiation, this is noticeable in the periods between the 10th to the 20th and between 24th to the 30th of November. In this month, the solar PV with the Sea-Salt battery is still capable of cover up to 65% of the demand however not the full demand. A similar case is observed for the Bever III (Figure 4.3c and 4.3d). During June 2016 the solar PV has a peak power of 15kWp on the sunniest day (4th of June) and the Sea-Salt battery SOC is above 12kW giving enough electricity to the Bever III during the month of June 2016. However, in November 2016 the solar PV produced a peak value of 7kWp on the sunniest day (10th of November) and the Sea-Salt battery is capable of covering the demand of electricity during almost 75% of the month. In both cases, the MBR and the Bever III are capable to work 100% off-grid in the month of June. However, in the month of November, both systems could power the DWWTPs only for around 70% of their demand.

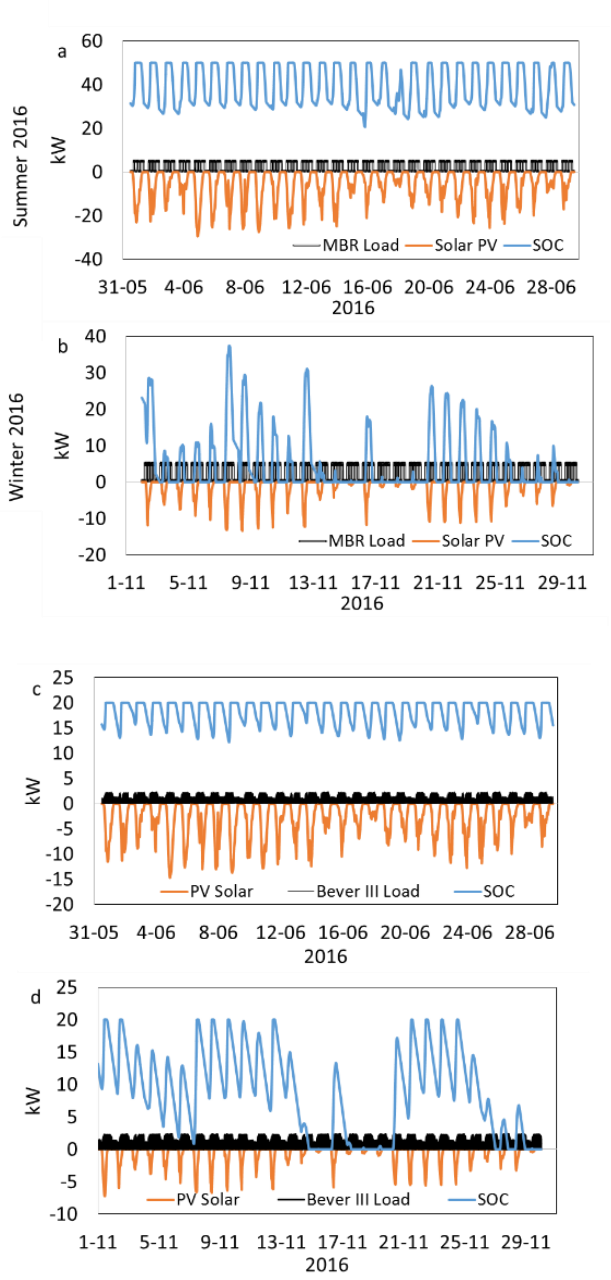

Figure 4.3 *Energy profiles of the DWWTP using solar PV and the Sea-salt battery in a 100% off-grid scenario a)MBR during June 2016 b) MBR during November 2016 c) Bever III during June 2016 and d) Bever III during November 2016.*

In order to achieve a 100% off-grid scenario for the DWWTPs during the month of November, the capacities of the solar PV and Sea-Salt battery were increased until a size of the off-grid system is found, which allows to provide the complete energy requirements over the year. Figure 4.4 shows the simulation results of the oversized energy profiles for the DWWTPs during the months of June and November 2016. As expected during June 2016 the MBR and the Bever III can work without energy shut down. In detail, in the case of MBR (Figure 4.4a), the solar PV shows a peak power of 240kWp on the sunniest day (4th of June) and a Sea-Salt battery with 60kW of electricity reserve during the entire month. In the case of the Bever III, the peak power is 50kWp on the sunniest day (4th of June) with a reserve battery SOC of 25kW (Figure 4.4c). Further, during the month of November 2016, both DWWTPs can be powered during the month in a 100% off grid mode. In detail, the MBR (Figure 4.4b), has a solar PV peak power of 100kWp during the sunniest day (10th of November) and a Sea-Salt battery SOC of 10kW. On the other hand, the Bever III has a peak power of 22kWp and a Sea-Salt battery with minimum SOC of 5kW during the entire month.

The cases considered in Figure 4.3 and 4.4, show that standard sizing of solar PV and battery as shown in Table 4.1 may not warrant a 100% off-grid scenario for DWWTP during a period of a year. Furthermore, simulations and smart power steering of the DWWTP allows to provide a degree of flexibility which leads to a reduction of the size of solar PV and battery. In the future, more research should be performed on cost analysis and alternative technologies to provide the electricity needed during low sunlight periods.

The results in Figure 4.4 indicate that quite some fraction of the battery capacity and the PV generation is just used for a small period of time (mainly during winter). Therefore, it is of interest to look for alternative solutions. One such alternative to create a 100% off-grid DWWTP is using a Solar PV, a Sea-Salt battery and a backup system. For this backup system, we used a Glycerol Fuel Cell which is described in more detail in Chapter 3.

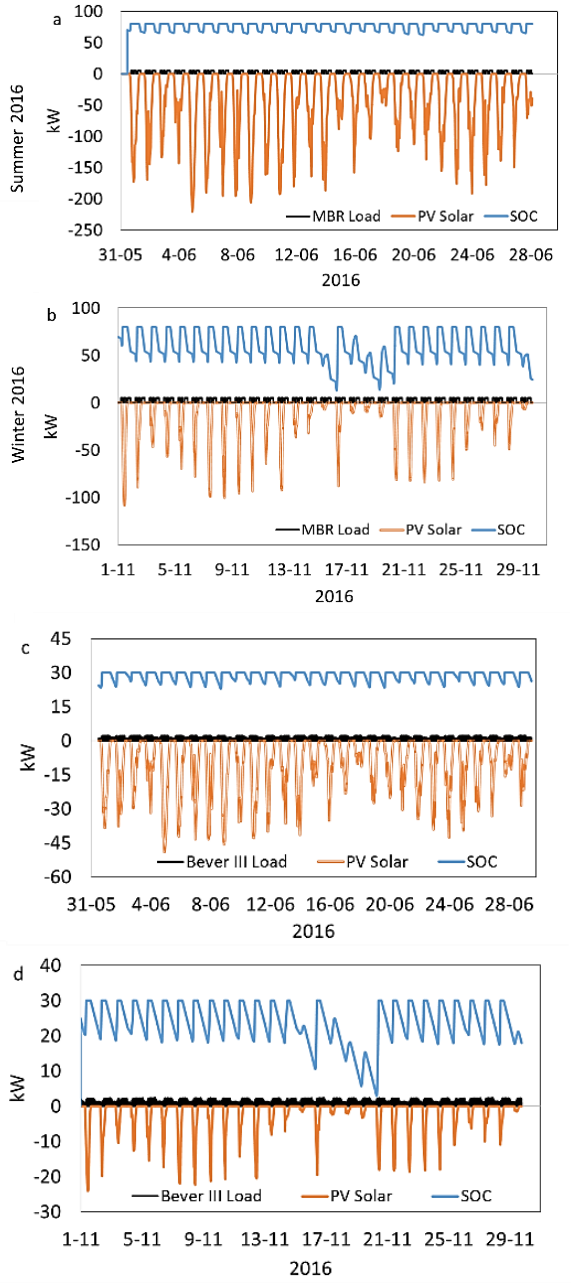

Figure 4.4 *Oversized energy profiles for the DWWTP using solar PV and the Sea-salt battery in a 100% off-grid scenario a)MBR during June 2016 b) MBR during November 2016 c) Bever III during June 2016 and d) Bever III during November 2016*

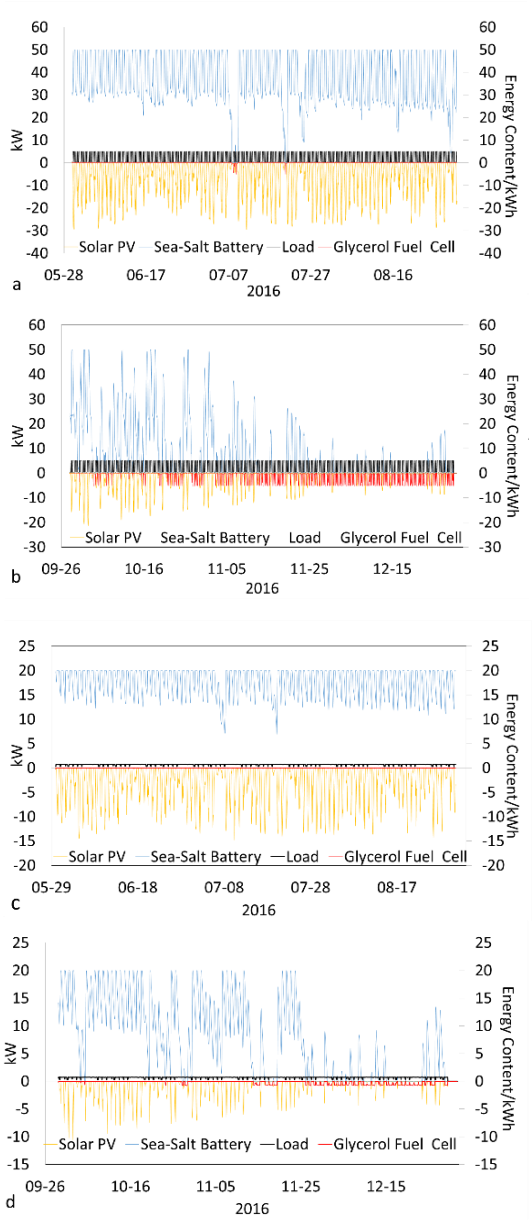

Figure 4.5 *Energy profiles for the DWWTP using solar PV, the Sea-salt battery and the Glycerol Fuel Cell in a 100% off-grid scenario a)MBR during June to August 2016 b) MBR during October to December 2016 c) Bever III during June to August 2016 and d) Bever III during October to December 2016.*

Figure 4.5 shows the energy profiles of the solar PV, Sea-Salt battery and the Glycerol Fuel Cell for the DWWTPs during two periods in 2016. In detail, the Glycerol Fuel Cell is used only when the solar PV and the Sea-Salt battery are not able to provide the electricity needed for the MBR and the Bever III. In the case of the MBR the Glycerol Fuel Cell is not used during the period of June to August of 2016 (see Figure 4.5). Furthermore, the MBR requires a Glycerol Fuel Cell of 6kW during the period between October to December 2016 and the fuel cell is used mostly in the months of November and December (see Figure 4.5b).

On the other hand, the Bever III the solar PV and the Sea-Salt battery can give the electricity necessary throughout almost all the tested time during June to August 2016, except for 2 days in the period (7th of July, 27th of July) (see red line Figure 4.5c). During the period of October to December 2016, the Bever III needs a Glycerol Fuel Cell of 2kW in order to be electrically self-sufficient.

4.5 Conclusion

This chapter shows a method that can be used to determine energy sizing/characterization for powering DWWTPs working in off-grid mode using renewable resources even during the months with low renewable generation. Concretely the results indicate that solar PV and a Sea-Salt battery can provide the energy required for the DWWTPs. However, in order to power the DWWTPs also during the months of low sunlight the dimensions of the solar PV and the Sea-Salt battery needs to be increased by a factor of three compared to the sizes resulting from a static analysis. More precisely, the simulations performed with the DEMKit tool show that a solar PV of 15kWp and a 20kWh Sea-Salt battery may provide 100% of the electricity necessary during the summer and up to 75% during the winter in the Netherlands for the Bever III. In case of the MBR, a PV system of 30kWp and a Sea-salt battery of 50kWh is necessary to provide 100% electricity during the summer and up to 65% during the winter in the Netherlands. In this scenario the deficit in the winter can be covered with a backup technology, such as a Glycerol Fuel Cell. For this we identified that the MBR requires a Glycerol Fuel Cell of 6kW and the Bever III a 2kW to cover the electricity needed for the periods of June to August and from October to December 2016. Notice, that the Glycerol Fuel Cell is mostly used during the periods of low solar PV generation.

5

Sizing of Electricity Storage For an "Off-Grid House"

Abstract: This chapter uses experimental data to estimate the size of storage needed for an islanded off-grid house in two different regions (Austin, Texas, US, and Nunspeet, NL). In our study, an off-grid house is considered to be supplied with 100% renewable energy during the summer period, and a solar photovoltaic (PV) system, the Sea-salt battery, and the Glycerol Fuel Cell are the main electrical energy providers [6].

5.1. Introduction

Power generated from sustainable energy by, e.g., solar photovoltaic (PV) cells, is an ideal option for generating renewable power for houses. However, the technology is constrained by weather conditions that influence renewable energy generation. Due to this variation in energy production, energy-storage technologies (e.g., batteries) are an option worth considering for providing energy at times when it is needed but not supplied by renewable energy [142].

It is expected that, in the future, 100% off-grid houses will be an important and interesting asset in electrical grids [143]. They can achieve two goals: bringing flexibility to the grid and providing electricity to remote places. The

[6] *Large parts of this chapter have been published in [DFQP 1 and 5]*

first goal, if achieved, would entail that a house will only be disconnected from the grid and work in standalone mode during blackouts or maintenance periods [144,145]. This option depends on the reliability of the grid, which has been investigated by various authors. Shivakumar [146] researched the estimation of electricity interruption costs for houses across the European Union (EU). It was found that the difference in cost resulting from interruptions in the electricity grid among EU member states is significant, ranging from 3.2 €/kWh in Bulgaria to 15.8 €/kWh in the Netherlands. The annual average for the value of lost load for the EU was calculated to be 8.7 €/kWh.

In another study, Hanser and Leuken [147] investigated the use of a solar PV system and batteries to create an off-grid house in the US. They concluded that the use of houses as flexible assets in the grid can bring advantages in cases of blackouts. However, a solar PV system coupled with batteries still needs a backup power generator to secure electricity supply. Furthermore, Ardito and Procaccianti [148] researched the current status of smart grids in Europe. They show that the European situation is slowly changing giving the priority to renewable energy with storage. However, the storage technologies still need to be evaluated in detail to be able to provide stable and reliable electricity for houses. From these studies, also was concluded that the reliability of the grid could change in the short term. Furthermore, a 100% off-grid house may also be an important asset for times of high energy demand. In such cases, it is possible that houses can be controlled as flexible assets in the grid (to be disconnected/connected when needed) or as a backup in case of blackouts.

The second possibility for 100% off-grid houses is that they can get access to electricity in remote places that are still not connected to the grid. These cases are more common in developing countries. For example, Khodayar [27] investigated the current trends in microgrid systems for Africa and the impact on cities with low access to electricity. Hirmer and Guthrie [149] researched the benefits of off-grid energy appliances for places with low access to electricity, and Hashemi [150] analyzed a low-income house in the tropical region that could solve the problem of energy shortage in a house in Uganda. These studies support the view that renewable energy coupled with storage is the most likely technology to be implemented for the next years to power houses not connected to the grid. However, the feasibility to implement an off-grid electrical system for houses depends on the reliability of the technology and the local economy. In order to achieve a 100% off-grid house, storage sizing is a crucial step. In the literature, storage sizing methods have been investigated. The focus has been in the development of

algorithms for storage sizing for smart grids [151,152], the economic feasibility of batteries for large scale storage of renewables [153,154], and hybrid renewable energy technologies combined with multiple storage systems [155,156], to name a few. These studies concluded that storage sizing is important in order to ensure 100% off-grid scenarios for houses. Furthermore, it is suggested that further research has to concentrate on showing that battery storage systems are reliable during long periods of constant operation.

With respect to the battery system, a new battery called the Sea-Salt battery [34] has been chosen. This battery has been measured and tested at the University of Twente and will be used in a project sponsored by the Dutch Government. In this project, 24 houses in the province of Gelderland will be equipped with batteries. If the project runs successfully, the Sea-Salt battery may become an important asset for the implementation of 100% off-grid houses. It is claimed that the battery manufacturing cost may be around 100 Euro/kWh and thereby may be lower than lithium-ion (400 Euro/kWh) [157] and comparable to lead-acid batteries (120 Euro/kWh). The first lab test indicates that the Sea-Salt battery may be able to be 100% discharged without damage and that it has a lifetime of at least 7000 cycles. These characteristics of the Sea-Salt battery show that the technology may play a role in the implementation of batteries in houses in the future.

We set out to determine whether the combination of a solar PV system and Sea-Salt battery is able to provide electrical power to a house for a summer period. For this research, we use a distributed energy management methodology (DEMkit) for smart grids developed by the University of Twente [38,158–160]. We focus on two specific cases for which we investigate the energy consumption and the solar PV production. The first house is located in Austin, Texas, US, and the second in Nunspeet, NL. In the case of Austin, the data for electricity consumption and solar PV production were collected from the Pecan Street database center [21] and in the case of Nunspeet, the data was measured locally. This data was then used to specify the electrical behavior of the houses. Based on this data, the size of the Sea-Salt battery necessary to operate in a 100% off-grid mode during the summer was determined.

This chapter is organized as follows. First, some background information is given about the two houses, the considered solar PV system, the Sea-Salt batteries, and the decentralized management methodology (DEMkit). Second, the experimental results are presented into two parts. Firstly, the analysis of the solar PV system and Sea-Salt batteries is given followed by the dynamic sizing/characterization of the solar PV system and the Sea-Salt

battery to power the two different houses. Secondly, we present an approach to test the Sea-Salt battery for off-grid application, in which a real battery is tested under scaled loads. The paper ends with some conclusions.

5.2. Background Information

In this section, the description of the considered houses in Austin and Nunspeet is presented together with an example of the load and solar PV profiles of one day. Afterward, the characteristics of the Sea-Salt battery are given followed by a short description of the used demand side management tool (DEMkit).

5.2.1. House Description

To characterize the electric load of an off-grid house in Texas, data provided by Pecan Street Inc. in Austin (Austin, TX, USA), Texas, was used. This data is part of an ongoing study for smart grids and demonstration studies [21]. The study utilizes a testbed of 300 modern, green-built homes built after 2007, and 160 homes ranging from 10 to 92 years of age. The homes are equipped with electricity, gas, and water metering devices. Of the 300 homes in the study, 185 have rooftop solar PV panels, which are metered separately from the electricity demand. This database has been used in previous smart grid studies [161–165]. In the case of the house in Nunspeet, the experimental data was taken from a single house with characteristics similar to those of the house in Austin. The data was collected in situ with commercial metering devices.

Figure 5.1 shows the description of the resulting electricity layout of the selected houses in Austin (Figure 5.1a) and in Nunspeet (Figure 5.1b). In the case of Austin, the house was selected by narrowing down the available data from the Pecan Street database to the house with the largest installed solar PV system and largest peak load and for which data for a whole year was available. Figure 5.1a shows that the selected Austin house has 148 solar PV panels of 280 Wp installed in a grid-connected mode. A DC-to-AC inverter is used in order to deliver the electricity to the grid at 120 V. The energy distributor is the company Austin Energy (Austin, TX, USA) [166]. Furthermore, the house has an electric hybrid-vehicle (EV), which is charged using the available electricity at the house (the electricity grid or the solar PV system). The EV, among all energy-consuming objects, has the highest energy consumption in the house with a power consumption of 3.7 kWp. In the case of Nunspeet (Figure 5.1b), the data was measured with the TED Pro Home real time [33] and an Energy Logger 4000 from the company Voltcraft [167]. All data was collected during the summer of 2016. The house has 48

solar PV panels connected to a DC-to-AC inverter in order to deliver the electricity to the grid at 230 V.

An example of the data recorded for a day in June 2016 for the houses in Austin and Nunspeet is presented in Figure 5.2. In the case of Austin (Figure 5. 2a), the load distribution during the day has an average of 4.7 kW. The maximum load is observed during the night (12.9 kW) and the lowest load during the early morning (1.3 kW). The maximum load may be produced due to an EV charging from 8:00 to 10:00 p.m., together with other appliances connected to the house (lights, TV, dishwasher, washing machine, etc.). The solar PV system generates electricity for approximately seven hours with an average production of 8.3 kW. The solar PV peak produced is 34.9 kW between 12:00 to 2:00 p.m.

Figure 5.2b shows a one-day energy distribution of the house in Nunspeet. The load observed in the house has an average power consumption of 0.8 kW, and a load peak of 5 kW that is observed at around 7:00 a.m. The solar PV system installed in the house produces an average of 3.2 kW of electricity during the day and a peak production of 10 kW at around 10:00 a.m. In both cases, the trend of the load and solar PV production has a similar structure, although the total values are much larger in Austin. During the night and early morning periods, there is none or only a very low production of electricity from the solar PV system. At such times, the house is working fully on grid power. After the sun rises, the electrical load of the house is partly supplied by the solar PV system. However, the solar PV power increases and at some time it is well beyond the load needed in the house. In this case, the solar PV surplus of electricity is injected to the grid. In order to create a 100% off-grid scenario, the solar PV excess of electricity may be stored in a battery instead of being transferred to the electrical grid. In order to perform the calculation of the size of storage needed for an off-grid scenario, the given energy profiles during the summer period of 2016 of these two houses are used.

5.2.2 The Sea Salt Battery

To determine the storage size needed for an off-grid house, we used as storage technology a Sea-Salt battery. The Sea-Salt battery may become an important for houses that are a part of smart grids [168,169]. The battery is part of the ongoing research of the company Dr Ten (Wezep, The Netherlands) for the development of environmentally friendly storage technologies, whereby the main focus has been on the development of the Sea-Salt battery [34] and the glycerol fuel cell [37,170]. The battery is made of carbon graphite and its electrolyte is based on sea salts (mostly NaCl). This

may make the Sea-Salt battery an environmentally friendly alternative. The charge voltage per cell of the battery is on average about 1.9 V with a stable electrolyte (where hydrogen and oxygen evolution has not been noticed).

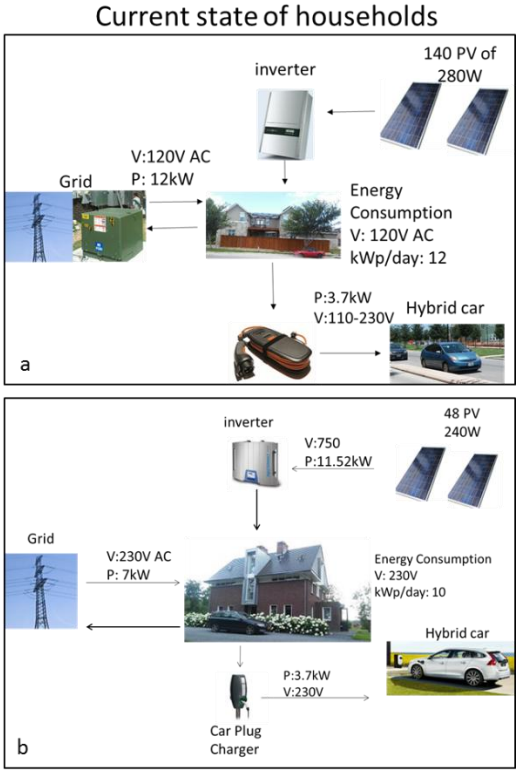

Figure 5.1. *Sketch of the electric layout of a house: (**a**) Austin, Texas, US; (**b**) Nunspeet, NL.*

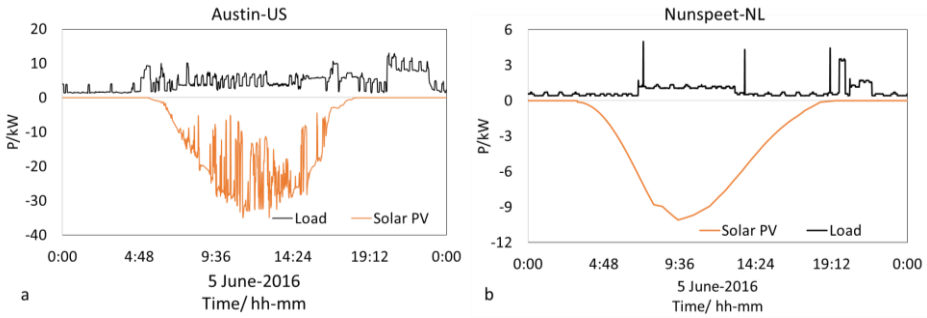

Figure 5.2. *Example of load and solar PV daily profiles in June 2016: (**a**) Austin; (**b**) Nunspeet.*

The low voltage per cell reduces the possibilities of electrolysis, thus diminishing the risk of explosion. These characteristics make the Sea-Salt battery a good candidate for in-home storage of electricity.

In this study, we use the Sea-Salt battery in two ways. First, as an ideal storage device in the DEMkit model of the houses where it is assumed that the device can be charged to 90% and discharged until 10% of its full capacity and second, as a real battery under scaled loads. In order to do this last part, the performance of the Sea-Salt battery was tested with a UBA5 charge/discharge battery analyzer from the company Vencon [171]. The device is directly connected to the battery and runs with the software Vencon-UBA Version 2017 with data recorded every five seconds.

5.2.3. The DEMkit Simulator

For the simulation study, the DEMKit simulation and demonstration toolkit was used [44]. As explained in Chapter 4 DEMKit makes use of discrete time-series dynamic simulations using a bottom-up modeling approach. A library with device, grid, and control components is available in the tool. Generic device components are available that describe the behavior of a device and its operation constraints, such as the buffer capacity. An attached control implementation can optimize the operation of the device using these constraints. On the other side, an interface allows the devices to be connected to a physical grid model, such that it can be used to evaluate the effects of control actions on the delivered power quality. Using these components, houses and other buildings can be modeled and connected to a physical (micro) grid model. On top of these physical components, a digital control system can be modeled. As a result, DEMKit can be used to perform simulations of cyber-physical systems, in which there is an interaction between the physical (devices and power grid infrastructure) and the digital (cyber) control system.

Using DEMkit to Determine Storage Size

The underlying model to study the feasibility of the envisioned Sea-Salt battery for an off-grid house consists of a battery storage system, house loads, and solar PV panels. Additionally, a control system is added that ensures that the power balance within the house is maintained. This results in the house model as shown in Figure 5.3. The static house load and PV production is provided using time series measurement data. Furthermore, an ideal battery model is used.

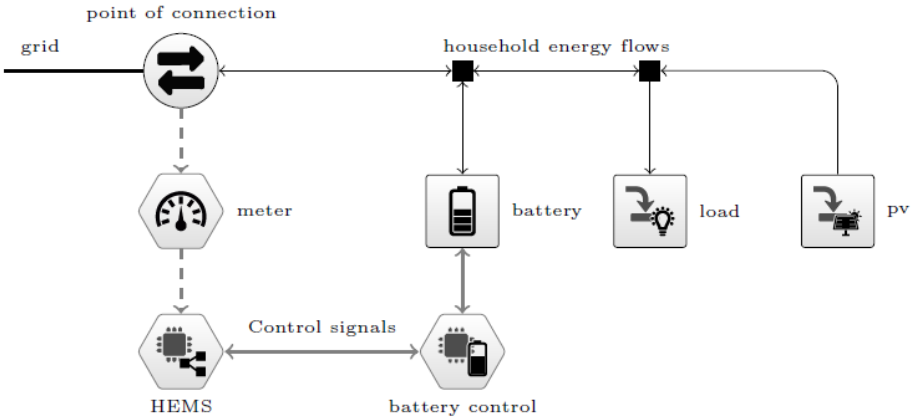

Figure 5.3. *Diagram of the house model within DEMKit.*

The power consumption of the devices (rectangular blocks) result in a power surplus/deficit at the point of connection, which is measured by the meter. The HEMS (home energy management system). and battery controller act on this information to balance the power consumption in the house.

The power consumption of the house is measured by the smart meter device model, which then communicates that information to the implemented HEMS Based on the observation of the power consumption ($P_{meter}(t) = P_{battery}(t) + P_{load}(t) + P_{pv}(t)$) at time t, the battery controller is instructed to inject or consume power to balance the house power consumption, i.e., to ensure no power is imported or exported in each time interval. Hence, the new power consumption of the battery is given by $P_{battery}(t+1) = P_{battery}(t) - P_{meter}(t)$. The battery controller verifies if this new power consumption is feasible, i.e., $P_{min,battery}(t) \leq P_{battery}(t) \leq P_{max,battery}(t)$ and whether battery capacity constraints are met. More details of device models and control algorithms are given in [44]. The required capacity of battery storage system capacity can be determined from the data to ensure that the house can be supplied with the required power at all times.

5.3. Results and Discussion

In this section, we derive, based on the available data of the two houses in the US and NL, the following. First, a simple baseline calculation for a possible storage size is given that is based on the assumption that the house should be able to be 100% off-grid for a short period of time (two days). In a second step, a simulation with the DEMkit tool is executed using the data of

the summer period of 2016 and the baseline storage sizing. The results of this simulation lead to a minimum sizing of the storage needed for the houses to be off-grid for the whole summer. Lastly, the results of the proof of concept for testing of a real Sea-Salt battery under scaled house loads and the solar PV system are given.

5.3.1. Initial Sizing of the Storage

To obtain an initial indication for the needed storage capacity, we use a common method described by Spiers [172]. This method is normally used by solar PV companies (e.g., [173]) for sizing batteries for off-grid scenarios. The method is shown in Equation (1), where B_C is the battery capacity, I_{BR} the total daily Ah required, t_R the recommended reserve time, and B_{UC} the percentage of battery useable capacity.

$$B_C = I_{BR} \times t_R / B_{uc}. \quad (1)$$

For the calculation, we assume that the battery is capable of fully support the house for a period of two days during the summer (also known as recommended reserved time); the two days refers to the average of continuous cloudy days. Therefore, we used the average consumption of the houses during the summer (4606 kWh/month in Austin and 918 kWh/month in Nunspeet). Additionally, the energy consumption of the houses is corrected with a 15% factor due to losses in the AC-to-DC inverter. Furthermore, we assume that, during the two days, the battery does not receive any input via charging. We also assume that the battery has 80% useable capacity and a working voltage of 48 V. The resulting values for sizing the battery are shown in Table 5. 1. A battery of 452 kWh for the house in Austin and a battery of 90 kWh for the house in Nunspeet are needed to cover the average load demand of the houses for two days.

Table 5.1. *Initial sizing of the battery based on the average power consumption of the houses in Austin and in Nunspeet.*

Battery Design	**Austin**	**Nunspeet**	**Unit**
Houses Avg. Energy Consumption during the summer	4606	918	KWh/month
AC/0.85 = DC Correction Factor (15%)	5419	1080	KWh/month
DC Consumption (L_p)	180.6	36.0	KWh/day
Voltage battery system V_B	48		V
Total daily Ah ($I_{BR} = L_p/V_B$)	3.76	0.750	kAh/day
Recommended reserve time (t_R)	2		day
Percentage of usable battery capacity (B_{UC})	80%		
Minimum battery capacity in kAh ($B_C = I_{BR} \times t_R/B_{uc}$)	9.41	1.875	kAh
Minimum battery capacity in kWh	452	90	kWh

5.3.2. Storage Sizing Simulation

The initial size for the storage is used as input for a simulation in order to research if this size of battery is enough to cover the load demand of the house in an off-grid scenario during the complete summer of 2016. These off-grid scenarios for the two houses are depicted in Figure 5. 4. The two houses in Austin (Figure 5.4a) and in Nunspeet (Figure 5.4b) require a solar PV system connected to a DC–DC inverter in order to charge the batteries at a voltage of 48 V. The battery and solar PV system require a DC-to-AC inverter to send the electricity from the battery to the house grid and power the appliances in the houses. Within the simulation, all the generated solar PV energy is either stored in the Sea-Salt battery, injected to the house electricity grid, or the surplus is curtailed.

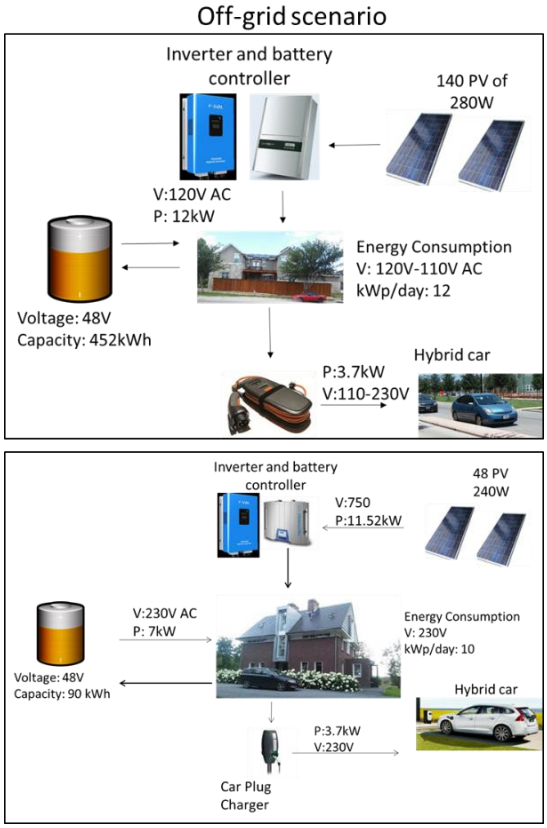

Figure 5.4. *Description of electricity distribution for off-grid scenario: (**a**) Austin; (**b**) Nunspeet.*

In the simulation with DEMkit, we used the available solar PV profiles (like the one in Figure 5.2) as input, the available house profiles, and the battery with a capacity as calculated in Section 5. 3.1. Within the simulation, the battery is charged with the excess of solar energy not needed for supplying the house and discharged during the periods where insufficient solar production is available to power the appliances in the houses. The output of the simulation is the resulting state-of-charge profile of the battery, which refers to the energy content (EC) of the battery in kWh.

Figure 5.5 shows the input profiles for the simulation and the resulting EC profile of the battery during the summer of 2016. In the case of Austin, the profiles of the solar PV system and load are shown in Figure 5.5a. The average load of the house is 4.6 kW with a peak load of 14.6 kW and the average solar PV energy generated is 7.7 kW with a peak production of 38.5 kW. Figure 5.5b shows the profile behavior of the Sea-Salt battery that is connected to the solar PV system for the off-grid house scenario. The results

show that the battery average EC is 421 kWh with a minimum EC of 275.7 kWh. Moreover, since the battery EC is always above the lowest possible value of 90 kWh (20% of the capacity) during the entire studied period, a full discharge of the battery does not occur.

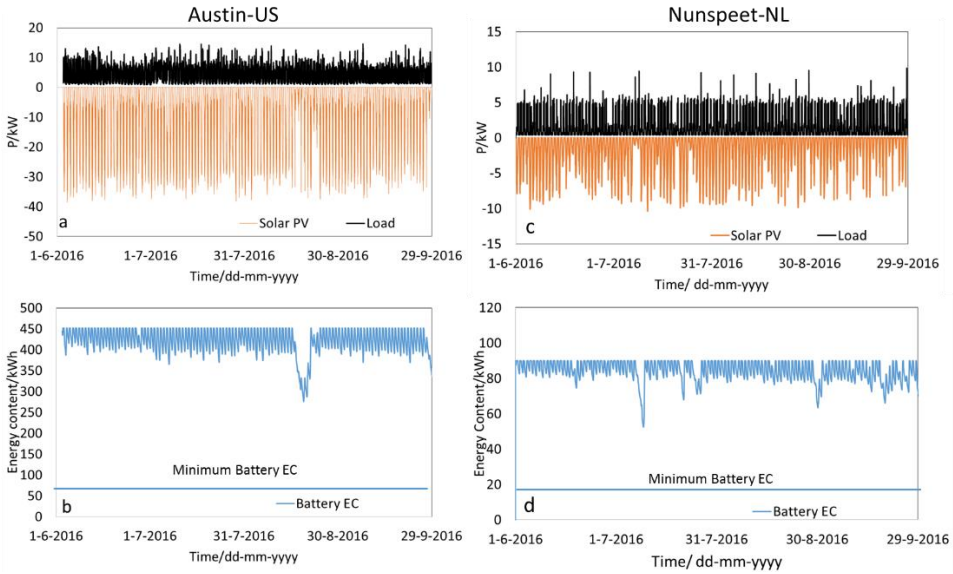

Figure 5.5. *Profiles resulting from simulating a house for the summer of 2016 using the initial capacity for the storage in (**a**) Austin (solar PV energy and load), (**b**) Austin (battery EC), (**c**) Nunspeet (solar PV energy and load), and (**d**) Nunspeet (battery EC).*

In the case of the house in Nunspeet, the average load during the period is 0.9 kW and the peak load is 9.8 kW. Furthermore, the average solar PV energy generated is 1.7 kW with a peak production of 10.4 kW (see Figure 5.5c). The battery behavior for the off-grid house in Nunspeet is shown in Figure 5.5d. The battery had an average EC of 82.4 kWh and the minimum EC observed is 52.9 kWh. Moreover, the minimum possible EC of 19 kWh is not reached during the entire summer.

In both cases, the modeled battery is able to provide 100% of the dynamic power deficit to the houses during the summer of 2016 (June–September 2016). In Austin, a battery of 452 kWh is necessary, and a battery of 90 kWh is needed in Nunspeet, and this is possible only with the available solar PV system. However, Figure 5.5 also shows that the chosen battery size is large enough to cover the house's electricity demand (the maximum discharge of the Sea-Salt battery is not reached). Based on the given results, a minimal battery size needed to create the 100% off-grid scenario can be estimated. For these values, we chose 226 kWh for Austin and 45 kWh for Nunspeet.

The results of the simulation of DEMkit using this capacity are presented in Figure 5.6.

In the case of Austin, the simulation results for a battery capacity of 226 kWh is presented in Figure 5.6a. The results indicate an average EC of 192 kWh. Furthermore, the minimum EC recorded is 49.8 kWh. This value is shown during the week with the lowest solar PV production (13–19 August). Figure 5.6b shows the profiles in the week with low solar PV energy in which the battery has the deepest discharge. In this week, the average solar PV production is only 4.4 kW with a peak of 37 kW. Moreover, the load in this week has an average of 3.9 kW and a peak of 12.5 kW.

For the Nunspeet case, the results for the reduced battery size are presented in Figure 5.6c. The average battery EC is 38.3 kWh. Moreover, a discharge of the battery below the minimum allowed EC is not observed during the studied period. The minimum observed EC is 9.8 kWh. This value occurs during the week with the lowest solar PV production (4–10 July; Figure 5.6d shows the profiles in this week). Here, the average solar PV production is 1.5 kW with a peak of 9.0 kW and the load has an average of 0.97 kW with a peak of 9.4 kW.

The results for the reduced size of the battery show that these capacities are sufficient to provide the necessary power to maintain the houses 100% off-grid without causing a shortage of electricity. Summarizing, the house in Austin requires a battery of 226 kWh and the house in Nunspeet a battery of 45 kWh. Note that these values are half of the capacities resulting from the method use in Section 5.3.1 (see Figure 5.5). This indicates that in case a solar PV system is available, a different approach should be developed. Such an approach should take into account the average or minimum amount of PV production in the considered period that the battery has to bridge.

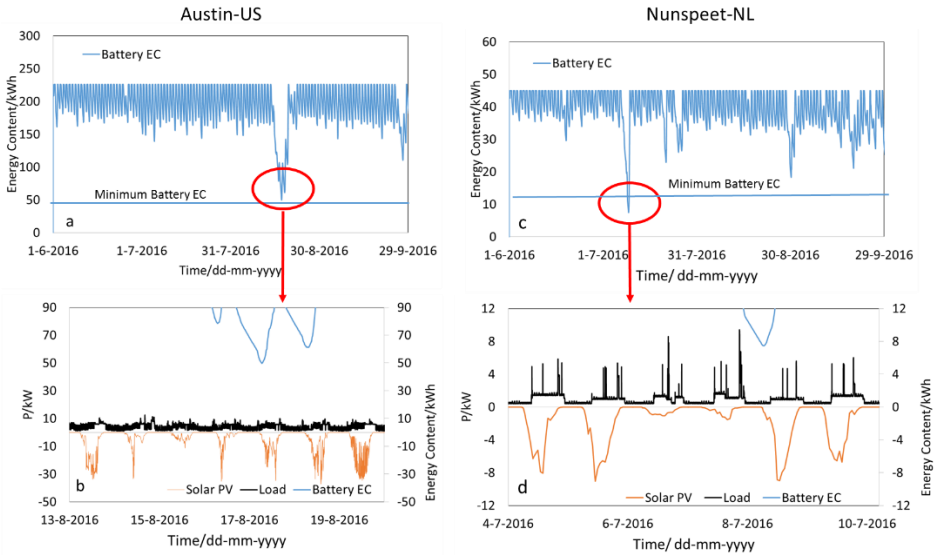

Figure 5.6. *Profiles of a house modeled with a solar PV system and a reduced storage size for the summer of 2016. (**a**) Complete summer in Austin. (**b**) Week with lowest solar PV production in Austin. (**c**) Complete summer in Nunspeet. (**d**) Week with lowest solar PV production in Nunspeet.*

5.3.3 A Case Study for a 100% Off-grid House in the Netherlands

In this section, we present a case study for an off-grid house. Here, we used a Glycerol Fuel Cell as backup system in order to create a more feasible off-grid house during the winter in the Netherlands, otherwise the sizing of the battery and solar PV can be too large for a possible implementation.

In principal, the goal of this study was to show that it is technically feasible to develop an off-grid house. The economic aspects of off-grid houses are beyond the scope of this research. Figure 5.7 shows the setup of an islanded off-grid house using new sustainable technologies developed in the Netherlands. In general, the setup uses various technologies to generate the electricity needed for a house, and it is designed to also supply electricity to a decentralized wastewater treatment plant (DWWTP). To achieve this, solar PV is used coupled with a battery.

During the day, solar PV provides electricity and during the night or during low solar irradiation, the battery is used as main electricity provider. Furthermore, a fuel cell is used as a backup power unit. The fuel cell is only used when solar PV and the battery are not capable of providing the electricity demand. The Sea-Salt battery and the Glycerol Fuel Cell are discussed in chapters 2 and 3.

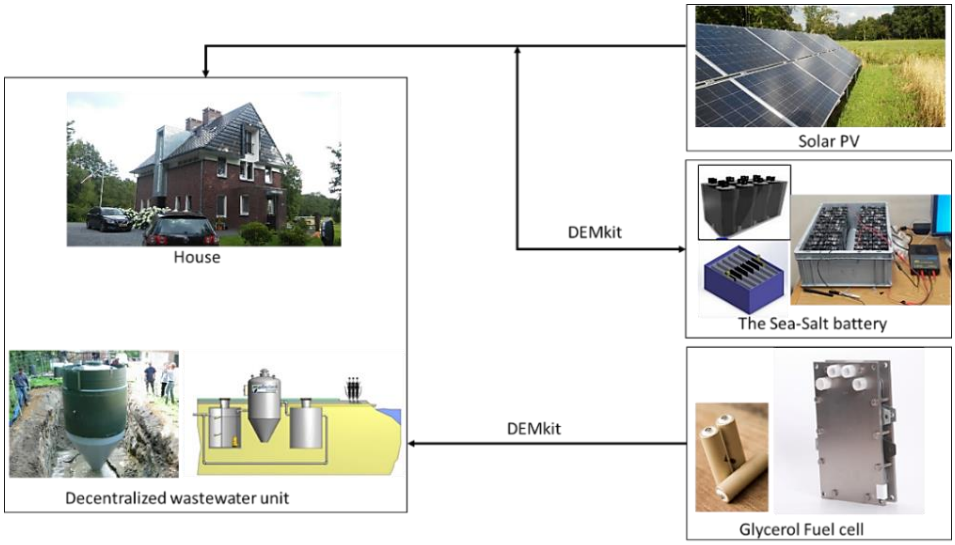

Figure 5.7. Prototype set up for an islanded off-grid house.

The given devices can be connected to a physical grid model, such that it is possible to evaluate the effects of control actions on the delivered power and power quality.

Using DEMkit the performance of an off-grid house equipped with solar PV, a sea-salt battery and a glycerol fuel cell was evaluated. Furthermore, the simulations could be used to determine suitable parameters of the appliances (e.g., size of PV panels, storage capacity of the batteries and fuel cell), such that the house may be used off-grid over a complete year.

The electricity consumption used for this simulation (see red line in Figure 5.8) has been recorded in a house consisting of 5 residents. The house is equipped with regular appliances (fridge, TVs, washing, and drying machines), and also equipped with a hybrid vehicle that is charged regularly.

The goal of the simulations with DEMkit was to investigate whether or not the house load could be covered by solar PV, the battery, and the backup unit. For the storage, the sea-salt battery has been used as an ideal device, meaning that the battery may be discharged for 100%. In contrast to Li-ion batteries, a sea-salt battery can withstand 100% discharge without damage. The glycerol fuel cell was considered as a back-up unit, only to be used when the sea-salt battery and the solar PV are not capable of providing the required electricity for the house. In DEMkit, the glycerol fuel cell is programmed to start when the battery is below 20% capacity.

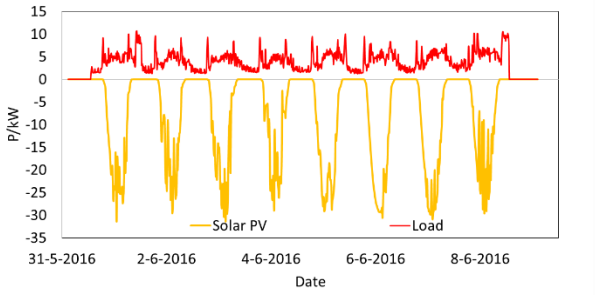

a) Solar PV and Load June 2016

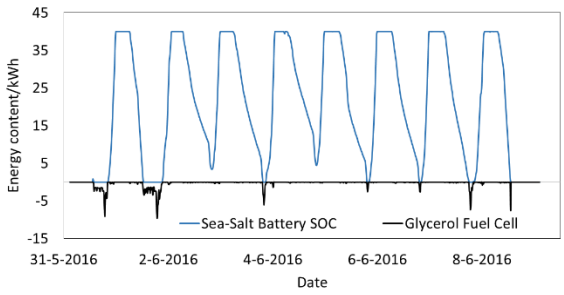

b) Sea-Salt battery and Glycerol Fuel Cell June 2016

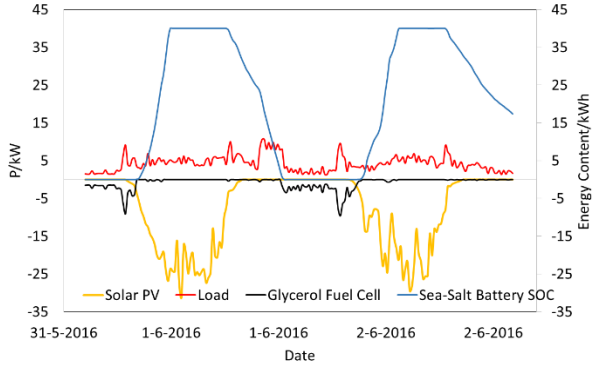

c) Combined technologies two days of June 2016

Figure 5.8. *DEMkit results of an off-grid house in the Netherlands with Solar PV, Sea-Salt battery and a Glycerol Fuel Cell during one week of summer 2016 showing (**a**) Solar PV and Load, (**b**) Sea-Salt battery SoC and Glycerol Fuel cell power and (**c**) a zoom in on June 1 and 2 2016 with Solar PV, Load, Sea-Salt battery and Glycerol Fuel Cell.*

Preliminary results using DEMkit for an off-grid house in the Netherlands using solar PV, a sea-salt battery, and a glycerol fuel cell, with energy profiles of one week during June 2016 are presented in Figure 5.8. The house load

(red line) and the solar PV profiles (yellow line) were recorded in a house in the Netherlands (the data has been provided by the company Alliander) [38].

5.3.3.1 Discussion of the Results

Figure 5.8a shows the data of electricity load and solar PV production during the first week of June 2016. Figure 5.8b shows the electricity content of the simulated sea-salt battery and the production of the backup glycerol fuel cell during the first week of June 2016, and Figure 5.8c shows the zoom in of the compiled data of the house load, solar PV, the sea-salt battery and the glycerol fuel cell in the first two days of June 2016. It was observed in detail that the overall profile of solar PV was constant throughout the days, and a maximum electricity production of 30 kW was observed. On the other hand, the house load showed a maximum value of 10 kW during the first week of June 2016 (see Figure 5.8a). In Figure 5.8b, it was observed that the sea-salt battery stored the surplus of electricity that was provided from the solar PV during the day. Furthermore, the sea-salt battery is discharged typically during the evening and night (the modelled battery has a size of 45 kWh). Moreover, during the night, it was observed that the sea-salt battery did not always cover the required house load. In such situations, the glycerol fuel cell of 11 kW (black line) covered this demand and was active until the solar PV covered the demand of the house on the next day. In Figure 5.8c, a more clear detail view of the interaction of the solar PV, the sea-salt battery, and the glycerol fuel cell is given for the first two days of June 2016.

Figure 5.9a shows the data of electricity load and solar PV production during a winter week in January 2016, and Figure 5.9b shows the corresponding electricity content of the simulated sea-salt battery with the backup glycerol fuel cell during the same week of January 2016. Furthermore, Figure 5.9c shows the zoom in of the compiled data of the house load, solar PV, sea-salt battery, and the glycerol fuel cell during two days of the same week. In detail, it was observed that overall, the profile of solar PV stayed constant over this week and the maximum electricity production was of 30 kW.

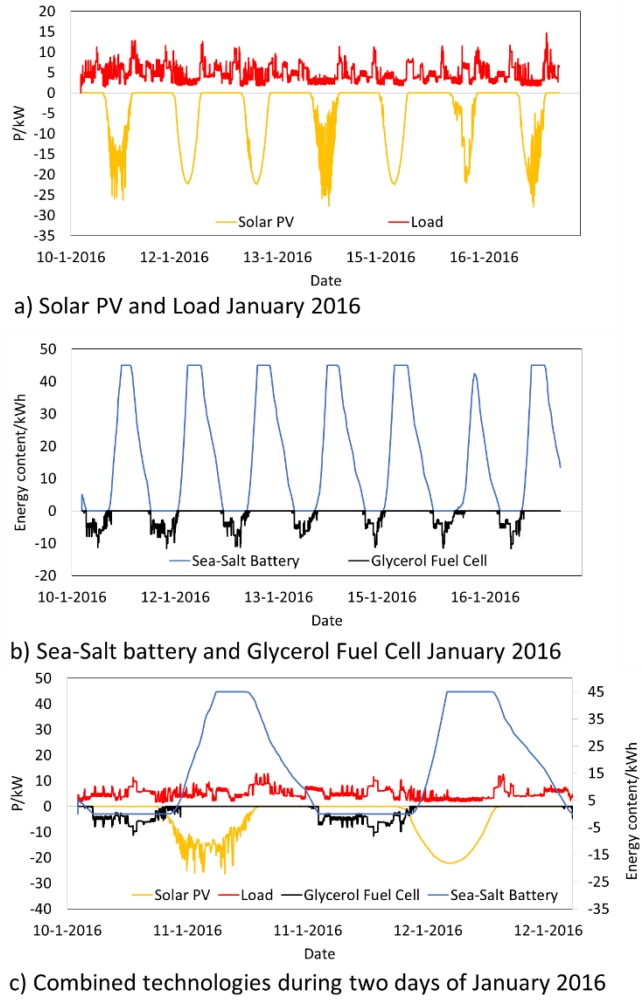

Figure 5.9. *DEMkit results of an off-grid house in the Netherlands with Solar PV, sea-salt battery and a glycerol fuel cell during one week of winter 2016 showing (**a**) Solar PV and Load, (**b**) Sea-Salt battery and glycerol fuel cell cell and (**c**) a zoom in on January 11 and 12 2016 with Solar PV, Load, Sea-Salt battery and glycerol fuel cell.*

On the other hand, the house load shows a maximum value of 15 kW during the week of January 2016 (see Figure 5.9a), which is higher than the load in the week of June 2016 (10 kW). In Figure 5.9b, it was observed that the sea-salt battery stored the surplus of electricity that was provided from the solar PV during the day. Furthermore, the sea-salt battery was typically discharged during the evening and night, and this occurred during longer periods of time than in the summer (the modelled battery has a size of 45 kWh). Moreover, during the winter night, it was observed that the sea-salt

battery did not always cover the required house load. In such situations, a glycerol fuel cell of 16 kW (black line) covered this demand and was active until solar PV covered the demand of the house on the next day. In Figure 5.9c, a clearer detailed view of the interaction of the solar PV, sea-salt battery, and glycerol fuel cell is given for the 10th to the 12th of January 2016.

To summarize, it was observed that a house in the presented scenario in the Netherlands was capable of being off-grid by having a solar PV of 30 kW with a sea-salt battery of 45 kWh and a glycerol fuel cell of 11 kWh during the aforementioned week in June 2016. In the case of the tested week in winter, it was observed that the size of the glycerol fuel cell had to increase to 15 kW but the solar PV and the sea-salt battery could work with the same size in the summer and in the winter.

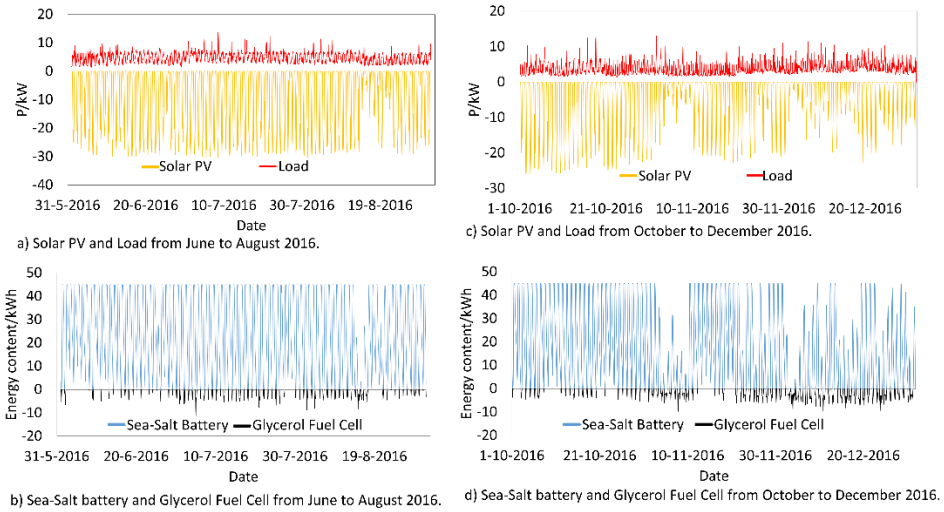

Figure 10. *DEMkit results of an off-grid house in the Netherlands with hourly data with Solar PV, sea-salt battery and a glycerol fuel cell during the months of June to December 2016 showing (**a**) Solar PV and Load from June to August 2016, (**b**) Sea-salt battery SoC and glycerol fuel cell power from June to August 2016, (**c**) Solar PV and Load from October to December 2016, (**d**) Sea-salt battery SoC and glycerol fuel cell power from October to December 2016.*

The above results are supported by the simulation created for longer periods of time, as shown in Figure 5.10. The simulation is presented over a 7 months period, from June to December 2016. It was observed in Figure 5.10 that the results support the simulation performed for the weeks of January and June (see Figures 5.8 and 5.9). Also, Figure 5.10 shows the same behavior as the simulation performed for the weeks in Figures 5.8 and 5.9. However, notice that during the months of November and December, the glycerol fuel cell is

used more often than during the more sunny periods. Nevertheless, this could have been expected, based on the weather differences.

5.3.4. Proof of Concept for Testing a Sea-Salt Battery under Scaled Load

The testing of batteries under scaled loads is a method using available electricity data to observe the behavior of a (smaller-sized) battery by using electricity inputs/outputs with the same variations as the available electricity data. This method may offer a less expensive alternative than a full-sized battery for testing. For the scenarios considered in this research, we use a small Sea-Salt battery as an example. This section is presented in two parts. First, some standard tests are performed to observe the battery capacity (performance under discharge) of the given Sea-Salt battery; secondly, the behavior of the Sea-Salt battery is tested under scaled loads using data from one week of summer from the house in Austin.

Figure 5.11a shows the voltage behavior of a single cell Sea-Salt battery using different constant discharge loads and Figure 5.11b shows multiple Sea-Salt batteries connected to form a battery pack. In the example in Figure 5.11a, the battery was charged with a constant current of 250 mA for 10 h. Furthermore, different discharge rates (C/10–C/5) were tested (C-rate corresponds to the maximum capacity of the battery divided by the desired discharge time). The results of the experiment are presented in detail in Table 5.2. The minimum and maximum current efficiency of the battery are 81% (C/10) and 93% (C/5), respectively. The OCP (open circuit potential) where no load is applied had an average of 1.74 V at the different C rates tested. The average discharge voltage had a minimum value of 1.36 V at C/5 and a maximum average voltage of 1.5 V at C/10. In all of the experiments, the battery was discharged until the output voltage was reduced to 0.2 V. When comparing the Sea-Salt battery power output for the different discharge rates, it was observed that the battery has the highest power output at C/9 (3.29 Wh) and the lowest at C/5 (3.18 Wh). This effect is possibly related to battery internal resistances (ohmic losses), measuring equipment (cables, and distance of the battery with the measuring device), and self-discharge effects. The presented results for the given battery show that the Sea-Salt battery has potential to be used in scenarios in which long periods with discharge load are present (such as for off-grid houses with a solar PV system).

To test this, a Sea-Salt battery was tested under scaled loads using the data from Austin. The goal of this test was to observe the changes that the battery undergoes under real loads, using only low power equipment. In order to

perform the test, the following steps were executed. First, a Sea-Salt battery was constructed and configured with 4 Wh and 6 V nominal voltage.

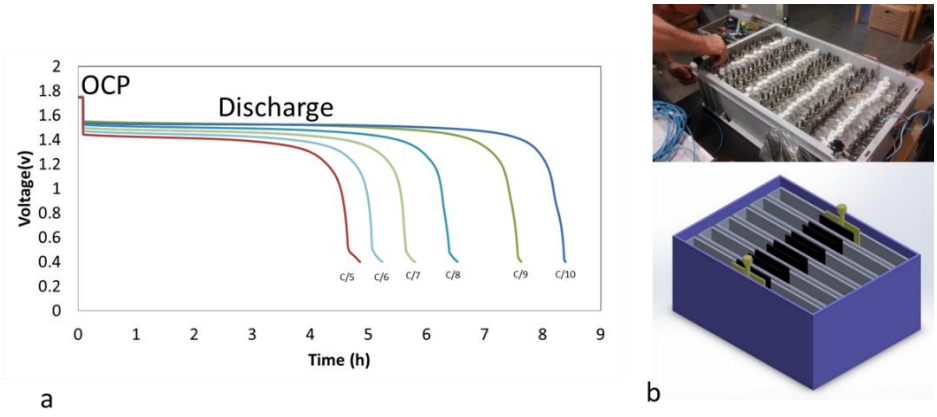

Figure 5.11. *(**a**) Voltage behavior of the Sea-Salt battery in one single cell at different C-rates. (**b**) Example of multiple Sea-Salt batteries connected to form a stack.*

Second, the house load and the solar PV system of Austin was scaled down 10,000 times. Lastly, the battery was connected to a UBA5 battery testing equipment in order to simulate the charge/discharge operation of the battery for the house in Austin. In the scaled period, one day is simulated every three hours, giving the possibility to test four days of the modeled off-grid conditions in one day. Figure 5.12 shows the profiles of the used input and the resulting profile of the battery. Note that, in this figure, the battery voltage is the indicator of the battery SoC (the Sea-Salt battery is 100% charged when the voltage reaches 7.9 V and fully discharges when the battery voltage is 5.1 V).

The results show that the load of the simulated house has a maximum value of 1 W, with an average consumption of 0.6 W, and the simulated solar PV system has a maximum energy production of 3 W with an average of 1.5 W. The Sea-Salt battery profile shows a similar shape during the four simulated days. In addition, the voltage charge limit was not reached, nor was the voltage discharge limit.

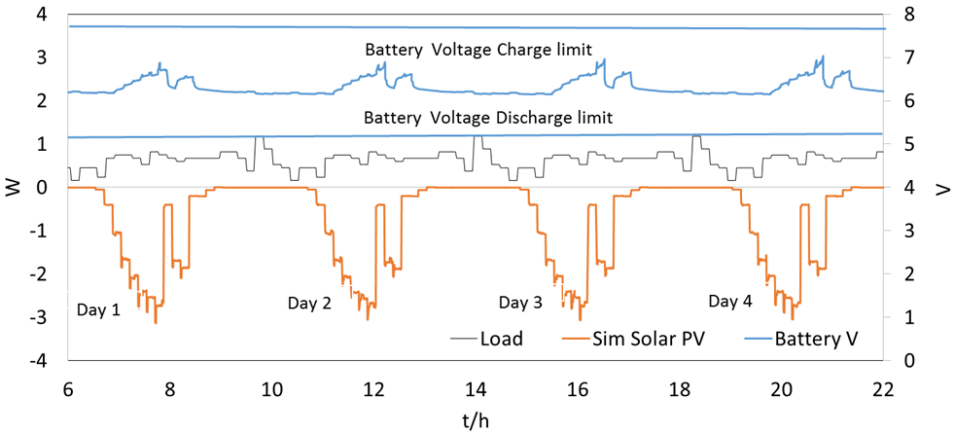

Figure 5.12. *Profiles testing of the Sea-Salt battery under scaled loads.*

Table 5. 2. *C-rate results for a single cell Sea-Salt battery.*

C rate	Charge Ah	Discharge Ah	Current Efficiency %	OCP	V Discharge Avg.	Capacity Wh
C/10	2.49938	2.03699	81%	1.7453	1.5026	3.060781174
C/9	2.49961	2.21013	88%	1.7406	1.4889	3.290662557
C/8	2.49923	2.26647	91%	1.7456	1.4345	3.251251215
C/7	2.49909	2.27749	91%	1.7412	1.4087	3.208300163
C/6	2.49913	2.28835	92%	1.7345	1.3867	3.173254945
C/5	2.49942	2.33479	93%	1.7456	1.3656	3.188389224

Thus, the experiment shows that the battery can deal with the offered profiles without being fully charged or fully discharged during the tested period. The minimum voltage observed was 6.1 V, and the highest charge voltage was 7 V. Although this method may give an indication of the battery behaviour for off-grid scenarios in houses, more research should be performed with real loads and non-scaled batteries so that a more reliable conclusion of the potential of the Sea-Salt battery can be made.

5.4. Conclusions

Based on the experimental data collected in the summer of 2016 for the houses in Austin and Nunspeet, it is concluded that during this period a PV

installation combined with a battery may provide the necessary electricity for a 100% off-grid house without showing a blackout. The Austin house needs a solar PV system of 38 kWp and a storage of 226 kWh, and the Nunspeet house needs a solar PV system of 11.5 kWp with a storage of 45 kWh. To achieve these results, the DEMkit simulation tool was used. Also, it is observed that a house in the Netherlands may be capable to be off-grid by having a solar PV of 30kW with a Sea-Salt battery of 45kWh and a Glycerol Fuel Cell of 11kWh during summer. Moreover, during a week of winter it is observed that the Glycerol Fuel Cell size has to increase to 15kW, to provide all the electricity demands.

Furthermore, solar PV and load data for one week was used to create down-scaled data for one day and was then used to test if a real Sea-Salt battery would be able to deal with the fluctuation of electricity for the considered off-grid scenario in Austin. The results of this test indicate that the Sea-Salt battery has the potential to be used for such off-grid applications, although more tests are needed to support this conclusion. A further conclusion of the research is that the presented down-scaling method may be a useful approach for battery testing under real electricity fluctuations.

The current research is only a first step that shows the interaction of the considered devices in such an off-grid situation. In further research we aim to use all technologies mentioned in this research to provide all the electricity needs to a real house.

6

Conclusions and Recommendations

In this chapter we summarize the results of this thesis in two parts. In the first part we show the conclusions of each chapter and in the second part we provide the answer to the research questions stated in Chapter 1. Finally, we present recommendations for further research.

6.1 Importance of off-grid houses

In Chapter 1 the role of off-grid houses in the energy transition is presented. These off-grid houses may be an important asset for the electrical grid, on the one hand, to increase the electricity access in the world and, on the other hand, to allow a better integration of renewable energy sources in the energy system. Initiatives to improve the access to electricity are plenty, but the rate of implementation of practical solutions is far below the UN Sustainable Development Goal 7 Energy (SDG 7) for 2030. It has been observed that this problem is most apparent in Sub-Saharan Africa, where the current trends of electricity access calculated by the World Bank indicate that they will not be able to achieve the SDG 7 targets by 2030. On the other hand, the current worldwide introduction of renewable energy generation at the local level leads to an unbalance of electricity in terms of generation and consumption, which in the future may cause a shortage of electricity in some periods of the year. Remarkably, the implementation of renewable energy generation using the bottom-up approach of off-grid houses is happening at a faster rate in developing countries than in developed countries.

6.2 The Sea-Salt battery analysis

In Chapter 2 a halide battery cathode material is studied as part of a Sea-Salt battery which is an energy storage technology for an off-grid house. In detail, the oxidation of halides, in particular bromide, is studied in aqueous solutions on graphite electrodes by voltammetry, electrochemical impedance spectroscopy (EIS) and UV-Vis spectroscopy in light of its application in halide/halogen batteries used for off-grid houses and for microgrids. Based on the study of the halide oxidation at carbon graphite we conclude with the following observations. The results with cyclic voltammetry indicated fairly large differences in current density between different halide salts, concentrations, cation type and pH. When comparing the absolute values of the tested aqueous solutions, current densities higher than 300mA cm^{-2} were observed at relative low electrode potentials (1.5V or 1.7 were no hydrogen evolution is observed). These current densities suggest a large capacity of the solution to accept electrons. Oxidation kinetics with NaBr solutions were much higher than $ZnBr_2$ at 7M while no large difference was observed at 2M. This may be related to the effect that positive ions (Na^+ and Zn^+) have an influence on the halide oxidation kinetics at large positive electrode potentials, which indicates that local ionic potential effects affect the oxidation rate of the reaction. EIS spectra go in line with the previous view, as there was a large resistance between $ZnBr_2$ and NaBr in the electrolyte phase transfer element. This difference is possibly related to different polybromide formation rates (from the reaction Br^- -> Br_x^- + x e-). All data can be fitted by one equivalent circuit using the procedure proposed of Baukamp [67]. The fitted circuit and Nyquist plots show the complexity of the reaction indicated by the presence of different resistors and capacitors. Furthermore, the UV-Vis spectra confirmed that the Br^- oxidation in an aqueous solution differs considerably between pure halogen, NaBr and $ZnBr_2$.

6.3 The Glycerol Fuel Cell

In Chapter 3 fundamental research is performed to understand the electrochemical mechanisms behind glycerol oxidation at a gold electrode. This is done to develop a Glycerol Fuel Cell that can be used as a backup power in an off-grid house. In detail, our analysis shows that gold has the highest current density for glycerol oxidation in alkaline media when compared with another catalysts at a potential of -0.2V (Pt, Ag, GC and Cu). It is furthermore observed that the gold surface can change in cyclic voltammetry. The current density shows linear behaviour with the scan rate at an exponential value of 1/5. One equivalent circuit fitted the data well at

potentials of -0.05V,-0.15V and -0.25V vs Ag/AgCl, with resistors and a Warburg element in parallel with the double layer capacitance. These elements are related to the possible presence of hydroxypyrovate and oxalate ions. Our results were consistent with the low-frequency error fitting analysis (10^{-4}), AC Simulink-Matlab fitting and the Kronig-Kramers transform test. The Zn-Au and the Cu-Au electrodes showed a cyclic voltammetry behaviour similar to the gold electrode at different scan rates. The discharge chronoamperometry test showed that the Zn-Au and Cu-Au electrode have higher current densities than the pure gold electrode at a potential of -0.25V vs Ag/AgCl (5 mA cm^{-2}, 4.5mA $cm^{-2,}$ and 3mA cm^{-2} respectively). Au, Zn-Au, and Cu-Au are possible catalyst candidates for glycerol oxidation, meaning that the gold coated metals are suitable electrodes for building a fuel cell. The air electrodes used in the fuel cell test suffered limited instability and in future research, stable air electrodes for a glycerol fuel cell will be addressed. Upon success in scaling up the fuel cell, these fuel cells may be used as backup systems in microgrids or as an alternative to replace diesel generators in some situations. However, more research is needed to validate this insight.

6.4 Using modelling to create off-grid devices

In Chapter 4 an example of supplying an off-grid device using Sea-Salt batteries and solar PV is presented. In this case, the considered device was a decentralized wastewater treatment plant (DWWTP). In detail, a method is presented that can be used to determine the sizing of sustainable energy sources for powering a DWWTP working in off-grid mode. As we considered solar PV generation as a special challenge to guarantee supply even during the months with low solar radiation. Concretely the results indicate that, in summer solar PV and a Sea-Salt battery can provide the energy requirements of the DWWTPs. However, in order to power the DWWTPs during the months of low sunlight the dimensions of the solar PV and the Sea-Salt battery needs to be increased by a factor of three. Alternatively another power source can be used in the winter, e.g. a Glycerol Fuel Cell. The simulations performed with the DEMKit tool shows that a solar PV of 15kWp and 20kWh Sea-Salt battery provide 100% of the electricity needed during the summer and up to 75% during the winter in the Netherlands for the Bever III DWWTP. In the case of the MBR DWWTP, a PV system of 30kWp and a Sea-salt battery of 50kWh is necessary to provide 100% electricity during the summer and up to 65% during the winter in the Netherlands.

6.5 Using modelling to size energy storage for off-grid houses and backup units

In Chapter 5 experimental data collected in the US and in the Netherlands for electricity consumption in houses and generation from solar PV is used in order to calculate the necessary size of storage needed to create an off-grid house. In detail, based on the experimental data collected in the summer of 2016 for the houses in Austin and Nunspeet, it is concluded that during this period a PV installation combined with a battery can provide the necessary electricity for a 100% off-grid house without showing a blackout. The house in Austin needs a solar PV system of 38 kWp and a storage of 226 kWh, and the Nunspeet house needs a solar PV system of 11.5 kWp with a storage of 45 kWh. Note that, these systems are dimensioned for the summer period. In an additional scenario, it was observed that this particular house in the Netherlands was able to be off-grid, by having a solar PV of 30 kWp with a sea-salt battery of 45 kWh and a glycerol fuel cell of 15 kWh working all year round.

In a second part, solar PV and load data for one week was used to create down-scaled data for one day, this data was then used to test if a real Sea-Salt battery would be able to deal with the fluctuation of electricity for the considered off-grid scenario in Austin. The results of this test indicate that the Sea-Salt battery may have the potential to be used for such off-grid applications, although more tests are needed to support this conclusion. A further conclusion is that the presented down-scaling method may be a useful approach for battery testing under real electricity fluctuations.

6.6 Answers to research questions

In this Section, answers to the research questions stated in Chapter 1 are provided. The central problem statement was formulated as follows:

- *How to identify a setup for an off-grid house based on renewable energy generation, sustainable energy storage technologies and sustainable energy backup unit?*

First, the thesis shows a setup for an off-grid house in which different technologies are used for this purpose. Our proposed setup uses Solar PV as energy generation, the Sea-Salt battery as energy storage and the Glycerol Fuel Cell as electricity backup. We identified that in order to use these technologies in an off-grid house, it is necessary to study these technologies from chemical and physical sides. For this we observed that electrochemical methods are an appropriate mechanism to research the energy storage and

backup technology. Furthermore, a modelling tool can be used in order to study the battery and the fuel cell in an off-grid house. For this, we identified that DEMkit is a capable tool to model and size the energy storage and backup technologies. Although, this study is only based on models and assumptions, our findings give a first approach for sizing energy storage for off-grid houses. However, it is still necessary to verify the model by creating a real scaled up test.

The sub questions are answered as follows:

- *How can a Sea-Salt battery be designed for storage in off-grid houses?*

In this thesis we used two methods to study the Sea-Salt battery. First, in Chapter 2 we showed the analysis of the chemical reactions that occur while charging the cathode material in the battery. For this, we provided an electrochemical analysis of halides, in particular bromide, and its oxidation behaviour at a graphite electrode. We found that the bromide oxidation reaction is a complex mechanism that is related to a multistep process which does not lead only to halogen generation but to a series of possible reactions (e.g. $Br^- > Br_x$). We also observed that bromide oxidation is also affected to some extent by the changes of metal cations e.g. Na^+ and Zn^+ in aqueous solutions. Second, in Chapter 4 and 5 a sizing characterization analysis of the Sea-Salt battery is provided in order to be used for an off-grid house. Using DEMkit we have found that battery sizing for off-grid scenarios can be performed, and that the size of the battery can be optimized in order to find the right size for an off-grid-house.

- *How can a fuel cell based on glycerol be designed as backup power for an off-grid house?*

We presented two methods to study the Glycerol Fuel Cell. First, in Chapter 3 we presented the analysis of the chemical reactions that occur while discharging the cathode material in the fuel cell. For this, we provided an electrochemical analysis of glycerol oxidation using a gold electrode catalyst on different substrates where the catalyst is deposited. Furthermore, we have shown that the glycerol oxidation reaction at gold has a complex mechanism that is related to multiple processes and the amount of catalyst is linked to the maximum voltage that the oxidation reaction can provide. We also observed that glycerol oxidation is also affected by changes in different substrate materials where gold is deposit on e.g. Cu, Zn and graphite. Second, in Chapter 4 and 5 a sizing characterization analysis of the Glycerol Fuel Cell is provided in order to create an off-grid house, using the fuel cell as backup unit. Using DEMkit we have found that the Glycerol Fuel Cell can be used for

off-grid scenarios, and also the right size of a fuel cell for an off-grid-house can be determined.

- *How can the near optimal sizing of energy storage units be determined for an off-grid house?*

It is demonstrated that when enough data of solar PV and energy consumption is available a model to characterize these sizing can be implemented. Using the DEMkit tool it is possible to size and observed the behaviour of energy storage units and create different scenarios in order to find a near optimal sizing of storage for off-grid houses.

- *How can the storage technologies and backup units be integrated in the energy management of an off-grid house?*

In Chapter 4 and 5 it is stated that in most cases in order to create an off-grid house it is necessary to have generation, storage and a backup system. We have shown that solar PV alone for energy generation in an off-grid house cannot provide all the electricity needs in a house for a complete year. However, the models presented in this thesis showed that by storing all the excess of electricity it is possible to provide almost all electricity requirements in an off-grid house. Nevertheless, in order to achieve this it is necessary to have a large quantity of storage. We have shown using DEMkit that is possible to model the interaction of electricity generation, storage and backup in order to optimize the design of an off-grid house. The model shows that a house can work 100% off-grid when a proper sizing of storage and backup power is specified.

6.7 Recommendations

Based on the research presented in this thesis, the following topics are seen as relevant for future research.

Testing models under real conditions: During our research we modelled a possible off-grid house that may become an important asset for increasing electricity access in the world. However, hardware has not been tested fully under real conditions in this research. We recommend that further analysis needs to be done in order to test the anticipated off-grid house under real conditions, taking into account our findings for storage sizing and backup power.

Electrochemical analysis: In this thesis we showed different methods to characterize electrochemically a battery. However, the exact reactions involved in the oxidation of halides were only analyzed by using

spectroscopic methods (EIS and UV-Vis). We recommend that deeper analysis of the reaction needs to be performed in order to validate our findings and to provide a better understanding of the halide oxidation.

In the case of glycerol oxidation, we have provided a mechanism for the oxidation of glycerol with a gold catalyst. We have observed that gold is a right catalyst for oxidizing glycerol. However, more analysis needs to be performed in order to understand the physical and mechanical characteristics of the electrode in order to arrive to a scaled prototype.

7

References

[1] Van Aubel P, Poll E. Smart metering in the Netherlands: What, how, and why. Int J Electr Power Energy Syst 2019;109:719–25. doi:10.1016/J.IJEPES.2019.01.001.

[2] Stijn A. Net-Metering RES LEGAL Europe 2019. http://www.res-legal.eu/search-by-country/netherlands/single/s/res-e/t/promotion/aid/net-metering-1/lastp/171/ (accessed May 8, 2019).

[3] Plug in the World. Home | Mobisol Group | Innovative Off-Grid Solar Solutions | Designed in Germany 2017. https://plugintheworld.com/ (accessed November 19, 2018).

[4] Koepke M, Groh S. Against the Odds: The Potential of Swarm Electrification for Small Island Development States. Energy Procedia 2016;103:363–8. doi:10.1016/J.EGYPRO.2016.11.300.

[5] SEforALL. About Us | Sustainable Energy for All (SEforALL) n.d. https://www.seforall.org/about-us (accessed July 16, 2018).

[6] The World Bank. Is the world on track to deliver energy access for all? May 23 2018. http://www.worldbank.org/en/news/feature/2018/05/18/sustainable-development-goal-7-energy-access-all (accessed May 25, 2018).

[7] Arlet J. Electricity Tariffs, Power Outages and Firm Performance: A Comparative Analysis. 2017.

[8] The World Bank. Energizing Africa : Achievements and Lessons from the Africa Renewable Energy and Access Program (AFREA) Phase I. 2015.

[9] The World Bank. Access to electricity (% of population) | Data 2017. https://data.worldbank.org/indicator/EG.ELC.ACCS.ZS?view=map (accessed October 27, 2018).

[10] International Energy Agency. Commentary: Electricity in every village in India 2018. https://www.iea.org/newsroom/news/2018/june/commentary-electricity-in-every-village-in-india.html (accessed October 29, 2018).

[11] Gamso J, Yuldashev F. Does rural development aid reduce international migration? World Dev 2018;110:268–82. doi:10.1016/J.WORLDDEV.2018.05.035.

[12] International Energy Agency. World Energy Outlook EXECUTIVE SUMMARY. 2017.

[13] European Commission. 2020 climate & energy package | Climate Action n.d. https://ec.europa.eu/clima/policies/strategies/2020_en (accessed July 26, 2018).

[14] European Union. SHARES (Renewables) - Eurostat n.d. http://ec.europa.eu/eurostat/web/energy/data/shares (accessed July 27, 2018).

[15] European Environment Agency (EEA). Trends and projections in Europe 2015: Tracking progress towards Europe's Climate and energy targets. 2015. doi:10.2800/985234.

[16] IqtiyaniIlham N, Hasanuzzaman M, Hosenuzzaman M. European smart grid

prospects, policies, and challenges. Renew Sustain Energy Rev 2017;67:776–90. doi:10.1016/J.RSER.2016.09.014.
[17] SEARS. State of Energy Access Report 2017. 2017. doi:10.1596/26646.
[18] EPA - West Coast Collaborative U. DERA 2016: American Samoa Achieves 100% Renewable Energy on Ta'u Island. n.d.
[19] Zelinka D. Energy Transition Initiative: Island Energy Snapshot - San Andres and Providencia (Fact Sheet), NREL(National Renewable Energy Laboratory). n.d.
[20] Laan M Van Der. GridFlex Heeten investigates feasibility of local energy market 2018. https://ict.eu/wp-content/uploads/2018/10/ICT-GROUP_Casestudy-Energy-GFH_UK_Dig.pdf.
[21] Pecan Street Inc. | 2013. http://www.pecanstreet.org/ (accessed March 8, 2017).
[22] Burke PJ, Kurniawati S. Electricity subsidy reform in Indonesia: Demand-side effects on electricity use. Energy Policy 2018;116:410–21. doi:10.1016/J.ENPOL.2018.02.018.
[23] Kennedy SF. Indonesia's energy transition and its contradictions: Emerging geographies of energy and finance. Energy Res Soc Sci 2018;41:230–7. doi:10.1016/J.ERSS.2018.04.023.
[24] Ali I, Shafiullah G, Urmee T. A preliminary feasibility of roof-mounted solar PV systems in the Maldives. Renew Sustain Energy Rev 2018;83:18–32. doi:10.1016/J.RSER.2017.10.019.
[25] Lysen EH. Report IEA-PVPS T9-12: 2012 : Pico Solar PV Systems for Remote Homes. IEA International Energy Agency; 2013.
[26] International Finance Corporation. Lighting Global: Off-grid Solar Market Trends Report 2018. 2018. doi:10.1017/CBO9781107415324.004.
[27] Khodayar ME. Rural electrification and expansion planning of off-grid microgrids. Electr J 2017;30:68–74. doi:10.1016/j.tej.2017.04.004.
[28] Graber S, Narayanan T, Alfaro J, Palit D. Solar microgrids in rural India: Consumers' willingness to pay for attributes of electricity. Energy Sustain Dev 2018;42:32–43. doi:10.1016/J.ESD.2017.10.002.
[29] Sanchez DL, Sivaram V. Saving innovative climate and energy research: Four recommendations for Mission Innovation. Energy Res Soc Sci 2017;29:123–6. doi:10.1016/J.ERSS.2017.05.022.
[30] Forde E. The ethics of energy provisioning: Living off-grid in rural Wales. Energy Res Soc Sci 2017;30:82–93. doi:10.1016/J.ERSS.2017.06.018.
[31] Menconi ME, dell'Anna S, Scarlato A, Grohmann D. Energy sovereignty in Italian inner areas: Off-grid renewable solutions for isolated systems and rural buildings. Renew Energy 2016;93:14–26. doi:10.1016/J.RENENE.2016.02.034.
[32] Alliander N.V. About Alliander | Alliander n.d. https://www.alliander.com (accessed September 7, 2017).
[33] TED The Energy Detective. TED Pro Home Store n.d. http://www.theenergydetective.com/prohomestore.html (accessed October 16, 2018).
[34] Ten Kortenaar M. Seasalt battery | Dr Ten BV 2013. http://www.drten.nl/zeezout-batterij/?lang=en (accessed September 5, 2017).
[35] Quintero Pulido D, Hoogsteen G, ten Kortenaar M, Hurink J, Hebner R, Smit G. Characterization of Storage Sizing for an Off-Grid House in the US and the Netherlands. Energies 2018;11:265. doi:10.3390/en11020265.
[36] Reijnders VMJJ, Hurink JL. Testing Grid-Based Electricity Prices and Batteries in a Field Test. CIRED Workshop - Ljubljana , 7-8 June 2018 Paper 0500, 2018, p. 7–8.
[37] Quintero Pulido D, Ten Kortenaar M, Hurink J, Smit G. A Practical Approach in Glycerol Oxidation for the Development of A Glycerol Fuel Cell. IMedPub J Trends

Green Chem 2017;3:1–17. doi:10.21767/2471-9889.100018.
[38] Hoogsteen G, Molderink A, Hurink JL, Smit GJM. Managing energy in time and space in smart grids using TRIANA. IEEE PES Innov Smart Grid Technol Conf Eur 2015:1–6. doi:10.1109/ISGTEurope.2014.7028973.
[39] Hoogsteen G. DEMKit : A Flexible Smart Grid Simulation and Demonstration Platform Written in Python. Present Energy Open Enschede 2017.
[40] Fares RL, Webber ME. Dynamic Modeling of Community Energy Storage for Lifetime Estimation During Islanding. ECS Trans 2013;53:17–28. doi:10.1149/05307.0017ecst.
[41] Tuttle DP, Baldick R. The evolution of plug-in electric vehicle-grid interactions. IEEE Trans Smart Grid 2012;3:500–5. doi:10.1109/TSG.2011.2168430.
[42] Rothrock H. Sustainable housing: Emergy evaluation of an off-grid residence. Energy Build 2014;85:287–92. doi:10.1016/j.enbuild.2014.08.002.
[43] van der Klauw T, Hurink J, Smit G. Scheduling of Electricity Storage for Peak Shaving with Minimal Device Wear. Energies 2016;9:465. doi:10.3390/en9060465.
[44] Hoogsteen G. A cyber-physical systems perspective on decentralized energy management. University of Twente, 2017. doi:10.3990/1.9789036544320.
[45] Elding LI, Gustafson L. A reaction mechanism for oxidative addition of halogen to platinum(II), reductive elimination of halide from platinum(IV) and halide assisted anations of platinum(IV) complexes. Inorganica Chim Acta 1976;19:165–71. doi:10.1016/S0020-1693(00)91090-9.
[46] Heinrich Danneel ESM. Electrochemistry Theoretical Electrochemistry and Its Physico-Chemical Foundations. First. New York: Jhon Wiley & Sons; 1907.
[47] Besenhard JO. Handbook of Battery Materials. First. Austria: 1999.
[48] Cedzynska K. Properties of modified electrolyte for zinc-bromine cells. Pergamon 1995;40:971–6.
[49] Cathro KJ, Cedzynska, K, Constable DC. Some properties of zinc/bromine battery. J Power Sources 1985;16:53–63.
[50] Eustace DJ. Bromine Complexation in Zinc-Bromine Circulating Batteries. J Electrochem Soc 1980;127:528–32.
[51] Barnartt S, Forejt DA. Bromine-Zinc Secondary Cells. J Electrochem Soc 1964;111:1201–4.
[52] Vafiadis H, Skyllas-kazacos M. Evaluation of membranes for the novel vanadium bromine redox flow cell 2006;279:394–402. doi:10.1016/j.memsci.2005.12.028.
[53] Scamman DP, Reade GW, Roberts EPL, Limited RT, Station AP, Cf G. Numerical modelling of a bromide-polysulphide redox flow battery . Part 2 : Evaluation of a utility-scale system 2009;189:1231–9. doi:10.1016/j.jpowsour.2009.01.076.
[54] Mastragostino M, Valcher S. Polymeric salt as bromine complexing agent in a Zn-Br2 model battery. Electrochim Acta 1983;28:501–5. doi:10.1016/0013-4686(83)85034-8.
[55] White RE, S.E L. A Model of the Bromine / Bromide Electrode Reaction at a Rotating Disk Electrode. J Electrochem Soc 1983;130:1096–103. doi:10.1149/1.2119890.
[56] Vogel I and MA. On Some Problems of the Zinc- Bromine system as an Electric Energy System of Higher Efficiency-I. Kinetics of the Bromine Electrode. Pergamon Press 1991;36:1403–8.
[57] Diaz MA. Thermodynamics of Cl-H2O, Br-H2O, I-H2O, Au-Cl-H2O, Au-Br-H2O and Au-I-H20 systems at 298 K. J Electroanal Chem 1993;361:13–24.
[58] Conway BE, Phillips Y, Qian SY. Surface Electrochemistry and Kinetics of Anodic Bromine Formation at Platinum. J Chem Soc Faraday Trans 1995;91:283–93.
[59] Heintz A, Illenberger C. Diffusion coefficients of Br2 in cation exchange membranes. J Memb Sci 1996;113:175–81.

[60] Pell W. Zinc/Bromine Battery Electrolytes: Electrochemical, Physicochemical and Spectroscopic Studies. Ottawa: Ottawa University; 1994.
[61] Walter S, Aym D, Walter S, Gabelica Z, Valange S. Evaluation of carbon cryogels used as cathodes for non-flowing zinc – bromine storage cells zinc – bromine storage cells 2008. doi:10.1016/j.jpowsour.2007.09.076.
[62] Faita G, Fiori G, Mussini T. Electrochemical processes of the bromine/ bromide system. Electrochim Acta 1968;13:1765–72. doi:10.1016/0013-4686(68)80084-2.
[63] Bennett B, Chang J, Bard AJ. Mechanism of the Br-/Br2 Redox Reaction on Platinum and Glassy Carbon Electrodes in Nitrobenzene by Cyclic Voltammetry. Electrochim Acta 2016;219:1–9. doi:10.1016/j.electacta.2016.09.129.
[64] Kolthoff IM, Coetzee JF. Polarography in Acetonitrile. II. Metal Ions Which Have Significantly Different Polarographic Properties in Acetonitrile and in Water. Anodic Waves. Voltammetry at Rotated Platinum Electrode. J Am Chem Soc 1957;79:1852–8. doi:10.1021/ja01565a023.
[65] Duhlev R, Brown ID, Faggiani R, IUCr. Zinc bromide dihydrate ZnBr2.2H2O: a double-salt structure. Acta Crystallogr Sect C Cryst Struct Commun 1988;44:1696–8. doi:10.1107/S0108270188006584.
[66] Haaf WR, Carpenter GB, IUCr. The crystal structure of sodium bromide dihydrate. Acta Crystallogr 1964;17:730–2. doi:10.1107/S0365110X64001797.
[67] Boukamp BA. a Package for Impedance/Admittance Data Analysis. Solid State Lonics 18 2014;19:1–5. doi:10.1007/s13398-014-0173-7.2.
[68] Boukamp BA. A Linear Kronig-Kramers Transform Test for Immittance Data Validation. J Electrochem Soc 1995;142:1885–94. doi:10.1149/1.2044210.
[69] Sigma A. Product Description 2019. https://www.sigmaaldrich.com/nederland.html (accessed June 6, 2019).
[70] Autolab M. Autolab PGSTAT101 2019. https://www.metrohm.com/en/products-overview/electrochemistry/autolab compact line/PGSTAT101 (accessed May 21, 2019).
[71] Instruments H. HI-9811-5 pH/EC/TDS/°C Portable Meter 2018. https://www.hannainstruments.co.uk/ph-ec-tds-c-portable-meter.html (accessed May 21, 2019).
[72] Instruments C. Product Index 2019. https://www.chinstruments.com/products.shtml (accessed May 21, 2019).
[73] Boukamp BA. A Nonlinear Least Squares Fit procedure for analysis of immittance data of electrochemical systems. Solid State Ionics 1986;20:31–44. doi:10.1016/0167-2738(86)90031-7.
[74] Boukamp BA. Electrochemical impedance spectroscopy in solid state ionics: Recent advances. Solid State Ionics 2004;169:65–73. doi:10.1016/j.ssi.2003.07.002.
[75] Arai K, Kusu F, Noguchi N, Takamura K, Osawa H. Selective Determination of Chloride and Bromide Ions in Serum by Cyclic Voltammetry 1996;113:109–13.
[76] Chen M, Huang S, Hsieh C, Lee J-Y, Tsai T. Electrochimica Acta Development of a Novel Iodine-Vitamin C / Vanadium Redox Flow Battery. Electrochim Acta 2014;141:241–7. doi:10.1016/j.electacta.2014.07.069.
[77] Simonet V, Calzavara Y, Hazemann JL, Argoud R, Geaymond O, Raoux D. Structure of aqueous ZnBr2 solution probed by x-ray absorption spectroscopy in normal and hydrothermal conditions. J Chem Phys 2002;116:2997–3006. doi:10.1063/1.1433499.
[78] Omta AW, Kropman MF, Woutersen S, Bakker HJ. Negligible Effect of Ions on the Hydrogen-Bond Structure in Liquid Water. Science (80-) 2003;301:347–9. doi:10.1126/science.1084801.
[79] Lin Y-S, Auer BM, Skinner JL. Water structure, dynamics, and vibrational

spectroscopy in sodium bromide solutions. J Chem Phys 2009;131:144511. doi:10.1063/1.3242083.

[80] Adanuvor PK, White RE, Lorimer SE. The Effect of the Tribromide Complex Reaction on the Oxidation/Reduction Current of the Br2 / Br − Electrode. J Electrochem Soc 1987;134:1450–4. doi:10.1149/1.2100688.

[81] Mastragostino M, Gramellini C. Kinetic study of the electrochemical processes of the bromine/bromine aqueous system on vitreous carbon electrodes. Electrochim Acta 1985;30:373–80. doi:10.1016/0013-4686(85)80198-5.

[82] Park S, Shin S, Jung D, Chae J, Chang J. Understanding Br− transfer into electrochemically generated discrete quaternary ammonium polybromide droplet on Pt ultramicroelectrode. J Electroanal Chem 2017;797:97–106. doi:10.1016/j.jelechem.2017.05.014.

[83] Izumi I, Sato J, Iwashita N, Inagaki M. Electrochemical intercalation of bromine into graphite in an aqueous electrolyte solution. Synth Met 1995;75:75–7.

[84] Gaier JR, Ditmars NF, Dillon AR. Aqueous electrochemical intercalation of bromine into graphite fibers. Carbon N Y 2005;43:189–93. doi:10.1016/j.carbon.2004.09.005.

[85] Bell JG, Wang J. Current and potential oscillations during the electro-oxidation of bromide ions. J Electroanal Chem 2015;754:133–7. doi:10.1016/j.jelechem.2015.07.016.

[86] Ciriminna R, Pina C Della, Rossi M, Pagliaro M. Understanding the glycerol market. Eur J Lipid Sci Technol 2014;116:1432–9. doi:10.1002/ejlt.201400229.

[87] He Q (Sophia), McNutt J, Yang J. Utilization of the residual glycerol from biodiesel production for renewable energy generation. Renew Sustain Energy Rev 2017;71:63–76. doi:10.1016/j.rser.2016.12.110.

[88] Ayoub M, Abdullah AZ. Critical review on the current scenario and significance of crude glycerol resulting from biodiesel industry towards more sustainable renewable energy industry. Renew Sustain Energy Rev 2012;16:2671–86. doi:10.1016/j.rser.2012.01.054.

[89] Waidhas M, Drenckhahn W, Preidel W, Landes H. Direct-fuelled fuel cells. J Power Sources 1996;61:91–7. doi:http://dx.doi.org/10.1016/S0378-7753(96)02343-9.

[90] Liu W, Webb CJ, Gray EM. Review of hydrogen storage in AB3 alloys targeting stationary fuel cell applications. Int J Hydrogen Energy 2016;41:3485–507. doi:10.1016/j.ijhydene.2015.12.054.

[91] Granot E, Filanovsky B, Presman I, Kuras I, Patolsky F. Hydrazine/air direct-liquid fuel cell based on nanostructured copper anodes. J Power Sources 2012;204:116–21. doi:10.1016/j.jpowsour.2011.12.008.

[92] Matos J, Borodzinski A, Zychora AM, Kedzierzawski P, Mierzwa B, Juchniewicz K, et al. Direct formic acid fuel cells on Pd catalysts supported on hybrid TiO2-C materials. Appl Catal B Environ 2015;163:167–78. doi:10.1016/j.apcatb.2014.07.063.

[93] Wang Z, Zhang B, Borthwick AGL, Feng C, Ni J. Utilization of single-chamber microbial fuel cells as renewable power sources for electrochemical degradation of nitrogen-containing organic compounds. Chem Eng J 2015;280:99–105. doi:10.1016/j.cej.2015.06.012.

[94] Wang FF, Shao S, Liu CL, Xu CL, Yang RZ, Dong WS. Selective oxidation of glycerol over Pt supported on mesoporous carbon nitride in base-free aqueous solution. Chem Eng J 2015;264:336–43. doi:10.1016/j.cej.2014.11.115.

[95] Falase A, Garcia K, Lau C, Atanassov P. Electrochemical and in situ IR characterization of PtRu catalysts for complete oxidation of ethylene glycol and glycerol. Electrochem Commun 2011;13:1488–91. doi:10.1016/j.elecom.2011.10.001.

[96] Habibi E, Razmi H. Glycerol electrooxidation on Pd, Pt and Au nanoparticles supported on carbon ceramic electrode in alkaline media. Int J Hydrogen Energy 2012;37:16800–9. doi:10.1016/j.ijhydene.2012.08.127.
[97] Geraldes AN, Da Silva DF, E Silva LGDA, Spinacé EV, Neto AO, Dos Santos MC. Binary and ternary palladium based electrocatalysts for alkaline direct glycerol fuel cell. J Power Sources 2015;293:823–30. doi:10.1016/j.jpowsour.2015.06.010.
[98] Wang Z, Xin L, Zhao X, Qiu Y, Zhang Z, Baturina OA, et al. Carbon supported Ag nanoparticles with different particle size as cathode catalysts for anion exchange membrane direct glycerol fuel cells. Renew Energy 2014;62:556–62. doi:10.1016/j.renene.2013.08.005.
[99] Burke LD, Nugent PF. The Electrochemistry of Gold: I The Redox Behaviour of the Metal in. Gold Bull 1997;30:43–53. doi:10.1007/BF03214756.
[100] Ureta-Zanartu MS, Berrios C, Gonzales T, Fernandez F, Baez D, Salazar R, et al. Electrocatalytic Oxidation of Alcohols at Gold Electrodes in Alkaline Media. Int J Electrochem Sci 2012;7:8905–28.
[101] Shi X, Simpson DE, Roy D. The role of chemisorbed hydroxyl species in alkaline electrocatalysis of glycerol on gold †. Phys Chem Chem Phys 2015;17:11432–44. doi:10.1039/C5CP00313J.
[102] Qi J, Xin L, Chadderdon DJ, Qiu Y, Jiang Y, Benipal N, et al. Electrocatalytic selective oxidation of glycerol to tartronate on Au/C anode catalysts in anion exchange membrane fuel cells with electricity cogeneration. Appl Catal B Environ 2014;154–155:360–8. doi:10.1016/j.apcatb.2014.02.040.
[103] Chornaja S, Kampars V, Zhizhkun S, Kulikova L. Oxidation of glycerol with oxygen in alkaline aqueous solutions in the presence of supported palladium catalysts prepared by the extractive- pyrolytic method. React Kinet Mech Catal 2013;108:341–57. doi:10.1007/s11144-012-0516-3.
[104] Marshall AT, Golovko V, Padayachee D. Electrochimica Acta In fl uence of gold nanoparticle loading in Au / C on the activity towards electrocatalytic glycerol oxidation. Electrochim Acta 2015;153:370–8. doi:10.1016/j.electacta.2014.11.186.
[105] Kwon Y, Schouten KJP, Koper MTM. Mechanism of the Catalytic Oxidation of Glycerol on Polycrystalline Gold and Platinum Electrodes. ChemCatChem 2011;3:1176–85. doi:10.1002/cctc.201100023.
[106] Kwon Y, Lai SCS, Rodriguez P, Koper MTM. Electrocatalytic Oxidation of Alcohols on Gold in Alkaline Media : J Am Chem Soc 2011;133:6914–7.
[107] Padayachee D, Golovko V, Marshall AT. The effect of MnO2 loading on the glycerol electrooxidation activity of Au/MnO2/C catalysts. Electrochim Acta 2013;98:208–17. doi:10.1016/j.electacta.2013.03.061.
[108] Hoogsteen G, Molderink A, Hurink JL, Smit GJM. Managing energy in time and space in smart grids using TRIANA. IEEE PES Innov. Smart Grid Technol. Conf. Eur., 2015. doi:10.1109/ISGTEurope.2014.7028973.
[109] Dimitrijević S, Rajčić-Vujasinović M, Trujić V. Non-cyanide electrolytes for gold plating - a review. Int J Electrochem Sci 2013;8:6620–46.
[110] Markiewicz M, Zalitis C, Kucernak A. Performance measurements and modelling of the ORR on fuel cell electrocatalysts - The modified double trap model. Electrochim Acta 2015;179:126–36. doi:10.1016/j.electacta.2015.04.066.
[111] Gewirth AA, Thorum MS. Electroreduction of dioxygen for fuel-cell applications: Materials and challenges. Inorg Chem 2010;49:3557–66. doi:10.1021/ic9022486.
[112] Carrettin S, Mcmorn P, Johnston P, Griffin K, Kiely CJ, Attard GA. Oxidation of glycerol using supported gold catalysts 2004;27.
[113] Song X, Zhang D. Bimetallic Ag-Ni/C particles as cathode catalyst in AFCs (alkaline fuel cells). Energy 2014;70:223–30. doi:10.1016/j.energy.2014.03.116.

[114] Othman MR, Riyanto. Electrochemical stability of Cu, Ni, Co, Pt and Ir metals sheet and their composite electrodes in potassium hydrox de solution. Int J Electrochem Sci 2012;7:8408–19.
[115] Chi-ucán SL, Castillo-atoche A, Borges PC, Manzanilla-cano JA, González-garcía G, Patiño R, et al. Inhibition Effect of Glycerol on the Corrosion of Copper in NaCl Solutions at Different pH Values. Hindawi Publ Corp J Chem 2014;2014:1–11.
[116] Avramov-Ivić ML, Leger JM, Lamy C, Jović VD, Petrović SD. The electro-oxidation of glycerol on the gold(100)-oriented single-crystal surface and poly crystalline surface in 0.1 M NaOH. J Electroanal Chem 1991;308:309–17. doi:10.1016/0022-0728(91)85075-Z.
[117] Singh PP. A Model for Ionic Behavior in Aqueous Solution. Activity Coefficients of Electrolytes at 298.15 K. J Am Chem Soc 1977;99:1312–5.
[118] Sobri S, Roy S, Aranyi D, Nagy PM, Papp K, Kalman E. Growth of electrodeposited gold on glassy carbon from a thiosulphate-sulphite electrolyte. Surf Interface Anal 2008;40:834–43. doi:10.1002/sia.2799.
[119] Hezard T, Fajerwerg K, Evrard D, Collire V, Behra P, Gros P. Gold nanoparticles electrodeposited on glassy carbon using cyclic voltammetry: Application to Hg(II) trace analysis. J Electroanal Chem 2012;664:46–52. doi:10.1016/j.jelechem.2011.10.014.
[120] Othman MR, Ahmad A. ELECTROCHEMICAL OXIDATION OF GLYCEROL USING GOLD ELECTRODE. Malaysian J Anal Sci 2015;19:291–9.
[121] Vilchis-Carbajal S, González I, Lapidus GT. Electrochemical study of gold cementation with zinc powder at low cyanide concentration in alkaline solutions. J Appl Electrochem 2000;30:217–29. doi:10.1023/A:1003820807315.
[122] Okinaka Y, Kato M. Electroless Deposition of Gold. Mod. Electroplat., 2011, p. 483–98. doi:10.1002/9780470602638.ch21.
[123] Guan YC, Han KN. The Electrochemical Study of the Deposition of Gold onto Copper and Zinc in Ammoniacal Solutions. J Electrochem Soc 1995;142:1139–43.
[124] Yongprapat S, Therdthianwong A, Therdthianwong S. Au / C catalyst prepared by polyvinyl alcohol protection method for direct alcohol alkaline exchange membrane fuel cell application 2012:483–90. doi:10.1007/s10800-012-0423-3.
[125] Palit D, Bandyopadhyay KR. Rural electricity access in India in retrospect: A critical rumination. Energy Policy 2017;109:109–20. doi:10.1016/j.enpol.2017.06.025.
[126] Kesselring R. The electricity crisis in Zambia: Blackouts and social stratification in new mining towns. Energy Res Soc Sci 2017. doi:10.1016/j.erss.2017.06.015.
[127] Burlando A. Transitory shocks and birth weights: Evidence from a blackout in Zanzibar. J Dev Econ 2014;108:154–68. doi:10.1016/j.jdeveco.2014.01.012.
[128] Olaya Y, Arango-Aramburo S, Larsen ER. How capacity mechanisms drive technology choice in power generation: The case of Colombia. Renew Sustain Energy Rev 2016;56:563–71. doi:10.1016/j.rser.2015.11.065.
[129] Olivero-Verbel J. Colombia: Environmental Health Issues. Encycl. Environ. Heal., 2011, p. 740–54. doi:10.1016/B978-0-444-52272-6.00395-0.
[130] Perfetti Del Corral M. Encuesta Nacional de Calidad de Vida. Bogota: 2017.
[131] Richards S, Withers PJA, Paterson E, McRoberts CW, Stutter M. Potential tracers for tracking septic tank effluent discharges in watercourses. Environ Pollut 2017;228:245–55. doi:10.1016/j.envpol.2017.05.044.
[132] Bousquet C, Samora I, Manso P, Rossi L, Heller P, Schleiss AJ. Assessment of hydropower potential in wastewater systems and application to Switzerland. Renew Energy 2017;113:64–73. doi:10.1016/j.renene.2017.05.062.
[133] Yang J, Chen B. Energy–water nexus of wind power generation systems. Appl Energy 2016;169:1–13. doi:10.1016/j.apenergy.2016.02.010.

[134] Naqvi M, Yan J, Dahlquist E, Naqvi SR. Off-grid electricity generation using mixed biomass compost: A scenario-based study with sensitivity analysis. Appl Energy 2017;201:363–70. doi:10.1016/j.apenergy.2017.02.005.
[135] Wang Y, Zhao Y, Xu L, Wang W, Doherty L, Tang C, et al. Constructed wetland integrated microbial fuel cell system: looking back, moving forward. Water Sci Technol 2017:wst2017190. doi:10.2166/wst.2017.190.
[136] Han C, Liu J, Liang H, Guo X, Li L. An innovative integrated system utilizing solar energy as power for the treatment of decentralized wastewater. J Environ Sci 2013;25:274–9. doi:10.1016/S1001-0742(12)60034-5.
[137] Gu Y, Li Y, Li X, Luo P, Wang H, Wang X, et al. Energy Self-sufficient Wastewater Treatment Plants: Feasibilities and Challenges. Energy Procedia 2017;105:3741–51. doi:10.1016/j.egypro.2017.03.868.
[138] Schäfer M, Hobus I, Schmitt TG. Energetic flexibility on wastewater treatment plants. Water Sci Technol 2017:wst2017308. doi:10.2166/wst.2017.308.
[139] Hoogsteen G, Molderink A, Hurink JL, Smit GJM, Schuring F, Kootstra BL. Impact of peak electricity demand in distribution grids: A stress test. 2015 IEEE Eindhoven PowerTech 2015:1–6. doi:10.1109/PTC.2015.7232412.
[140] Barreto CM, Garcia HA, Hooijmans CM, Herrera A, Brdjanovic D. Assessing the performance of an MBR operated at high biomass concentrations. Int Biodeterior Biodegradation 2017;119:528–37. doi:10.1016/j.ibiod.2016.10.006.
[141] Boule De Jong J. Bever IIIA - Afmitech Friesland 2016. http://afmitech.nl/producten/bever-iiia/?lang=en (accessed March 30, 2017).
[142] Parra D, Swierczynski M, Stroe DI, Norman SA, Abdon A, Worlitschek J, et al. An interdisciplinary review of energy storage for communities: Challenges and perspectives. Renew Sustain Energy Rev 2017;79:730–49. doi:10.1016/J.RSER.2017.05.003.
[143] Olabi AG. Renewable energy and energy storage systems. Energy 2017;136:1–6. doi:10.1016/J.ENERGY.2017.07.054.
[144] Mohler D, Sowder D. Energy Storage and the Need for Flexibility on the Grid. Renew. Energy Integr., Elsevier; 2017, p. 309–16. doi:10.1016/B978-0-12-809592-8.00023-8.
[145] Ghafoor, Abdul;Munir A. Design and economics analysis of an off-grid PV system for household electrification. Renew Sustain Energy Rev 2015;42:496–502. doi:10.1016/J.RSER.2014.10.012.
[146] Shivakumar A, Welsch M, Taliotis C, Jakšić D, Baričević T, Howells M, et al. Valuing blackouts and lost leisure: Estimating electricity interruption costs for households across the European Union. Energy Res Soc Sci 2017;34:39–48. doi:10.1016/j.erss.2017.05.010.
[147] Hanser P, Lueken R, Gorman W, Mashal J. The practicality of distributed PV-battery systems to reduce household grid reliance. Util Policy 2017;46:22–32. doi:10.1016/j.jup.2017.03.004.
[148] Ardito L, Procaccianti G, Menga G, Morisio M. Smart Grid Technologies in Europe: An Overview. Energies 2013;6:251–81. doi:10.3390/en6010251.
[149] Hirmer S, Guthrie P. The benefits of energy appliances in the off-grid energy sector based on seven off-grid initiatives in rural Uganda. Renew Sustain Energy Rev 2017;79:924–34. doi:10.1016/j.rser.2017.05.152.
[150] Hashemi A, Arman. Climate Resilient Low-Income Tropical Housing. Energies 2016;9:468. doi:10.3390/en9060468.
[151] Fossati JP, Galarza A, Martín-Villate A, Fontán L. A method for optimal sizing energy storage systems for microgrids. Renew Energy 2015;77:539–49. doi:10.1016/j.renene.2014.12.039.

[152] Schneider M, Biel K, Pfaller S, Schaede H, Rinderknecht S, Glock CH. Using inventory models for sizing energy storage systems: An interdisciplinary approach. J Energy Storage 2016;8:339–48. doi:10.1016/j.est.2016.02.009.
[153] Grantham A, Pudney P, Ward LA, Whaley D, Boland J. The viability of electrical energy storage for low-energy households. Sol Energy 2017;155:1216–24. doi:10.1016/j.solener.2017.07.063.
[154] Bruch M, Müller M. Calculation of the Cost-effectiveness of a PV Battery System. Energy Procedia 2014;46:262–70. doi:10.1016/j.egypro.2014.01.181.
[155] Balcombe P, Rigby D, Azapagic A. Energy self-sufficiency, grid demand variability and consumer costs: Integrating solar PV, Stirling engine CHP and battery storage. Appl Energy 2015;155:393–408. doi:10.1016/j.apenergy.2015.06.017.
[156] Bianchi M, Branchini L, De Pascale A, Melino F. Storage Solutions for Renewable Production in Household Sector. Energy Procedia 2014;61:242–5. doi:10.1016/j.egypro.2014.11.1098.
[157] Ciez RE, Whitacre JF. The cost of lithium is unlikely to upend the price of Li-ion storage systems. J Power Sources 2016;320:310–3. doi:10.1016/j.jpowsour.2016.04.073.
[158] Perez KX, Baldea M, Edgar TF, Hoogsteen G, van Leeuwen RP, van der Klauw T, et al. Soft-islanding a group of houses through scheduling of CHP, PV and storage. 2016 IEEE Int. Energy Conf., IEEE; 2016, p. 1–6. doi:10.1109/ENERGYCON.2016.7513972.
[159] Gerards MET, Toersche HA, Hoogsteen G, van der Klauw T, Hurink JL, Smit GJM. Demand side management using profile steering. 2015 IEEE Eindhoven PowerTech, IEEE; 2015, p. 1–6. doi:10.1109/PTC.2015.7232328.
[160] Bakker V, Molderink A, Bosman MGC, Hurink JL, Smit GJM. On simulating the effect on the energy efficiency of smart grid technologies. Proc. 2010 Winter Simul. Conf., IEEE; 2010, p. 393–404. doi:10.1109/WSC.2010.5679146.
[161] Fares RL, Webber ME. Combining a dynamic battery model with high-resolution smart grid data to assess microgrid islanding lifetime. Appl Energy 2015;137:482–9. doi:10.1016/j.apenergy.2014.04.049.
[162] Obinna U, Joore P, Wauben L, Reinders A. Comparison of two residential Smart Grid pilots in the Netherlands and in the USA, focusing on energy performance and user experiences. Appl Energy 2017;191:264–75. doi:10.1016/j.apenergy.2017.01.086.
[163] Muralitharan K, Sakthivel R, Vishnuvarthan R. Neural Network based Optimization Approach for Energy Demand Prediction in Smart Grid. Neurocomputing 2017. doi:10.1016/j.neucom.2017.08.017.
[164] van der Klauw T, Hoogsteen G, Gerards MET, Hurink JL, Xianyong Feng X, Hebner RE. Assessing the potential of residential HVAC systems for demand-side management. 2016 IEEE Power Energy Soc. Innov. Smart Grid Technol. Conf., IEEE; 2016, p. 1–5. doi:10.1109/ISGT.2016.7781193.
[165] Hoogsteen G, van der Klauw T, Molderink A, Hurink JL, Smit GJM, Feng X, et al. Balancing islanded residential microgrids using demand side management. 2016 IEEE Power Energy Soc. Innov. Smart Grid Technol. Conf., IEEE; 2016, p. 1–5. doi:10.1109/ISGT.2016.7781167.
[166] Austin Energy. Home 2016. https://austinenergy.com (accessed September 6, 2017).
[167] Voltcraft. VOLTCRAFT ENERGY-LOGGER 4000 Energiekostenmeter Instelbaar stroomtarief, Kostenprognose | Conrad.nl 2019. https://www.conrad.nl/p/voltcraft-energy-logger-4000-energiekostenmeter-instelbaar-stroomtarief-kostenprognose-125444?WT.mc_id=gshop&gclid=Cj0KCQjw3uboBRDCARIsAO2XcYBTbXXr2JaP9A

vltqWtOt6851X4zIYwqJSN9w7mtRak5P3HM6VzrfEaAjM9EALw_wcB&tid=1749191029_67243245 (accessed July 1, 2019).
[168] Energy Storage NL. Dr Ten Innovatie & Prestatie : Energy Storage NL n.d. http://www.energystoragenl.nl/lidbedrijf/dr-ten?lang=en (accessed September 9, 2017).
[169] Holland trade and Investment. Sea-salt Battery | Showcases | Holland Trade and Invest n.d. https://www.hollandtradeandinvest.com/showcases/sustainable-dutch-solutions/clean-energy/sea-salt-storage-battery (accessed September 9, 2017).
[170] Ten Kortenaar M V. Anodic Oxidation of Formaldehyde on Gold Studied by Electrochemical Impedance Spectroscopy: An Equivalent Circuit Approach. J Electrochem Soc 1999;146:2146–55. doi:10.1149/1.1391905.
[171] Vencon. UBA5 Battery Analyzer & Charger - PC Peripheral | Vencon 2019. https://www.vencon.com/ (accessed July 1, 2019).
[172] Spiers D. Batteries in PV Systems. McEvoy's Handb. Photovoltaics, Elsevier; 2018, p. 789–843. doi:10.1016/B978-0-12-809921-6.00021-5.
[173] Affordable Solar. Off-grid System Sizing - Affordable Solar n.d. http://www.affordable-solar.com/learning-center/solar-basics/off-grid-system-sizing/ (accessed December 27, 2017).
[174] Jacobson AJ, Nazar LF. Intercalation Chemistry. Encycl. Inorg. Bioinorg. Chem., Chichester, UK: John Wiley & Sons, Ltd; 2011. doi:10.1002/9781119951438.eibc0093.

Publications, Presentations and Prizes

Publications

DFQP 1. D.F. Quintero Pulido, Ten Kortenaar, J. Hurink, and G. Smit "The Role of Off-Grid Houses in the Energy Transition with a Case Study in the Netherlands". ***Energies*** **2019,** *12*, 2033 https://doi.org/10.3390/en12102033.

DFQP 2. D.F. Quintero Pulido, M. Ten Kortenaar, J. Hurink, and G. Smit, "Characteristics of Halide Oxidation at Graphite Electrode for Use in Halide Batteries". **Sustainable Energy Technologies and Assessments**. Volume 33, June 2019, Pages 14-23 https://doi.org/10.1016/j.seta.2019.03.001

DFQP 3. D.F. Quintero Pulido, M. Ten Kortenaar, J. Hurink, and G. Smit, "A Practical Approach in Glycerol Oxidation for the Development of A Glycerol Fuel Cell". ***IMedPub J. Trends Green Chem.***, vol. 3, no. 1:4, pp. 1–17, 2017 doi: 10.21767/2471-9889.100018

DFQP 4. D. F. Quintero Pulido, G. Hoogsteen, M. ten Kortenaar, J. Hurink, R. Hebner, and G. Smit, "Characterization of Storage Sizing for an Off-Grid House in the US and the Netherlands". ***Energies***, vol. 11, no. 2, p. 265, Jan. 2018 https://doi.org/10.3390/en11020265.

DFQP 5. D.F. Quintero Pulido, Ten Kortenaar, J. Hurink, and G. Smit "Simulation of sizing of energy storage for off-grid decentralized wastewater treatment units: A case study in the Netherlands" .***Water Practice & Technology*** Vol 13 No 4 doi: 10.2166/wpt.2018.087

Presentations

DFQP 6. D.F. Quintero Pulido, Ten Kortenaar M.V, Hurink J.L.,Smit G.J.M. "Electrochemical Behavior of Halogens Redox Couples at Carbon Graphite Electrode in Aqueous Solutions" , Presentation in Changchun-China the meeting-conference of the ***International Electrochemical Society*** 2015

DFQP 7. D.F. Quintero Pulido Ten Kortenaar M.V , Hurink J.L. . Smit G.J.M."Electrochemical Oxidation of Glycerol in Alkaline, Aqueous Solution on Gold and Different Gold Alloys for Fuel Cell Application". Abstract accepted and presented in Oakland, New Zealand at the conference ***International Electrochemical society 19th topic Meeting*** 2016

DFQP 8. D.F. Quintero Pulido, C.M. Barreto, M.V. Ten Kortenaar, J.L. Hurink , D. Brdjanovic, G.J.M.Smit . "An Off-Grid Energy Management System for Operating Decentralized Wastewater Treatment Units in Smart grids", ***8th conference Young Water Professionals IWA*** conference Cape town South Africa, 2017.

DFQP 9. D.F. Quintero Pulido, Ten Kortenaar M.V, Hurink J.L.,Smit G.J.M. "The Effect of Positive Ions in the Oxidation of Halides for Use in Electricity Storage" Presentation in Brisbane-Australia at the ***meeting-conference International Electrochemical Society,*** 2019

Prizes

- Universidad de la Salle. San Juan Bautista De La Salle Prize for career achievement "Development of New Technologies to Increase the Access to Water and Energy in the world". Bogotá-Colombia 2018.
- UNLEASH 2018 prize for the best idea in the 'SDG 6 Water and Sanitation' category and the Award for Global Scalability Potential, for the idea Beehive toilets for slums, with the group "Savvy Sanitation Solutions", Singapore 2018.

2eN Design - Godert Hoenderkamp & Anne-Marie van Bueren with DE COOBRAA FOUNDATION 2019 "Future practical implementation of this research".

ABOUT THE AUTHOR

Diego F. Quintero Pulido originates from Colombia where he achieved a bachelor degree in Environmental and Sanitary Engineering at La Salle University in Bogotá with a focus in decentralized water treatment systems. After that, he moved to the Netherlands in 2009 to follow a Master program in Sustainable Energy Technologies at TU Delft. Here he came in contact with the company Dr Ten and developed during an internship and his Master thesis new water based electricity storage systems (batteries and fuel cells).

He has been working at Dr Ten since 2011 doing research and development on products of the company for markets in developing countries.

His PhD research focused on the integration of new high tech technologies to enable the feasibility of off-grid houses for developed and developing countries. This thesis is part of the I-Care project at the chairs CAES and DMMP at the University of Twente. During the PhD project Diego cooperated with the University of Texas in Austin (USA), IHE Delft Institute for Water Education (the Netherlands), La Universidad de La Salle (Colombia) and the company Dr Ten (the Netherlands, Israel).